

AFIT/GAE/AA/81D-30

AN EXPERIMENTAL INVESTIGATION OF THE
FLOW FIELD OF AN EJECTOR WING DESIGN
EMPLOYING A PHOTON CORRELATION
LASER VELOCIMETER

THESIS

AFIT/GAE/AA/81D-30

DAMON G. STEPHENS
Captain USAF

S DTIC
ELECTE
FEB 1 9 1982
A

Approved for public release; distribution unlimited

PII Redacted

AFIT/GAE/AA/81D-30

AN EXPERIMENTAL INVESTIGATION OF THE
FLOW FIELD OF AN EJECTOR WING DESIGN
EMPLOYING A PHOTON CORRELATION LASER VELOCIMETER

THESIS

Presented to the Faculty of the School of Engineering
of the Air Force Institute of Technology
Air University
in Partial Fulfillment of the Requirements
for the Degree of Master of Science

by

Damon G. Stephens, B.S.
Captain USAF

Graduate Aeronautical Engineering
December 1981

Accession	
DTIC	
Unannounced	
Justification	
Availability Codes	
Dist	
A	

Approved for public release; distribution unlimited



PREFACE

This thesis arose out of a need by the Air Force Flight Dynamics Laboratory (AFFDL) for mean velocity and turbulence intensity data in the flow field of an ejector wing design. The design was conceived by the Vought Corporation while under contract with AFFDL and represents a unique and exciting airfoil/ejector mating

As a novice to the world of research and technical writing, I greatly appreciated the guidance and expert assistance of many talented individuals. My sincere thanks to Dr. Harold Wright, my principal faculty advisor, for the opportunity to work on this project and for his assistance in dealing with the many equipment problems that impeded its progress. Sincere thanks also to Dr. George Catalano for sharing with me his wealth of laser velocimeter experimental experience. I also wish to thank Maj. Mike Smith for his assistance in finding answers to questions that arose.

For their efforts in setting up and maintaining the experimental apparatus I wish to thank Mr. William Baker and Mr. Leroy Cannon. Also a word of appreciation and thanks to Mr. Nick Yardich and Mr. Scotty Whitt for their dedication to keeping the "Blue Beast" (AFIT Smoke Tunnel) in operation throughout my research. And for their useful suggestions and fine craftsmanship in the construction and modification of the ejector wing model, I wish to thank Mr. Carl Shortt, Mr. Russel Murray, and Mr. Jack Tiffany of the AFIT School Shop. Also, for their excellent photographic support I wish to thank Mr.

Ed Fields and Mr. Dave Cunningham of the Technical Photo
Division.

In addition, and most importantly, I wish to express my
deepest gratitude to my wife, Kathy, for her patience, love,
and understanding during the course of study required in the
preparation of this thesis.

CONTENTS

	<u>Page</u>
Preface.....	ii
List of Figures.....	v
List of Symbols.....	vii
Abstract.....	ix
I. Introduction.....	1
Background.....	1
High Lift Configurations.....	2
Objectives.....	3
Approach.....	3
II. Experimental Apparatus and Procedure.....	5
Flow System.....	5
Ejector Wing Design Model.....	7
Laser Doppler Velocimeter.....	14
III. Sources of Error and Equipment Limitations.....	20
IV. Results and Analysis.....	23
Flow Visualization.....	23
Laser Velocimeter.....	32
ACA = 15°.....	32
AOA = 0°.....	64
V. Conclusions.....	80
VI. Recommendations.....	83
Bibliography.....	86
Appendix A: Autocorrelation Function.....	88
Appendix B: Mean Velocity.....	94
Appendix C: Turbulence Intensity.....	98
Appendix D: Sample Calculations.....	101
Vita.....	109

LIST OF FIGURES

<u>Figure</u>	<u>Title</u>	<u>Page</u>
1	Flow System	6
2	Ejector Wing Design	8
3	Mercury Manometer Calibration Setup	9
4	Ejector	11
5	Ejector Velocity Profile	12
6	Ejector Velocity/Mercury Manometer Calibration	12
7	Laser Velocimeter System (Top View)	15
8	Optical Bench Showing Optical Path (Side View)	15
9	Laser Beam Control Volume	16
10	Oscilloscope Autocorrelation Display	17
11	Pictorial View of Experimental Apparatus	19
12	Laser Beams Oblique to Airfoil	20
13-26	Flow Visualization Photographs	25-31
27	Leading Edge Stagnation Point Movement	36
28	Survey Locations, $AOA = 15^\circ$	37
29-41	Mean Velocity Profiles, $AOA = 15^\circ$	38-50
42-54	Turbulence Intensity Profiles, $AOA = 15^\circ$	51-63
55	Wake Survey	66
56	Survey Locations, $AOA = 0^\circ$	68
57-62	Mean Velocity Profiles, $AOA = 0^\circ$	69-74

<u>Figure</u>	<u>Title</u>	<u>Page</u>
63-67	Turbulence Intensity Profiles, AOA = 0°	75-79
68	Autocorrelation of $u(t)$ and $u(t+\tau)$	88
69	Autocorrelation Function	89
70	Oscilloscope Displayed Autocorrelation Function	91
71	Displayed Skewed Autocorrelation Function	92
72	Replotted Unskewed Autocorrelation Function	92
73	Autocorrelation Function	93
74	Mean Velocity	94
75	Illustration of L, D, θ	95
76	Autocorrelation Peaks and Valleys	96
77	Velocity Fluctuations	98
78	High Turbulence Displayed Autocorrelation Function	102
79	Plot of Displayed Skewed Autocorrelation Function(Sample Calculations)	103
80	Least Squares Fit(Sample Calculations)	104
81	Least Squares Fit(Sample Calculations)	106
82	Unskewed Autocorrelation Function (Sample Calculations)	107
83	Nondimensional Autocorrelation Function(Sample Calculations)	107

SYMBOLS

<u>Symbol</u>	<u>Description</u>	<u>Units</u>
AOA	angle of attack	degrees
C	chord length of model	cm
D	distance the two laser beams are apart at a perpendicular reference surface(See L)	inches
D'	drag per unit span	lb _f /ft
ETA	turbulence Intensity	
F _d	doppler shift frequency	KHz
F _d [*]	doppler shift frequency with Phase Modulation	KHz
ΔF	frequency shift imposed on the two laser beams by the Phase Modulator	KHz
G(t)	autocorrelation function	
G ₁	first valley in the autocorrelation function	
G ₂	first peak after the first valley (G ₁) in the autocorrelation function	
G ₃	second valley in the autocorrelation function	
L	distance from the laser beam intersection point (control volume) to a perpendicular reference surface upon which the beams shine	inches
LDV	laser doppler velocimeter	
N	number of fringes in half of control volume	
PM Tube	photomultiplier tube	

<u>Symbol</u>	<u>Description</u>	<u>Units</u>
r_0	laser beam radius	mm
S	fringe spacing	m
T	sample time	sec
U_e	ejector velocity	m/sec
U_e/U_{fs}	ejector blowing ratio	
U_{fs}	free stream velocity	m/sec
U_{mX}	mean velocity component parallel to the free stream	m/sec
U_{mX}^*	mean velocity component parallel to the free stream with Phase Modulation	m/sec
U_{RMS}	root mean square velocity	m/sec
X	direction parallel to free stream	
x'	chordwise length dimension from leading edge of airfoil	cm
y'	spanwise length dimension	cm
z'	vertical length dimension from the chordline of airfoil	cm
z	vertical length dimension measured from the surface of airfoil at each survey location	cm
θ	half angle between the inter- secting laser beams	degrees
λ	wavelength of the he-ne laser	m
μ	refractive Index of Air	
ρ	air density	lb _m /ft ³
τ	delay time	sec

ABSTRACT

The flow field about a dual element airfoil model employing an ejector for aerodynamic blowing was investigated. Flow visualization was obtained by smoke tunnel testing. Mean velocities (mean velocity components parallel to the free stream), and turbulence intensities were determined at various flow field locations. All data was obtained through the use of a laser doppler velocimeter (LDV) using a photon correlation processing scheme. Flow field properties were computed from the LDV generated autocorrelation function.

The free stream velocity and Reynolds number, based on model chord length, were 8 m/sec and 325,000, respectively. The ejector wing model was tested with $U_{\text{ejector}}/U_{\text{free stream}}$ (U_e/U_{fs}) = 2.0 and no ejector flow. The $U_e/U_{fs} = 2.0$ blowing ratio delivers 0.046 lb_m/sec or 0.60 ft³/sec at the ejector face. Flow visualization photography was conducted at seven angles of attack: -5°, 0°, 5°, 10°, 15°, 20°, and 25° and LDV data was acquired at 0° and 15° angles of attack.

The results are presented in the form of flow visualization photographs and profiles of mean velocities and turbulence intensities. The ejector wing design achieves superior performance (enhanced lift, reduced drag) over an equivalent solid airfoil.

I. INTRODUCTION

Background

The ejector wing design analyzed in this paper was conceived by the Vought Corporation while under contract with the Air Force Flight Dynamics Laboratory (AFFDL) at Wright-Patterson AFB, Ohio (Reference 11). The model was fabricated and mounted in the Air Force Institute of Technology (AFIT) two-dimensional smoke tunnel at Wright-Patterson AFB prior to this present investigation. A schematic of the ejector wing design is presented in Figure 2. The thrust of this project is to study the flow field about the model as an aid to the Flight Dynamics Laboratory's investigation of the ejector wing design for possible V/STOL application.

The Air Force Institute of Technology's Laser Doppler Velocimeter (LDV) system incorporating a photon correlation processing scheme is used to obtain the experimental data. Flow visualization through kerosene smoke generation is used to assist in determining the overall flow field variations caused by ejector operation. There is a great deal of theoretical analysis and experimental documentation of simple ejectors available in the literature; however, very little information is available concerning the flow field about a wing incorporating an ejector. Hopefully, an experimental investigation of this unique design will contribute to a better understanding of this concept.

High Lift Configurations

Multi-element airfoils have long been recognized as beneficial in obtaining increased lift and reduced drag. The benefits include: increased circulation, decreased wake region, and enhanced boundary layer adhesion. The increased circulation is due to the location of the downstream element near the rear of the upstream element. The constriction to flow and the circulation about the downstream element places the trailing edge of the upstream element in a region of high velocity. In order for the flow on the upper surface of the upstream element to meet the decreased pressure at its trailing edge it must accelerate. This serves to increase the circulation about the entire airfoil and decrease the adverse pressure gradient on the upper surface of the upstream element. Thus, lift is increased and, since separation is delayed, the wake region and its associated drag are decreased. The introduction of an ejector blowing high velocity air into the constricted duct and over the upper surface of the downstream element further enhances these effects. Also, the high energy air from the ejector aids in keeping the downstream element's boundary layer attached. For further information on high lift devices, an excellent article by A.O.M. Smith (Reference 19) should be consulted.

Objectives

The objectives of this study are:

1. Using the two dimensional AFIT smoke tunnel obtain flow visualization photographs of the ejector wing model at various angles of attack: -5° , 0° , 5° , 10° , 15° , 20° , 25° , and ejector blowing ratios: $U_e/U_{fs} = 0.0$ and 2.0 .
2. Using a Laser Doppler Velocimeter obtain and plot mean velocity and turbulence intensity profiles at various flow field locations.
3. From the acquired data draw conclusions as to the aerodynamic benefit of this ejector wing design.

Approach

In order to meet the objectives of this study two different investigative schemes will be conducted:

1. Flow visualization photography through the use of kerosene smoke.
2. Mean velocity and turbulence intensity data at designated flow field locations obtained by a LDV.

Both investigative schemes will be employed with smoke tunnel free stream velocity (U_{fs}) of 8 m/sec and ejector blowing ratios, U_e/U_{fs} , of 0.0 and 2.0. Flow visualization photographs will be taken at -5° , 0° , 5° , 10° , 15° , 20° , and 25° angles of attack.

LDV data will be obtained at 0° and 15° angles of attack. At 15° angle of attack data will be taken with the ejector duct open. At 0° angle of attack, a comparison of the ejector

wing design with an equivalent solid airfoil will be conducted. Also, mean velocity wake surveys will be obtained and plotted in an attempt to determine relative drag.

II. EXPERIMENTAL APPARATUS AND PROCEDURE

Flow System

In order to provide a uniform free stream flow, the Air Force Institute of Technology's two dimensional smoke tunnel (Figure 1) is used. The smoke tunnel also provides the flow field visualization capability as well as an artificially seeded flow compatible with the LDV system. Maximum tunnel velocity is 23 m/sec using an open return flow system obtained by two diffuser isolated 1.5 hp motors. For this study a free stream velocity of 8 m/sec and a Reynolds Number based on model chord length of 325,000 is established. This velocity is obtained and monitored by a Prandtl type pitot-static probe and a 20 inch micromanometer. The free stream velocity is maintainable to within ± 0.1 m/sec or within 1.25% of the established free stream velocity. The test section measures 1.5 m in length, 1.0 m in height, and .07 m in width. The front wall is removable for ease of model access and its frame can accommodate any 0.635 cm thick glass material, such as, plexiglass or plate-glass. The rear wall, into which the model is mounted, is 0.635 cm laminated plateglass. Smoke (kerosene vapor) is generated by two 900 watt inconel heaters which boil the kerosene fuel at 910°R. The vapor particles are then mixed with cool compressed laboratory air, passed through a water condenser, and injected into the flow field upstream of the test section. The dense, white smoke produced is nontoxic, noncorrosive, and provides excellent visualization capabilities.

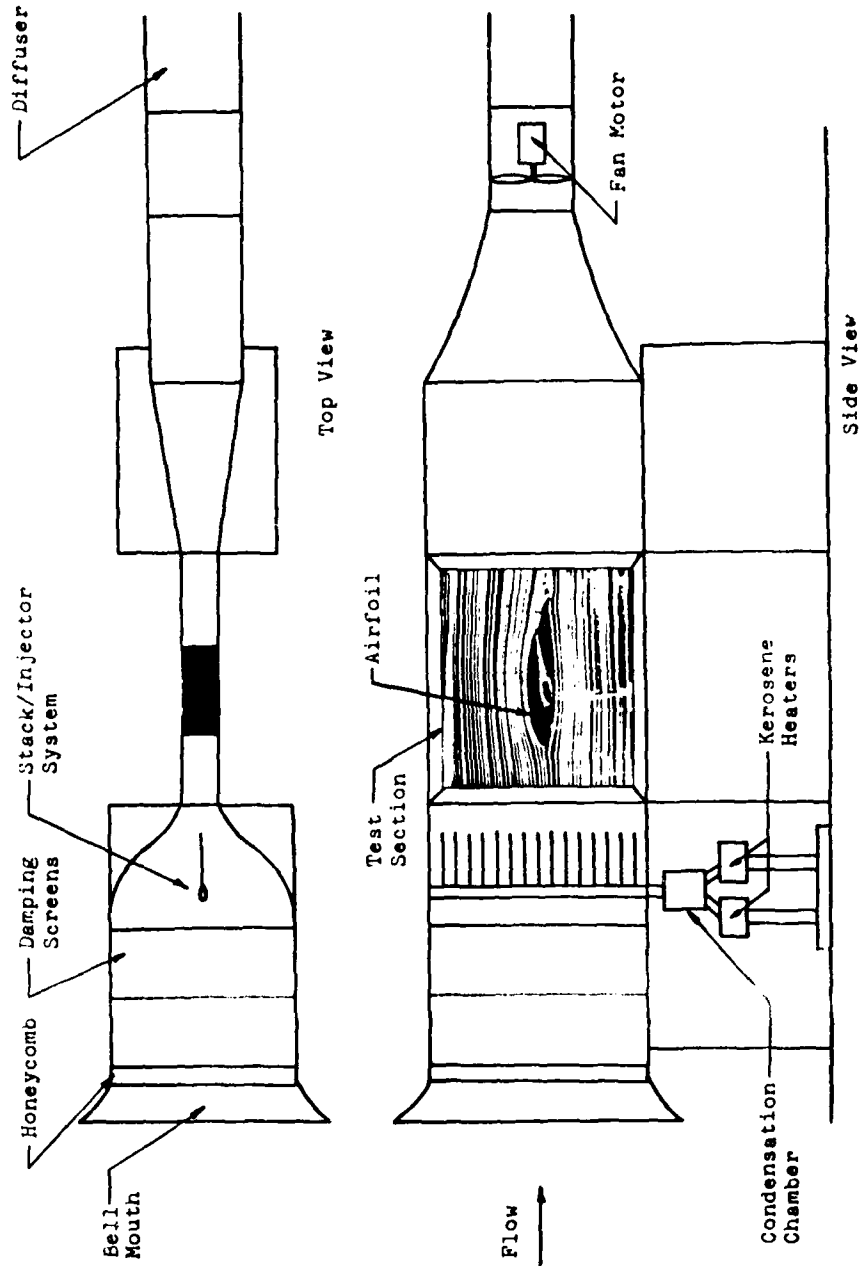


Figure 1 Flow System (Reference 23)

Ejector Wing Design Model

The model consists of a dual element airfoil with an incorporated ejector (Figure 2). It is constructed of wood and aluminum with a smooth flat black surface to minimize light scattering. The forward and aft airfoils and ejector are permanently secured to a plexiglass mounting plate and thus remain in the same configuration relative to each other as shown. The free space area or duct between the forward and aft airfoils where the ejector is located is referred to as the ejector duct. The entire airfoil is mounted to the back wall of the smoke tunnel at approximately the center of the test section. Two dimensional flow is assured by closing the test section securely against the model about its mounting apparatus. Test section blockage caused by the model ranges from 11% at 0° angle of attack to 29% at 25° angle of attack. The air is blown into the ejector in a spanwise direction and ejected in a chordwise direction at the ejector face. The laboratory compressed air reservoir supplies the ejector enabling various flow rates to be achieved.

The first task in this study was to determine the ejector velocity (U_e). A pitot-static tube was inserted in the front wall of the test section to probe the center of the ejector face in a spanwise direction (Figure 3). This probe was conducted with the model at 0° angle of attack. Since the pitot tube would interfere with the flow field and laser data acquisition, a pressure tap connected to a mercury manometer was

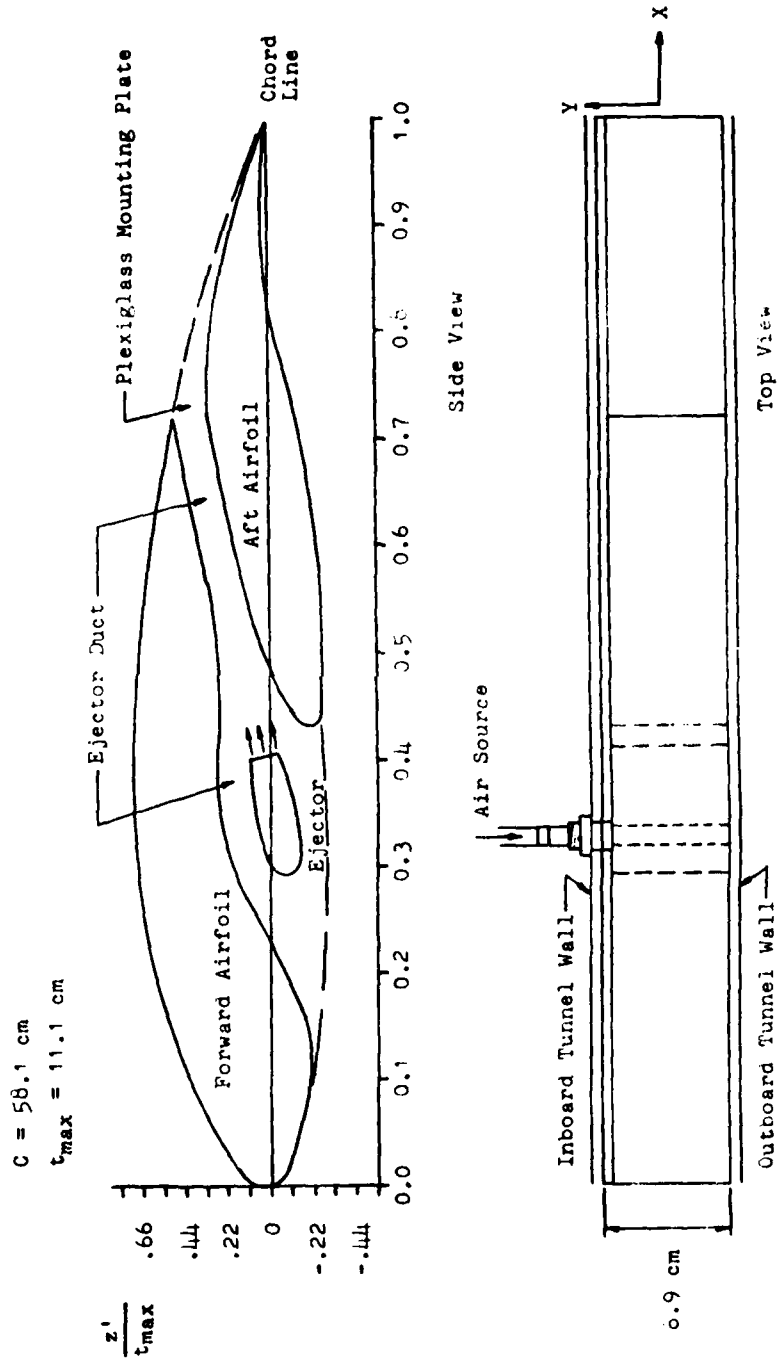


Figure 2 Ejector Wing Design

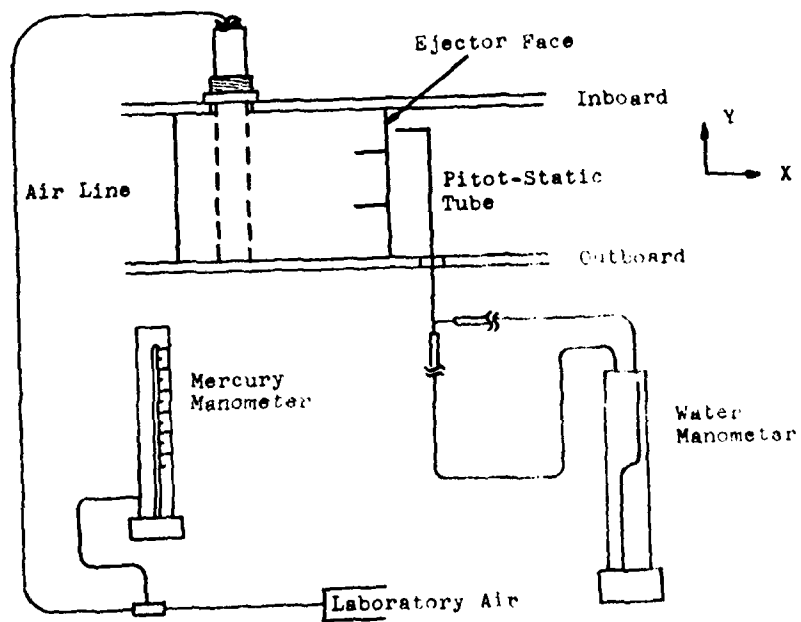
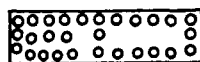
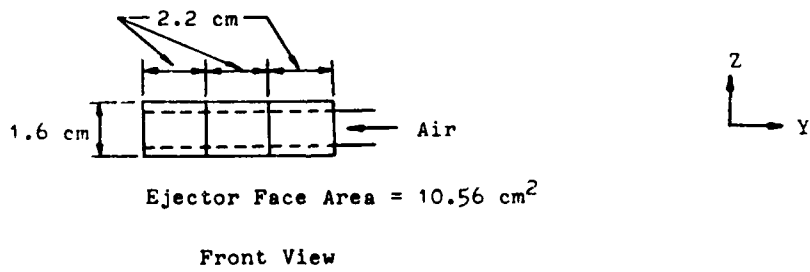
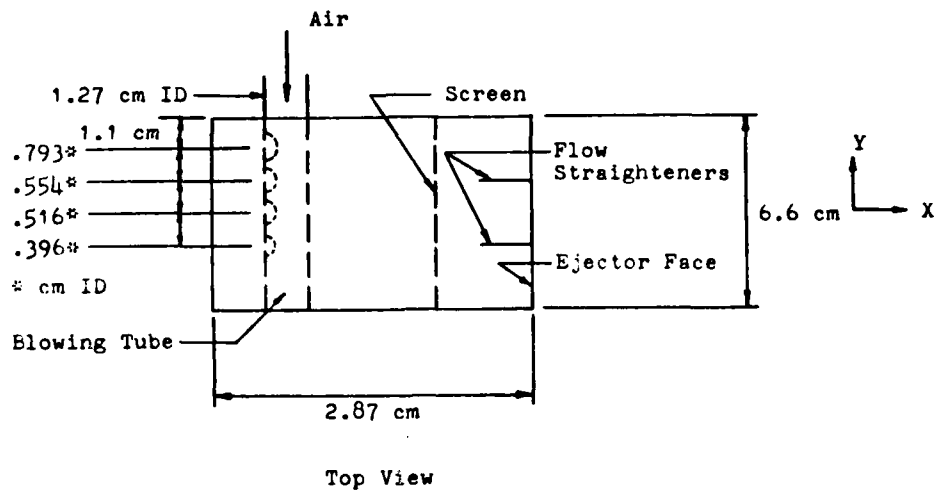


Figure 3 Mercury Manometer Calibration Setup

placed in the blowing line (air line). By determining the ejector velocity at various pressures, the manometer could be calibrated and its readings used to reestablish desired ejector velocities during the investigation. In addition to determining the ejector velocity, the pitot tube setup was used to modify the original ejector design to achieve a nearly uniform spanwise velocity profile at the ejector face. The new design was needed due to the nonuniform characteristics of right angle blowing, i.e., excessive ejector face velocities at the outboard section and near stagnation conditions at the inboard section. Use of a blowing tube with decreasing diameter holes inboard to outboard with a screen downstream of the tube provided the desired uniform spanwise velocity profile (Figure 4). Blockage of the ejector face caused by the screen is 67%, allowing back pressure to develop which aided in yielding the nearly uniform velocity profile. Figure 5 shows the velocity profile for $U_e = 16.0$ m/sec which is the ejector on velocity used throughout this investigation ($U_e/U_{fs} = 2.0$). After achieving the desired velocity profile, the mercury manometer was then calibrated (Figure 6).

In addition to ejector internal modifications, a method for changing the angle of attack of the model from outside the test section was devised and implemented. Rotation of the model exterior to the test section was accomplished by the use of strong magnets. Several strong magnets were embedded in the aft airfoil flush with the



225 Holes
 .132 cm ID each
 Screen Hole Area = 3.49 cm²

Screen

Figure 4 Ejector

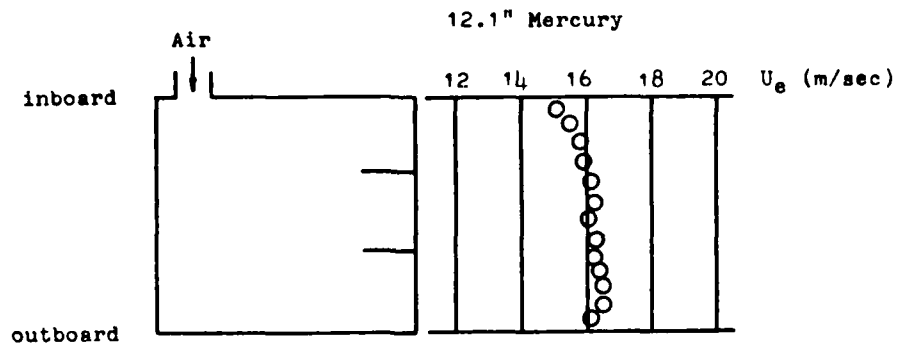


Figure 5 Ejector Velocity Profile

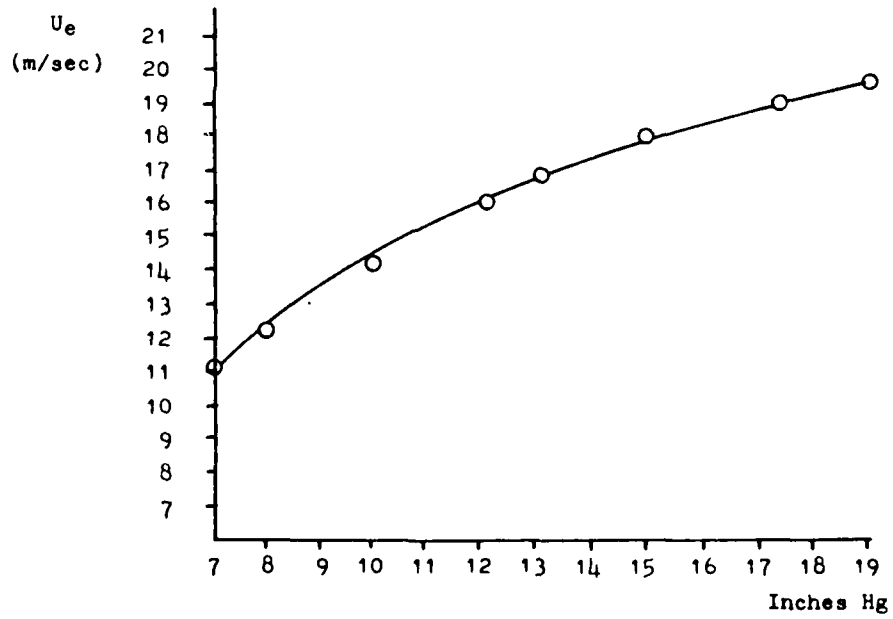


Figure 6 Ejector Velocity/Mercury Manometer Calibration

plexiglass mounting plate. Additional magnets were then used to rotate the model from outside of the test section. By drawing reference lines on the back wall of the test section, various angles of attack could be achieved.

Laser Doppler Velocimeter

In order to obtain the mean velocity and turbulence intensity profiles for this investigation a Malvern Doppler Velocimeter (LDV) was employed (Figures 7 and 8). The experimental benefit of the LDV system for determination of flow properties is due to its inherent noninterference with the flow. In addition, no calibration is required. The laser beams, unlike hot wire anemometers, pitot tubes, and pressure transducers do not create disturbances or pressure losses and do not suffer damage from the flow environment. However, the correct optical alignment is critical and thus requires constant monitoring. Also, light paths into and out of a transparent fluid containing suitable light scattering particles is required.

The Laser Velocimeter consisting of a Spectra-Physics 15 milliwatt helium-neon laser, Malvern beamsplitter and phase modulator, two silvered plane mirrors, a 100 cm focal length convex focusing lens, Malvern photomultiplier tube (PM Tube), Malvern digital photon correlator, oscilloscope, supporting optical benches, and associated power units was constructed for a previous AFIT master's thesis by Walterick (Reference 23).

A brief outline of the velocimeter's operation is presented. For more detailed operation and theory References 16, 17, and 23 should be consulted.

The he-ne laser provides a single 1.1 mm diameter monochromatic ($\lambda = 6328 \mu\text{m}$) red beam which is split into two

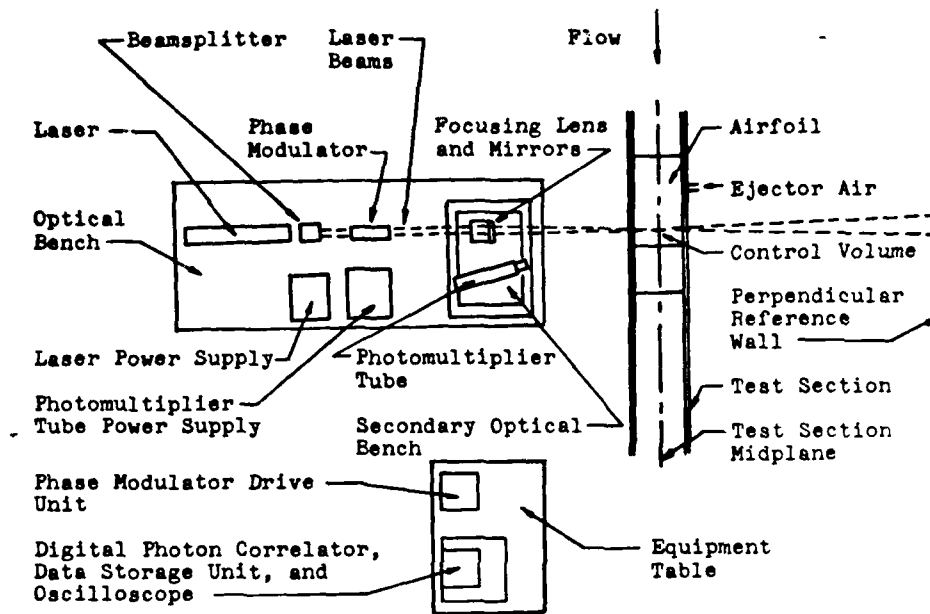


Figure 7 Laser Velocimeter System (Top View)

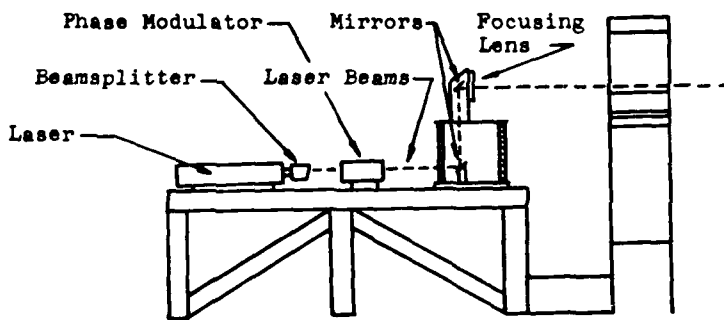


Figure 8 Optical Bench Showing Optical Path (Side View)

beams by a beamsplitter. The two beams pass through a phase modulator and are then transmitted along the optical path to the convex focusing lens by two silvered plane mirrors. As a result of passing through the lens the beams intersect at the focal point and form an ellipsoidal control volume composed of alternating constructive (light) and destructive (dark) interference fringes (Figure 9).

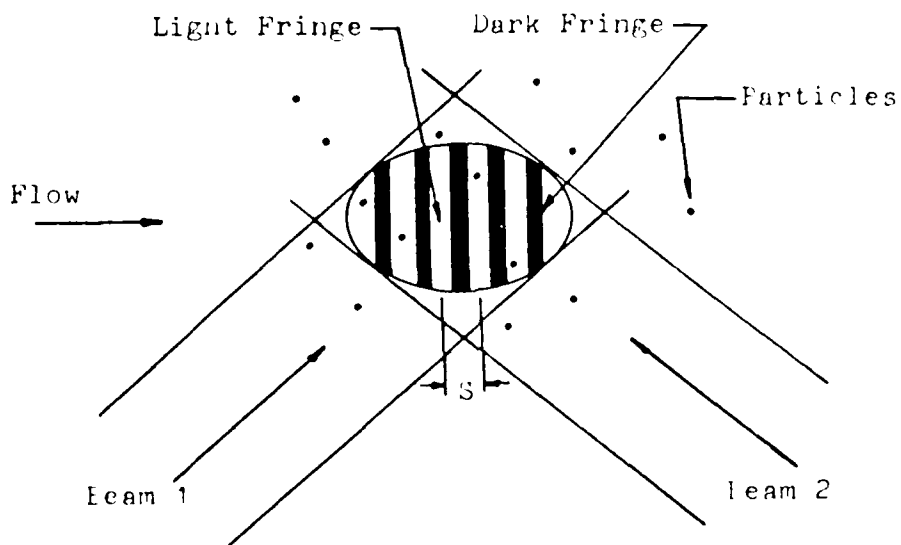


Figure 9 Laser Beam Control Volume

Mean velocity and turbulence intensity data can then be obtained by focusing a photomultiplier tube (PM tube) on the control volume as naturally occurring particles augmented by kerosene vapor pass through these light and dark fringes. Since the control volume fringes are oriented perpendicular to the free stream flow, only mean velocity components parallel to the free stream can be obtained. The PM tube detects the

the photons scattered by the particles and in conjunction with a digital photon correlator generates an autocorrelation function which is displayed on an oscilloscope (Figure 10).

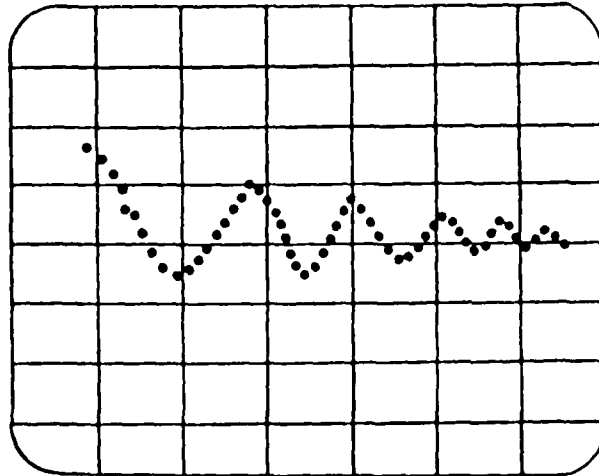


Figure 10 Oscilloscope Autocorrelation Display

In order to generate an adequate autocorrelation function, i.e., one with a damped sinusoidal shape, under certain adverse conditions a phase modulator unit is employed. Flow which is too slow, too fast, or too turbulent cannot be adequately evaluated without the phase modulator. Also, flow direction cannot be determined unless a phase modulator is used. Without phase modulation the interference fringes in the control volume are stationary with respect to the flow. By employing a phase modulator the fringes can be made to move either with or against the flow by applying an appropriate frequency shift to each beam. Attainable frequency shifts are 20 KHz to 1 MHz. By moving the fringes with the flow, for example, a fast flow can be "slowed" allowing more photon scattering and thus

improving the PM tube's efficiency and yielding a better autocorrelation function. In addition, by controlling the direction of fringe movement flow direction can be evaluated.

All data in this investigation was taken at the spanwise (y-direction) midplane of the test section (see Figure 7). Therefore, the LDV control volume was positioned at the test section midplane. Traversing of the control volume in the chordwise (x-direction) is accomplished by translation of the entire bench. Traverses in the z-direction are accomplished by translation of a secondary table through a chain and sprocket mechanism (Figures 7 and 8).

A brief explanation and discussion of the autocorrelation function plus definitions and discussions of turbulence properties are presented in the Appendix. In addition, the reduction of autocorrelation data, both with and without phase modulator employment, into mean velocities and turbulence intensities is presented in Appendices B and C.

A pictorial view of the entire experimental apparatus is presented in Figure 11.

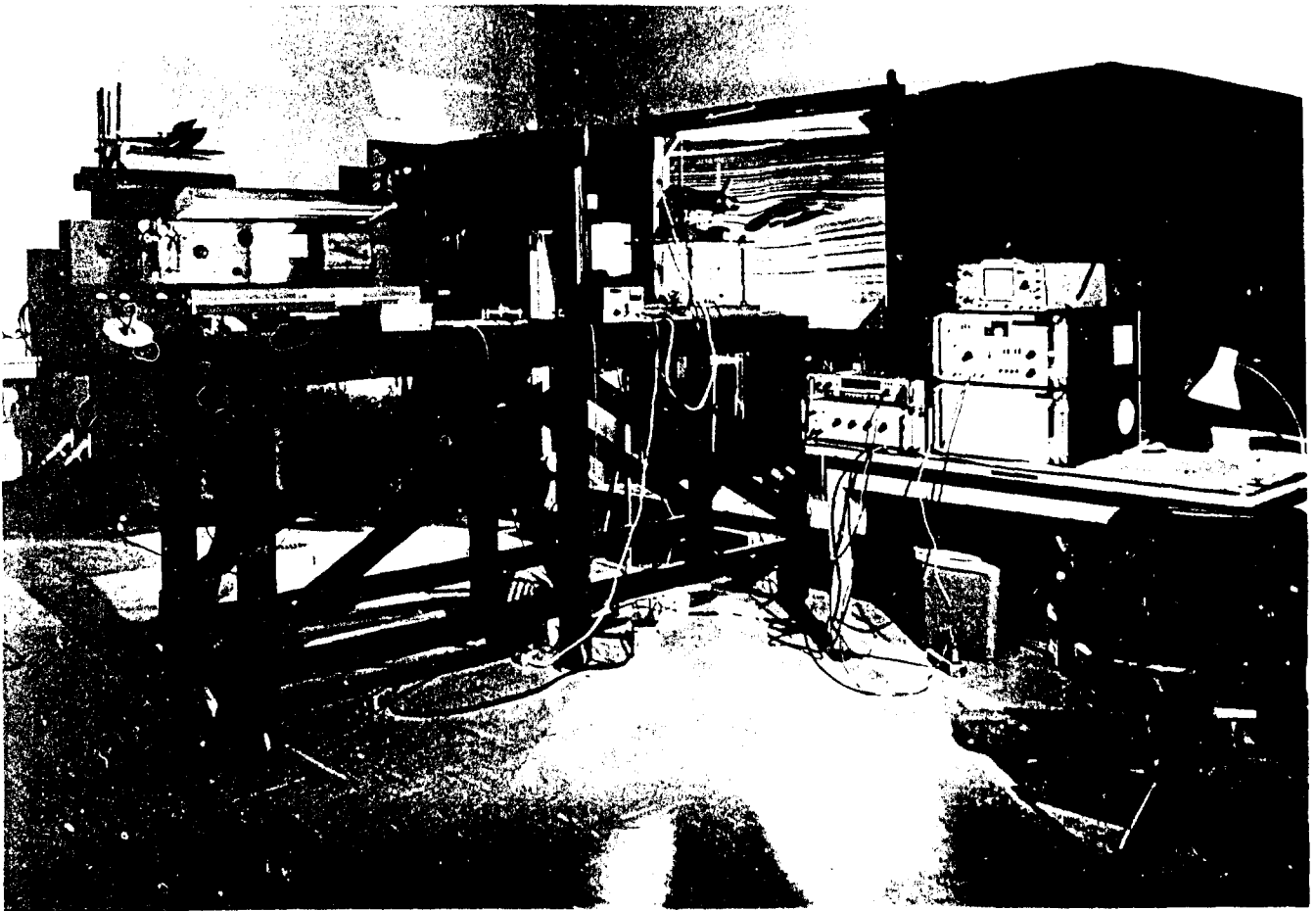


Figure 11 Fictorial View of Experimental Apparatus

III. SOURCES OF ERROR AND EQUIPMENT LIMITATIONS

Before presenting the results and subsequent conclusions and recommendations, the possible sources of error and limitations of the equipment are presented below:

1. The LDV optical alignment, in the absence of a rigid optical table, was very sensitive and required constant monitoring and frequent realignment.
2. Background light which results in optical noise, although minimized to the greatest extent possible, may still have yielded excessive noise and adversely affected the data.
3. It was found that data could not be obtained on the surface of the model nor within 2-3 mm of the surface due to the following:
 - a. The path at which the laser beams enter the test section is not parallel to the airfoil's surface as a result of floor/optical bench irregularities (Figure 12).

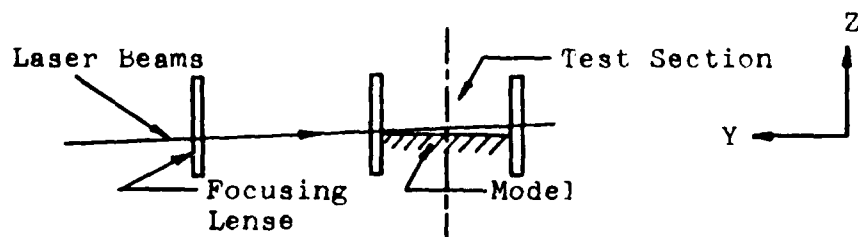


Figure 12 Laser Beams Oblique to the Airfoil

If the beams are lowered below that shown in Figure 12, the airfoil surface would block them.

b. Near the surface the beams caused excessive reflections which tended to overpower the PM tube and mask usable data.

c. Occasionally, the turbulence at the surface was in excess of the system's capability. This indicated a need for higher phase modulation than 1 MHz.

As a result of these limitations, data nearer than 2 to 3 mm from the surface was impossible to obtain. Therefore, useful data within the boundary layer could not be accurately acquired. In addition, all mean velocities obtained are not total velocity vectors but only components aligned with the free stream. Therefore, no meaningful boundary layer analysis could be conducted using this equipment and this model size.

4. Due to limitations imposed by the optical benches, the maximum downward (negative z-direction) movement of the control volume was approximately 12 cm below the center of the test section.

5. Initially, plexiglass, used for prior research applications for safety reasons, was used as the front wall of the smoke tunnel's test section. However, due to the softness of the plexiglass material it was easily scratched during normal use. These scratch marks along

with the refractive variations of the material caused by stresses induced a large scattering of laser light which, at times, generated overwhelming optical noise. Therefore, the plexiglass was replaced by plate glass. This reduced the optical noise and yielded a better signal.

IV. RESULTS AND ANALYSIS

The results are presented in the order in which they were experimentally obtained:

1. Flow Visualization Photographs
2. LDV Experimental Data

The main purpose of obtaining flow visualization photographs is to gain an appreciation of the overall changes in the flow field due to ejector employment. In addition, the photographs serve as a very useful aid in determining the locations at which LDV data should be acquired. Hence, the reason for the experimental sequence.

Flow Visualization

The visual effects of ejector operation on the flow field are documented in Figures 13 through 26. In all photographs the ejector duct is open. The arrows in each figure (photograph) identify a common streak line which can be used as an aid in flow field comparisons between the ejector off and ejector on operational modes.

Two observations can be readily made. First, the fluid, here visualized by streak lines, is drawn up from its original position before ejector employment. Second, the streak lines in the airfoil wake region directly above the aft airfoil appear less diffused and more well defined with ejector operation. An excellent illustration of the first observation occurs at $AOA = 10^\circ$ (Figures 19 and 20). The arrow in Figure 19 indicates a streak line which flows under the forward airfoil and into the ejector duct without ejector operation. The same streak line, identified

by the arrow in Figure 20, flows over the upper surface of the forward airfoil with ejector operation. This phenomenon, as discussed earlier, is attributable to the ejector's creation of a high velocity region at the trailing edge of the forward airfoil. This causes an acceleration of the flow on the upper surface and a drop in static pressure or increase in suction. This effect draws fluid up from its original position before ejector employment. The net result is a greater pressure differential and an increase in effective angle of attack yielding greater lift. The second observation would seem to indicate a smaller, more well behaved wake region which could lead to a drag reduction. An excellent illustration of this wake region phenomenon occurs at $AOA = 15^\circ$ (Figures 21 and 22). Note the apparent decrease in wake region size above the aft airfoil as well as the less diffused, more definable flow pattern.

It can be seen that the leading edge stagnation point appears to move down or in a counterclockwise direction at the nose with the ejector on. This indicates an increase in circulation. A final observation is the appearance that more flow is being entrained into the ejector duct region during ejector operation. Note this effect at $AOA = 5^\circ$ (Figures 17 and 18). More fluid can be seen within the ejector duct with the ejector on than with it off. This is an expected ejector benefit and should contribute to enhanced performance.



Figure 13 AOA = 5° , Ejector OFF

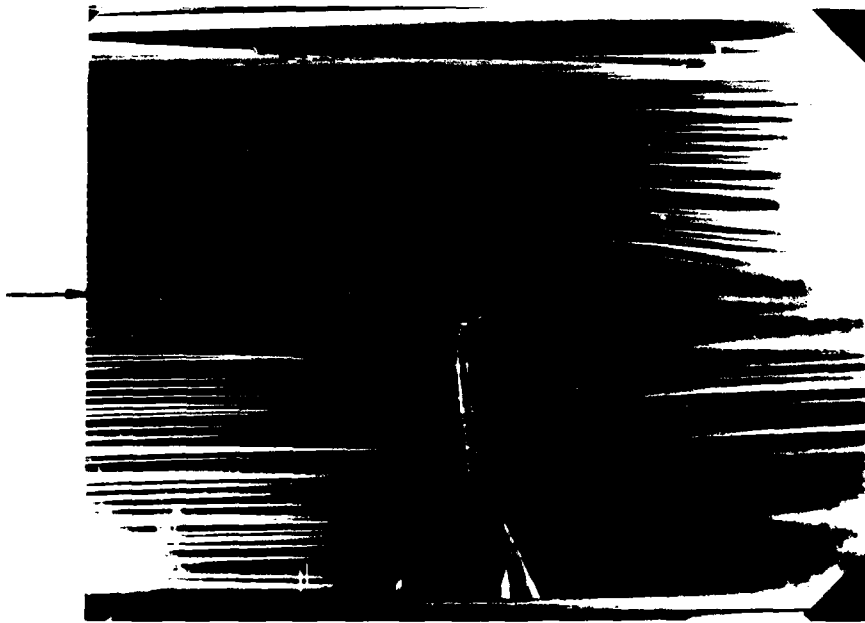


Figure 14 AOA = -5° , Ejector ON

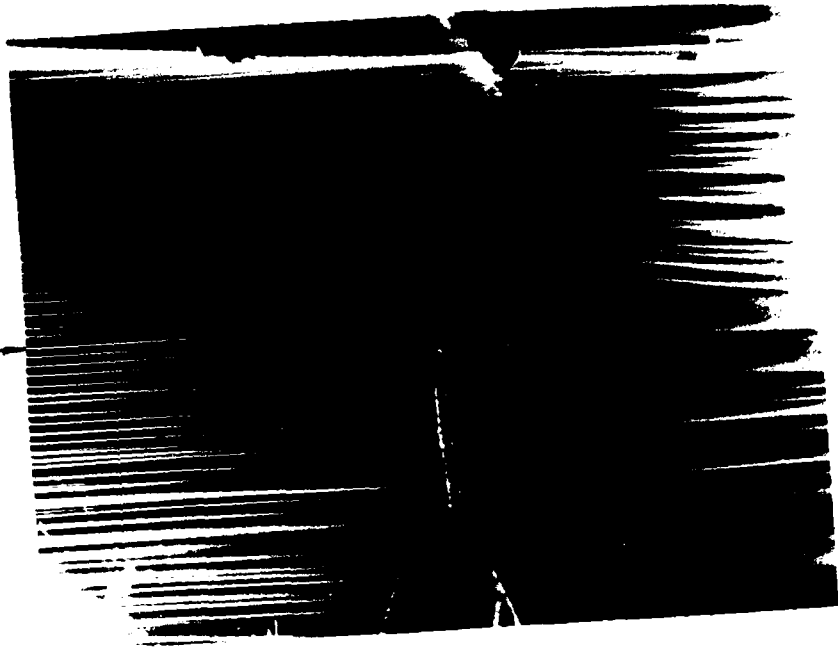


Figure 15 AOA = 0°, Ejector OFF

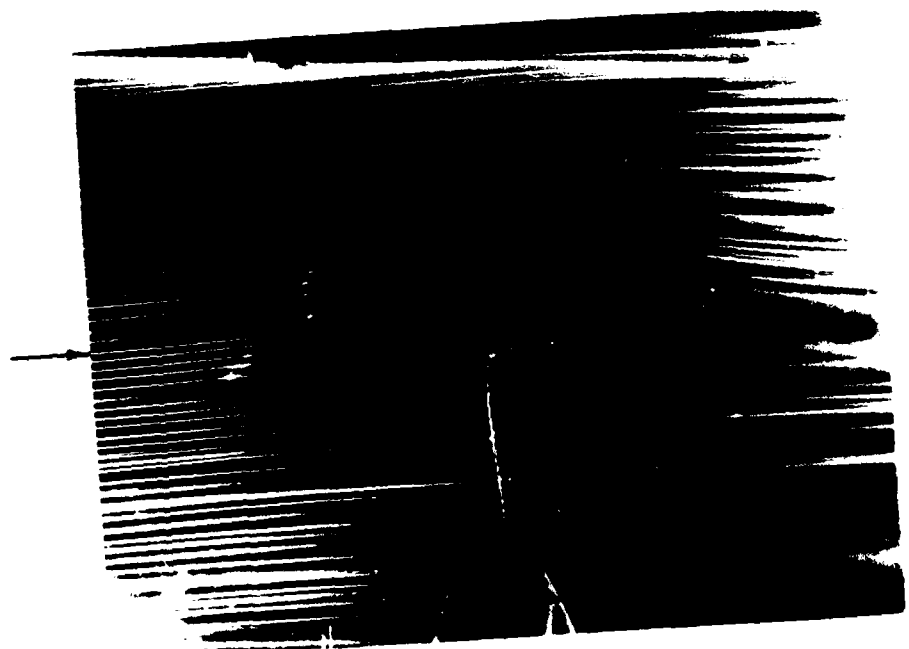


Figure 16 AOA = 0°, Ejector ON

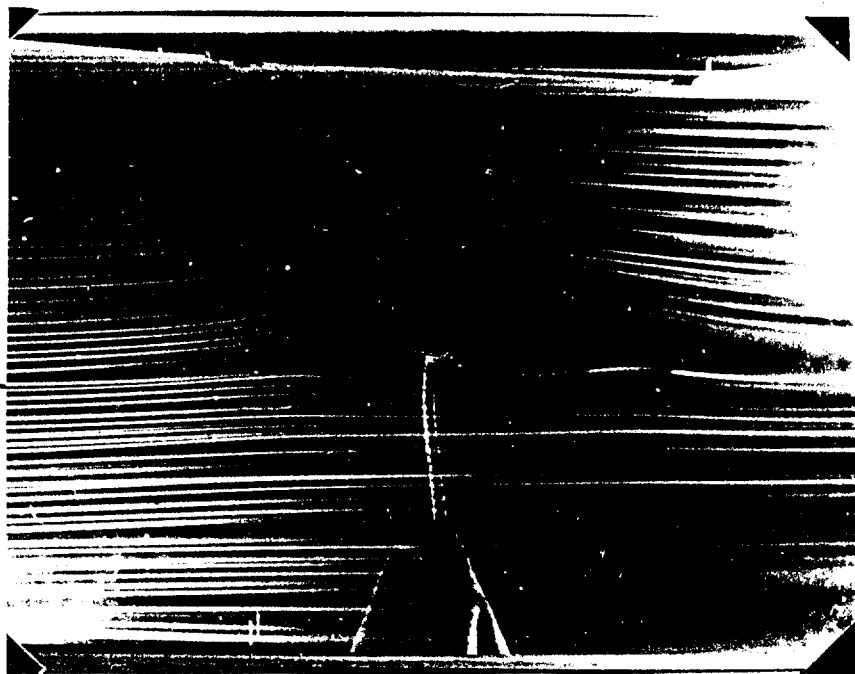


Figure 17 AOA = 5° , Ejector OFF

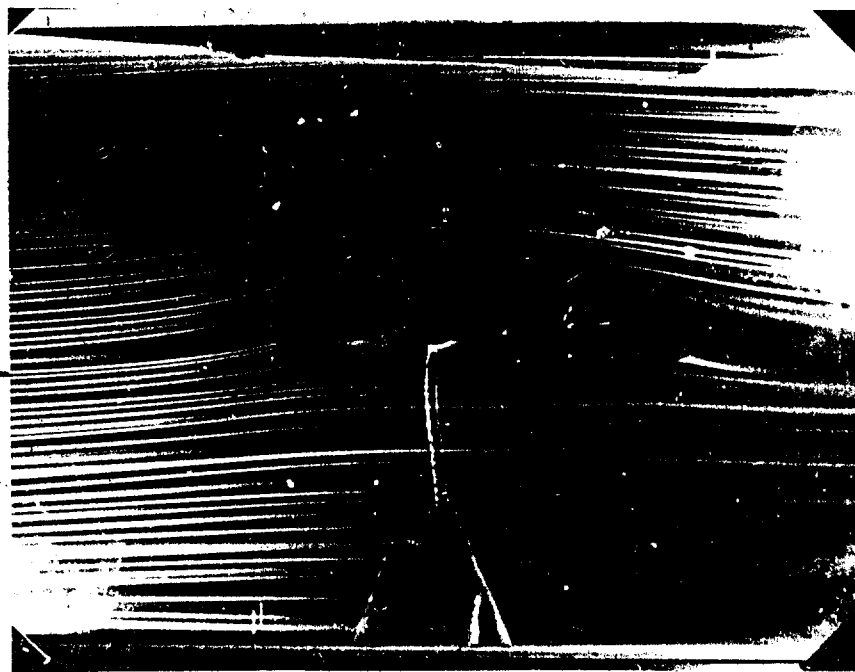


Figure 18 AOA = 5° , Ejector ON

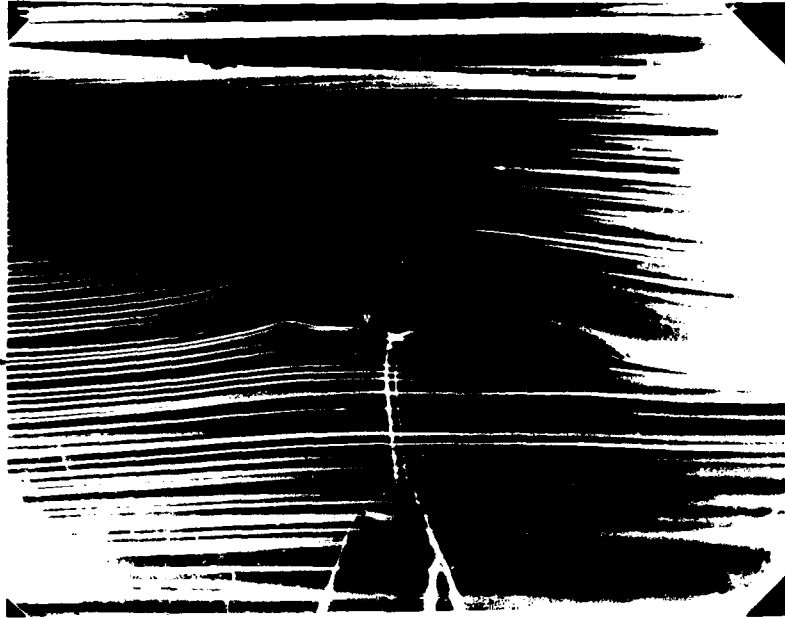


Figure 19 AOA = 10°, Ejector OFF

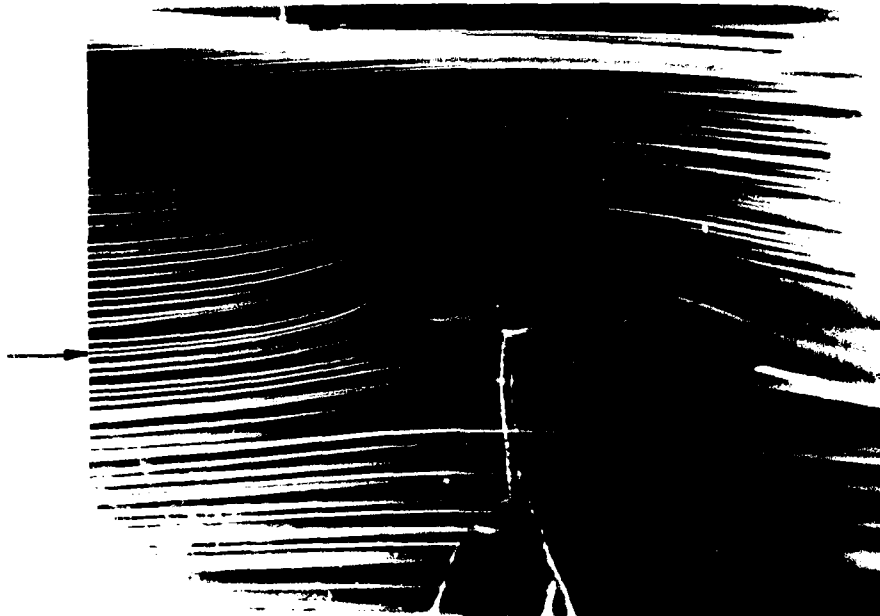


Figure 20 AOA = 10°, Ejector ON

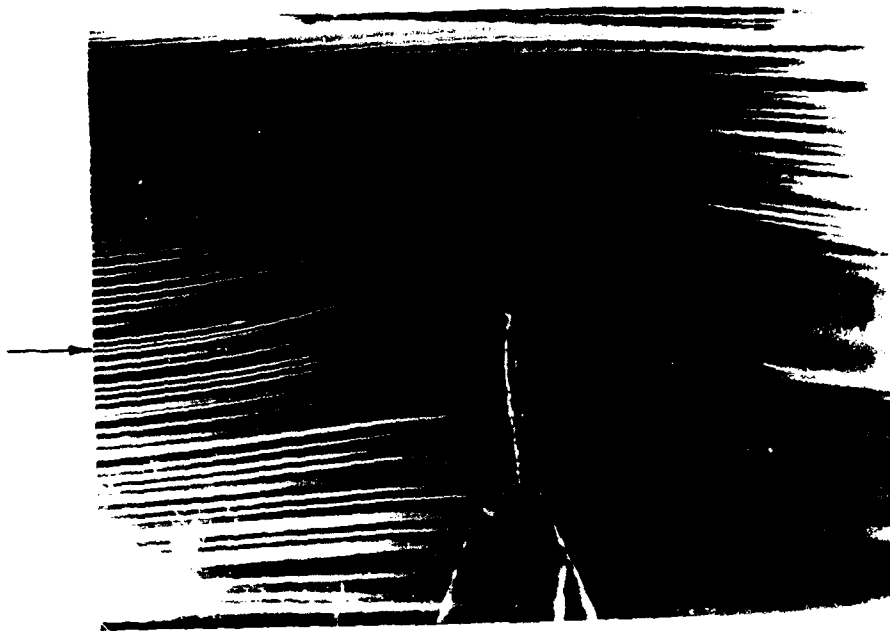


Figure 21 AOA = 15° , Ejector OFF

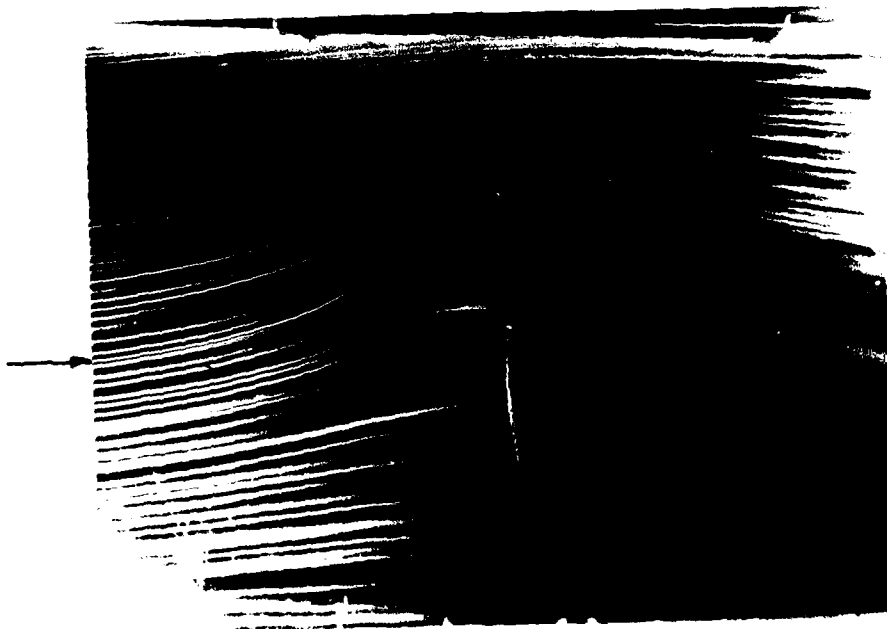


Figure 22 AOA = 15° , Ejector ON



Figure 23 ACA = 20^o , Ejector OFF



Figure 24 AOA = 20^o , Ejector ON



Figure 25 AOA = 25° , Ejector OFF



Figure 26 AOA = 25° , Ejector ON

In summary, the visual effects of ejector operation are:

1. The appearance of an increase in pressure differential due to the upward movement of the streak lines.
2. The appearance of an increase in effective angle of attack and increased circulation as evidenced by movement of the leading edge stagnation point.
3. The appearance of a more well defined, less turbulent wake region above the aft airfoil.
4. The evidence of increased entrainment due to the ejector's employment.

Based on an analysis of the flow visualization photographs, locations for obtaining LDV data were selected. The LDV results for $AOA = 15^\circ$ and $AOA = 0^\circ$ are presented below.

Laser Velocimeter

$AOA = 15^\circ$:

The first LDV results presented are for an angle of attack of 15° with the ejector duct open. Figure 28 shows the survey locations, lettered A through M, which were conducted. Approximately 130 points were evaluated both with and without blowing. Mean velocity profiles, U_{mx} vs. z , and turbulence intensity profiles, ETA vs. z , are presented in Figures 29 through 54. Please note carefully the z -ordinate for each profile: z' indicates a displacement from the chord line, while z indicates a displacement from the surface of the airfoil.

The first survey presented, Survey A (Figure 29), is

that of the free stream conducted at a point 0.85C ahead of the airfoil's leading edge. The mean velocities were sufficiently close to the pitot tube established tunnel speed of 8 m/sec to give confidence in the pitot tube as a means of setting tunnel speed. Also, to within the accuracy and ability of the LDV, the smoke tunnel free stream exhibits zero turbulence intensity (Figure 42).

In reviewing the results of the $AOA = 15^\circ$ Surveys B through M, several observations can be made. First, the mean velocities with ejector operation were consistently greater on the upper surface and slower on the lower surface. Thus a greater pressure differential exists between the suction and pressure sides of the overall airfoil. In addition, the higher velocity fluid on the upper surface is better able to overcome the adverse pressure gradient and thus delay separation. Secondly, with ejector employment there was an increase in turbulence near the airfoil surface, coupled with a more rapid decrease in turbulence back to the free stream value as the control volume was displaced from the surface. The further aft of the leading edge the more this trend intensified as evidenced by noting the turbulence intensity profiles of Surveys F, I, and K (Figures 47, 50, and 52). Also, the trend is evident on both the upper and lower surfaces, as Surveys G and L (Figures 48 and 53) will illustrate. This increase in turbulence near the surface with ejector operation should further energize the fluid and delay separation. The observation of a more rapid decrease in turbulence intensity to the

free stream value with ejector operation at Surveys K and M (Figures 52 and 54) tends to confirm the flow visualization interpretation of a smaller, more well defined wake region above the aft airfoil. Although a more turbulent fluid layer suffers more viscous drag, a delay in separation coupled with a smaller wake region should improve overall performance. Also, note the effect of the converging ejector duct on the flow near the surface of the aft airfoil in Surveys K and M. The higher than free stream velocities indicates greater energy flow on the aft airfoil surface. The effect is enhanced by the additional momentum flux of the ejector. A third observation at this AOA concerns Survey J (Figures 38 and 51) which was conducted in the ejector duct downstream of the ejector face. Without the ejector an increase in mean velocity above free stream is noted due to the constricting duct and flow over the aft airfoil's surface. However, with the addition of the ejector flux a larger mean velocity is obtained. Additionally, the turbulence level is greater with ejector operation. This indicates an increased mixing of the primary ejector fluid and the secondary entrained fluid. Thus higher energy flow exits the duct and energizes the aft airfoil's upper surface boundary layer.

Another interesting result of ejector employment is illustrated by Survey H (Figure 36). This survey was conducted approximately 0.80 cm aft of the ejector face and shows the entrainment of secondary fluid into the ejector duct region by the ejector. The velocities with ejector operation are larger in the areas above and below the ejector. Also, it

can be seen that without the ejector on, near stagnation conditions are present at the ejector face. With the ejector on, however, the established ejector velocity of approximately 16.0 m/sec is attained. Note also with ejector operation in Figure 49 the increase in turbulence within the duct and the characteristic more rapid decrease in turbulence as the control volume was moved away from the airfoil.

A final important effect of ejector operation documented at $AOA = 15^\circ$ was the apparent downward or counterclockwise movement of the leading edge stagnation point. In an attempt to quantitatively confirm this movement, Surveys D and E were taken (Figures 32 and 33). Surveys D and E are located 1 cm and 1.4 cm, respectively, behind the leading edge of the model. Thus Survey E is located further down the airfoil's surface, i.e., in a counterclockwise direction. As previously observed in the flow visualization photographs a trend of stagnation point movement in a counterclockwise direction is noted. Both surveys indicate a definite decrease in mean velocity with ejector operation. Near the surface at Survey D the velocity without blowing is near zero, indicating close proximity to the stagnation point. The mean velocity near the surface with ejector operation, however, is negative. Looking at Survey E the velocity near the surface with blowing is still negative and thus has not achieved stagnation, while the velocity without blowing has accelerated past the stagnation point to a positive value. This can best be visualized as in Figure 27. At Survey D the velocity without blowing is nearly zero, whereas,

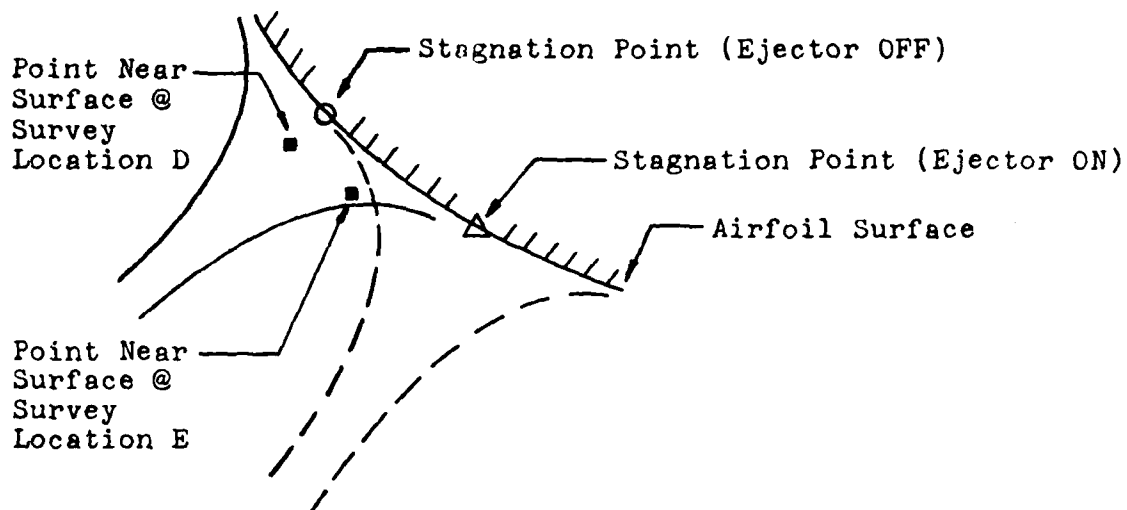


Figure 27 Leading Edge Stagnation Point Movement

with blowing it is negative and thus proceeding against the free stream apparently on its way to flowing over the top of the airfoil. At Survey E, however, the velocity without blowing has accelerated past its stagnation point to a small positive value on its way to flowing beneath the airfoil. The velocity with blowing is still negative but slightly slower as it accelerates (although in a negative direction) to Survey D and then over the top of the airfoil. Therefore, it can be observed that the stagnation point without blowing has apparently occurred prior to Survey E, while the stagnation point with blowing would occur slightly further down the airfoil surface from Survey E. This is a highly simplified model of the actual flow, but the trend of stagnation point movement is the important point. This trend indicates a stagnation point movement in a direction that would yield greater circulation with ejector employment.

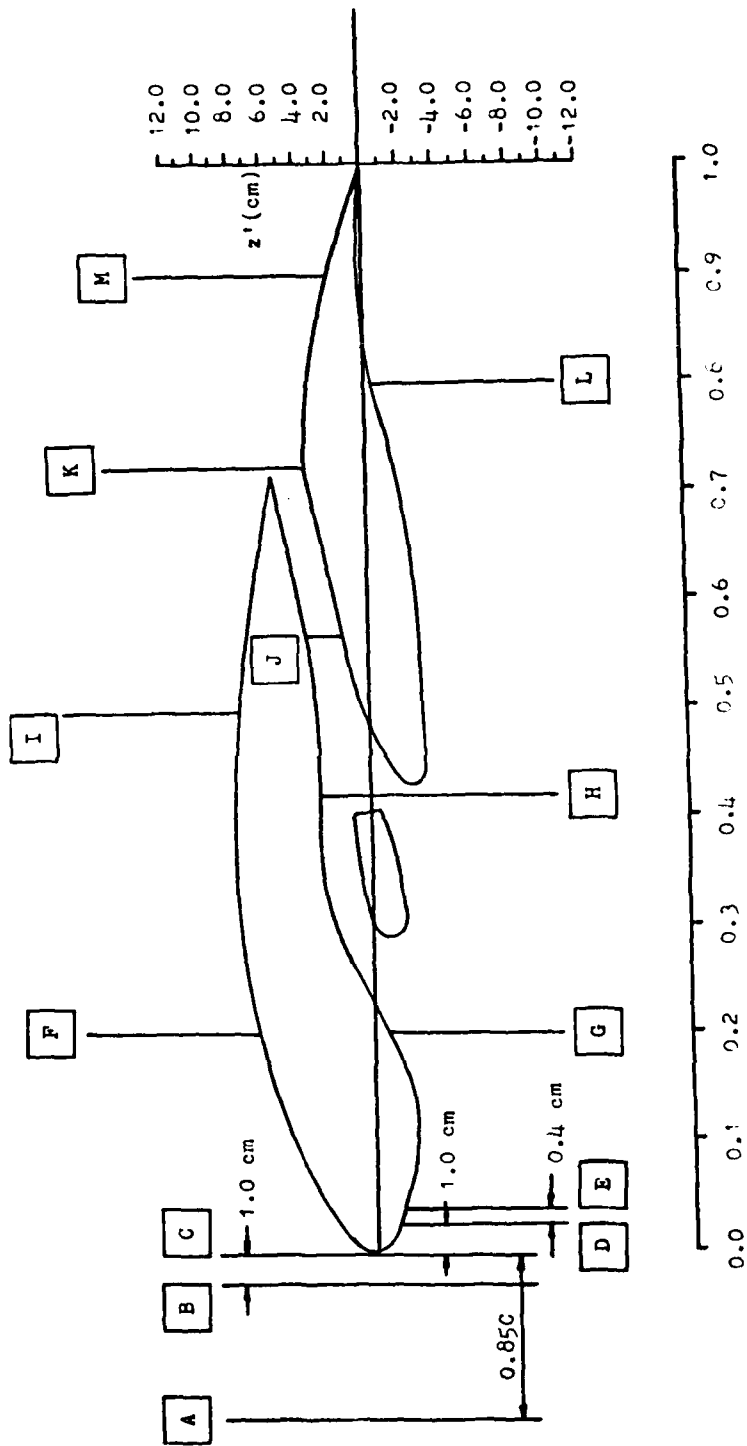


Figure 2b Survey Locations, $AOA \approx 15^\circ$

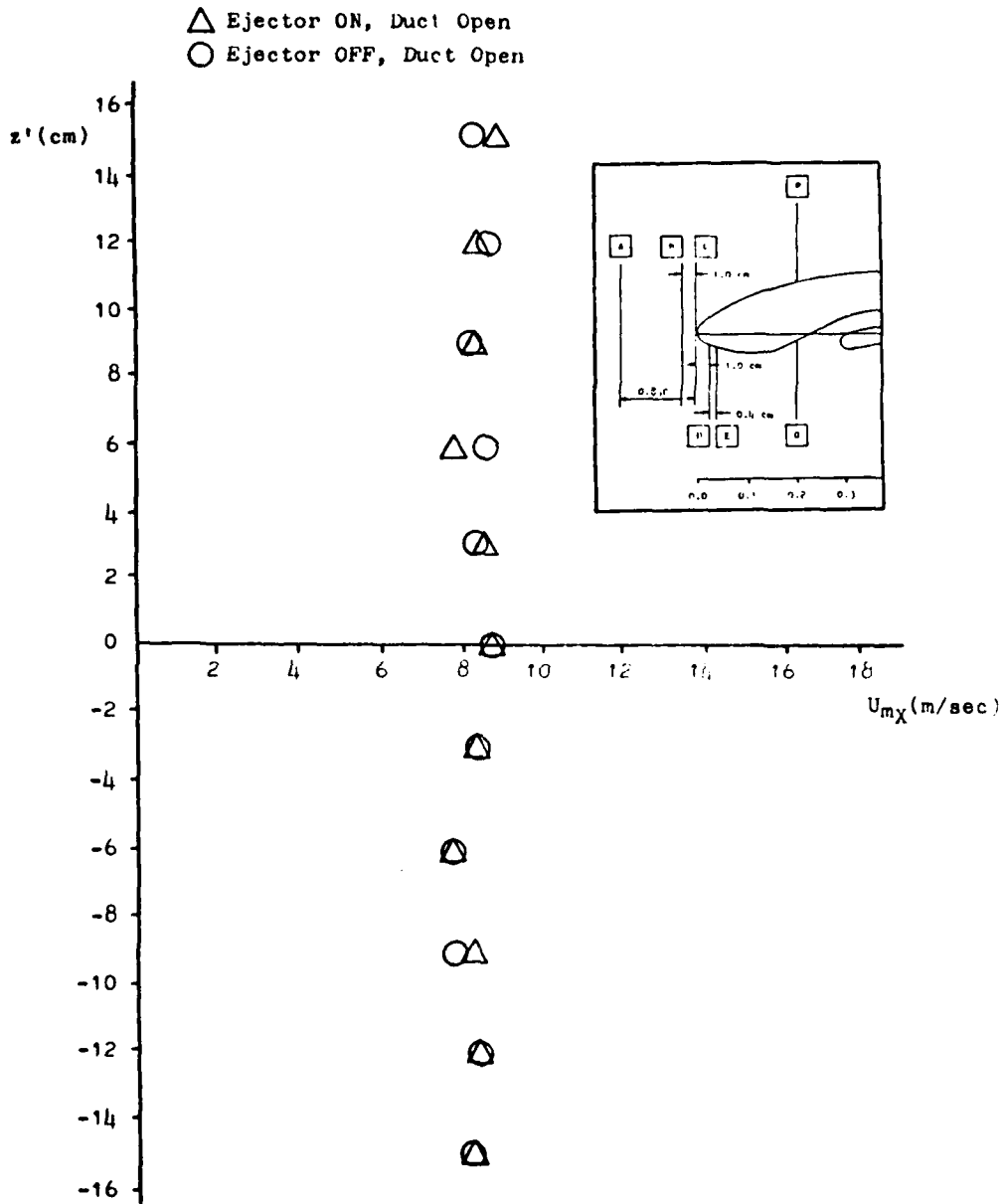


Figure 29 Mean Velocity Profile, Survey Location A, AOA = 15°

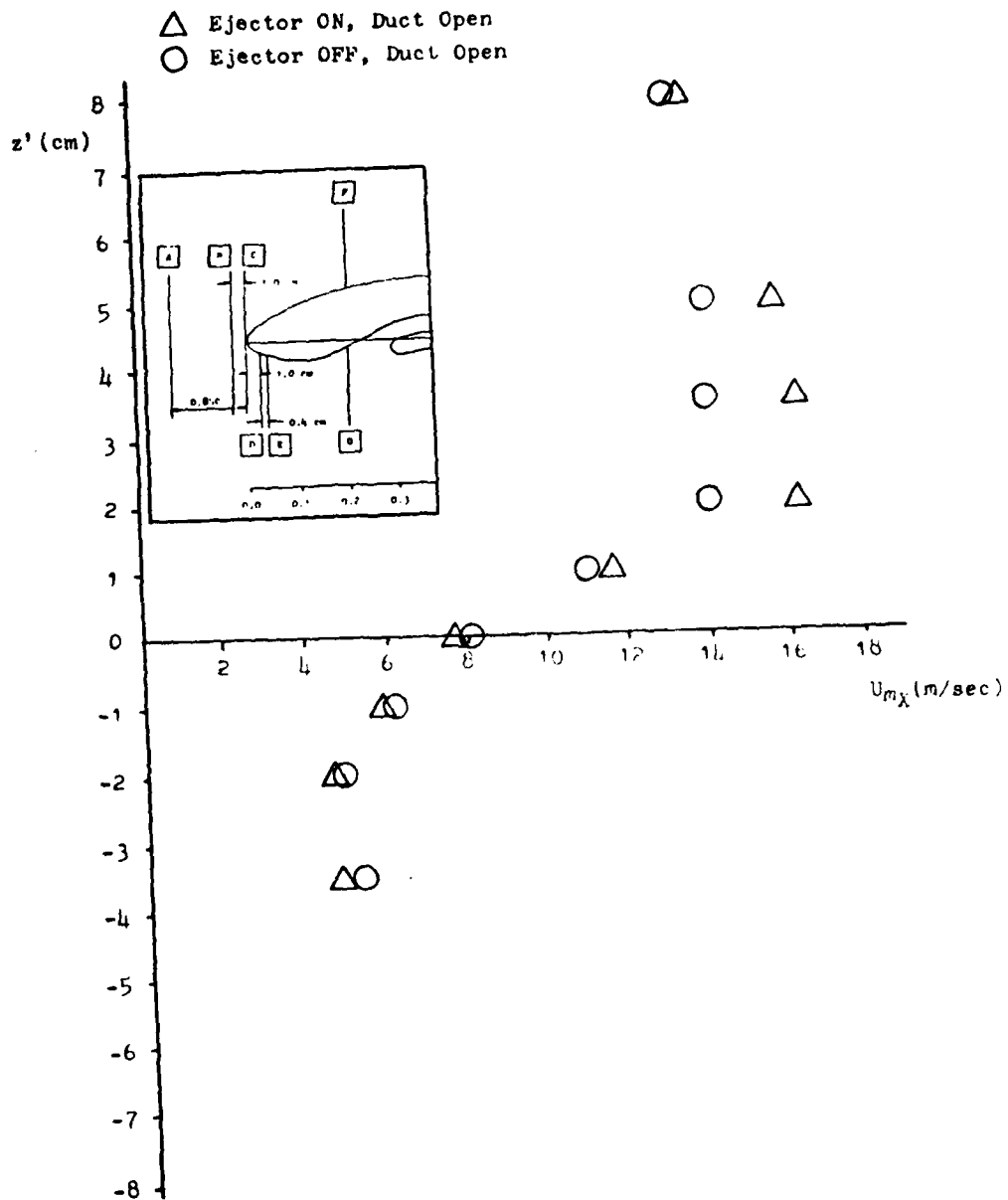


Figure 30 Mean Velocity Profile, Survey Location **B**, AOA = 15°

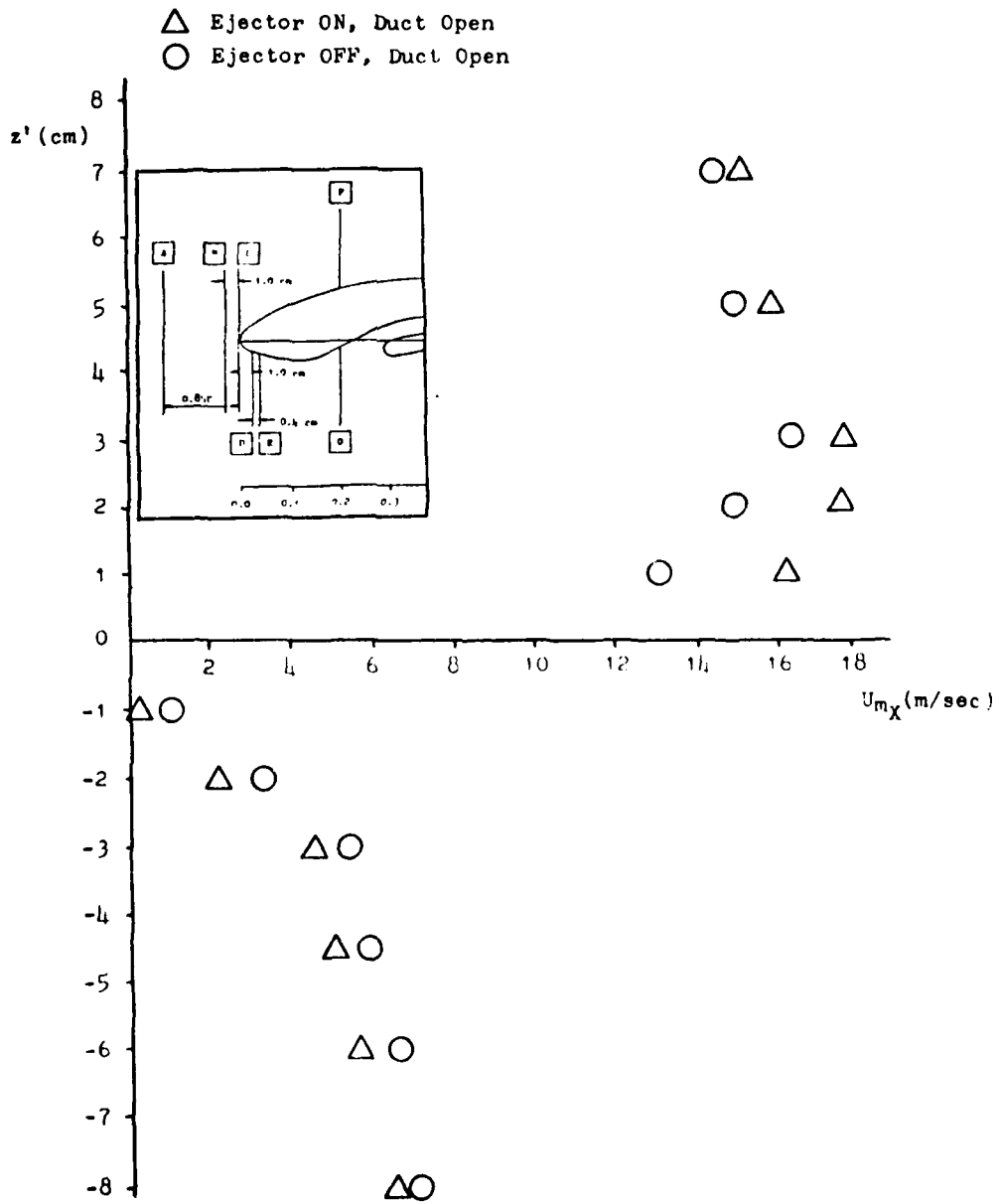


Figure 31 Mean Velocity Profile, Survey Location **C**, AOA = 15°

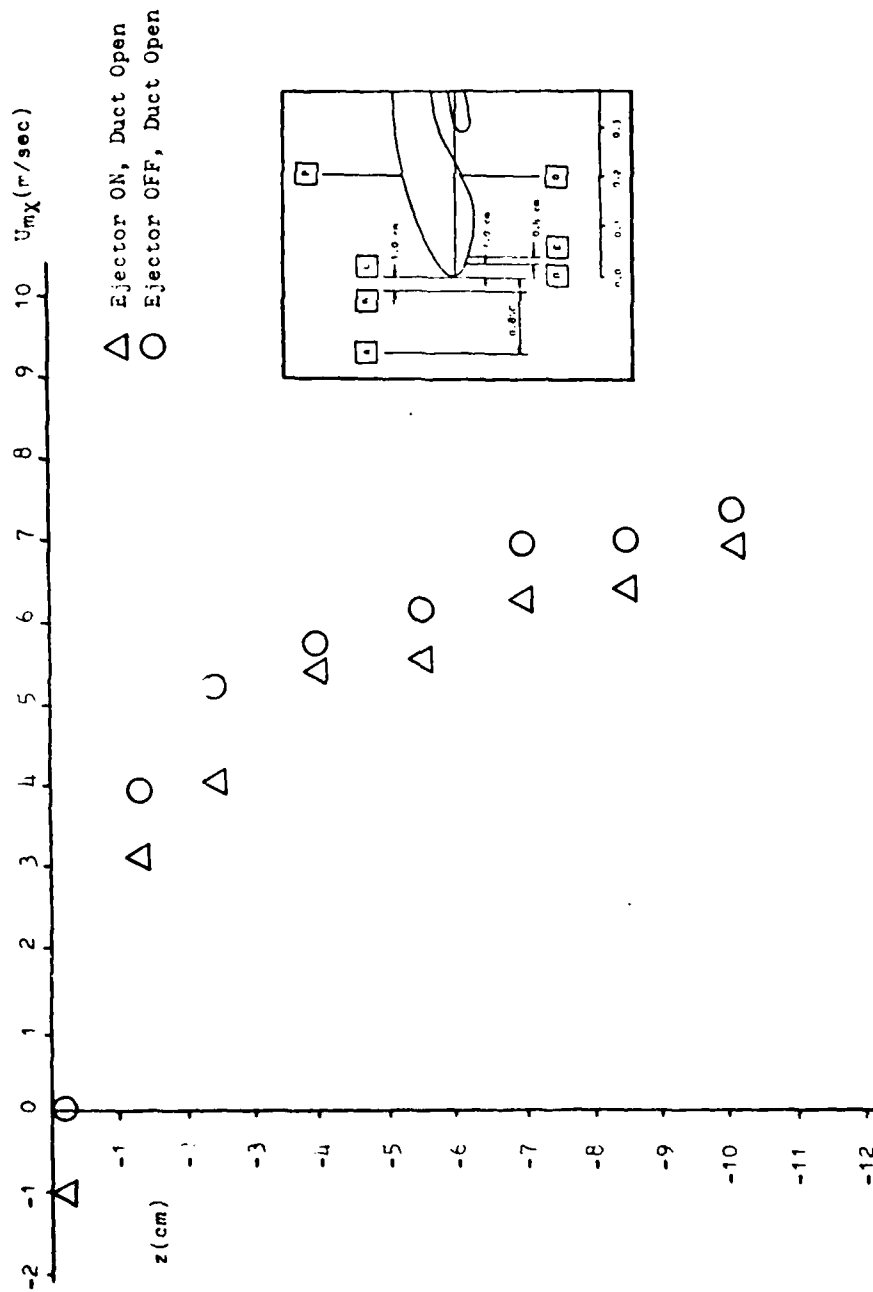


Figure 32 Mean Velocity Profile, Survey Location D, AOA = 15°

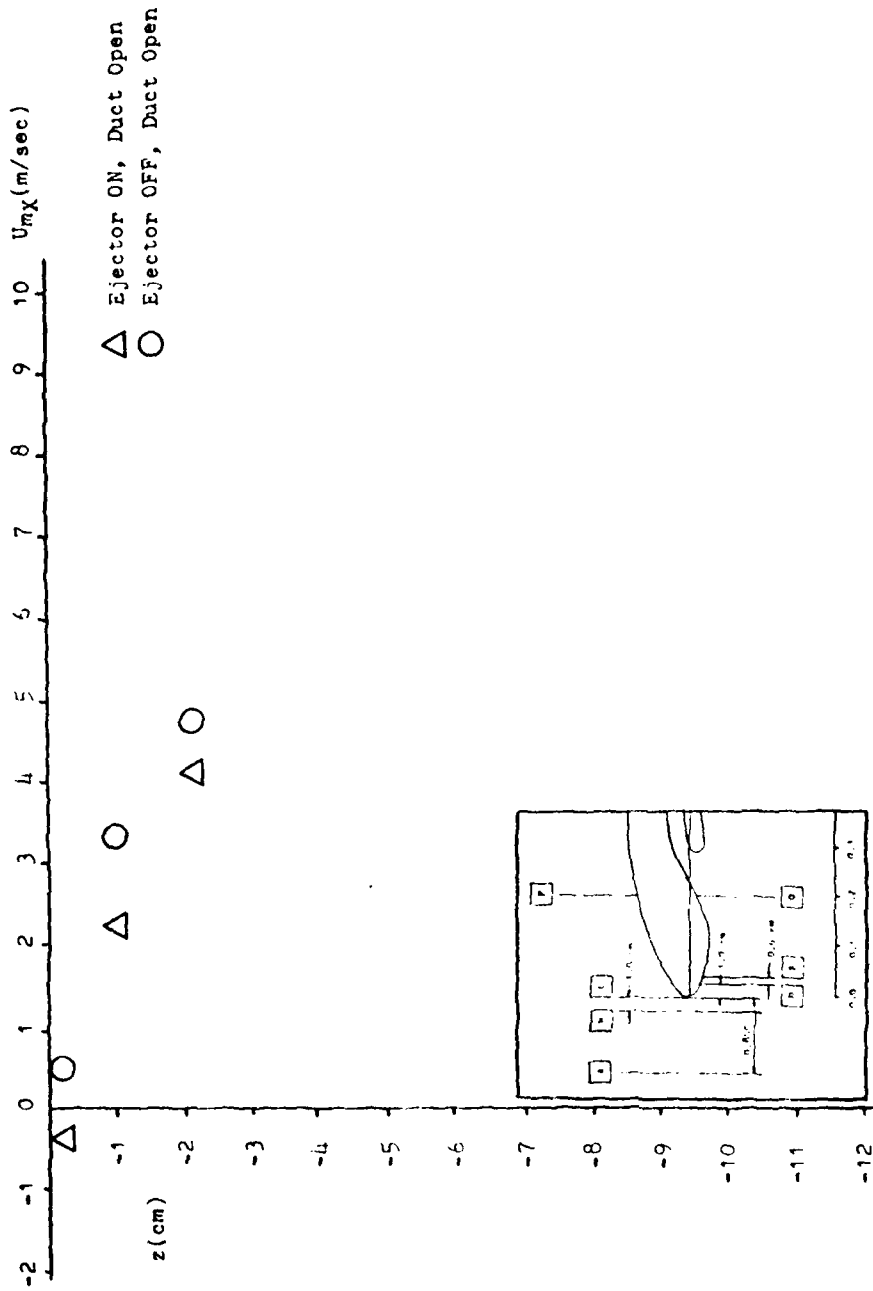


Figure 33 Mean Velocity Profile, Survey Location E, AOA = 15°

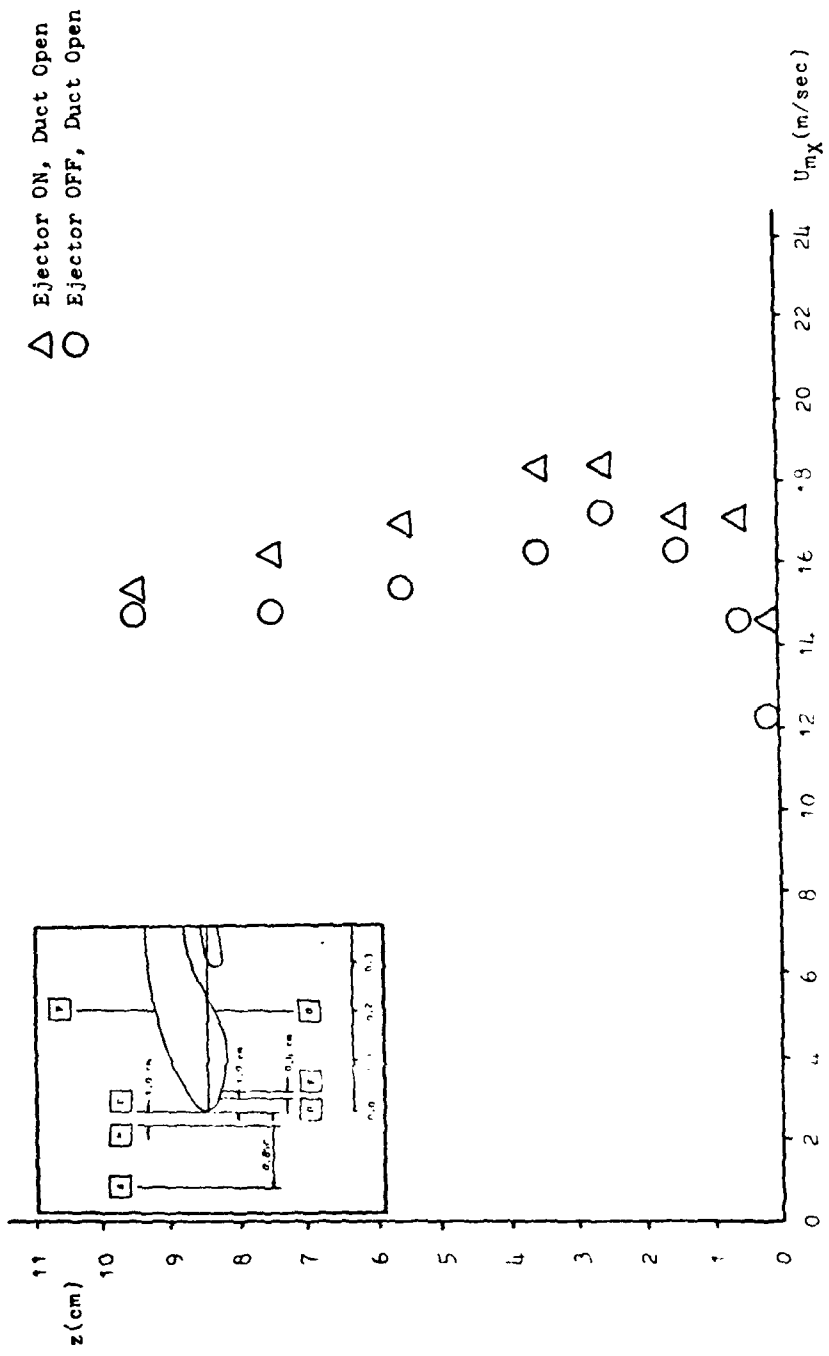


Figure 34 Mean Velocity Profile, Survey Location **F**, $AOA = 15^\circ$

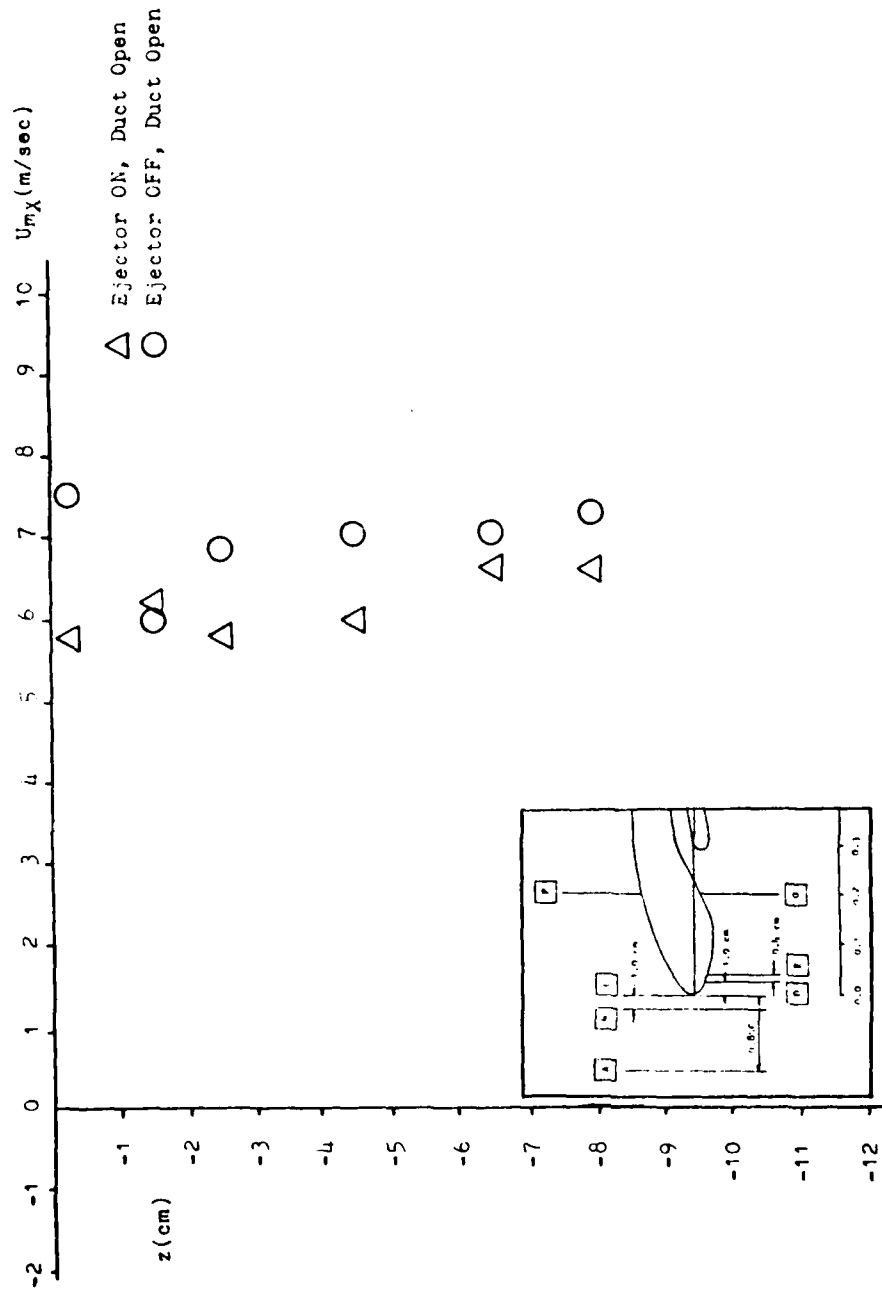


Figure 35 Mean Velocity Profile, Survey Location G , AOA = 15°

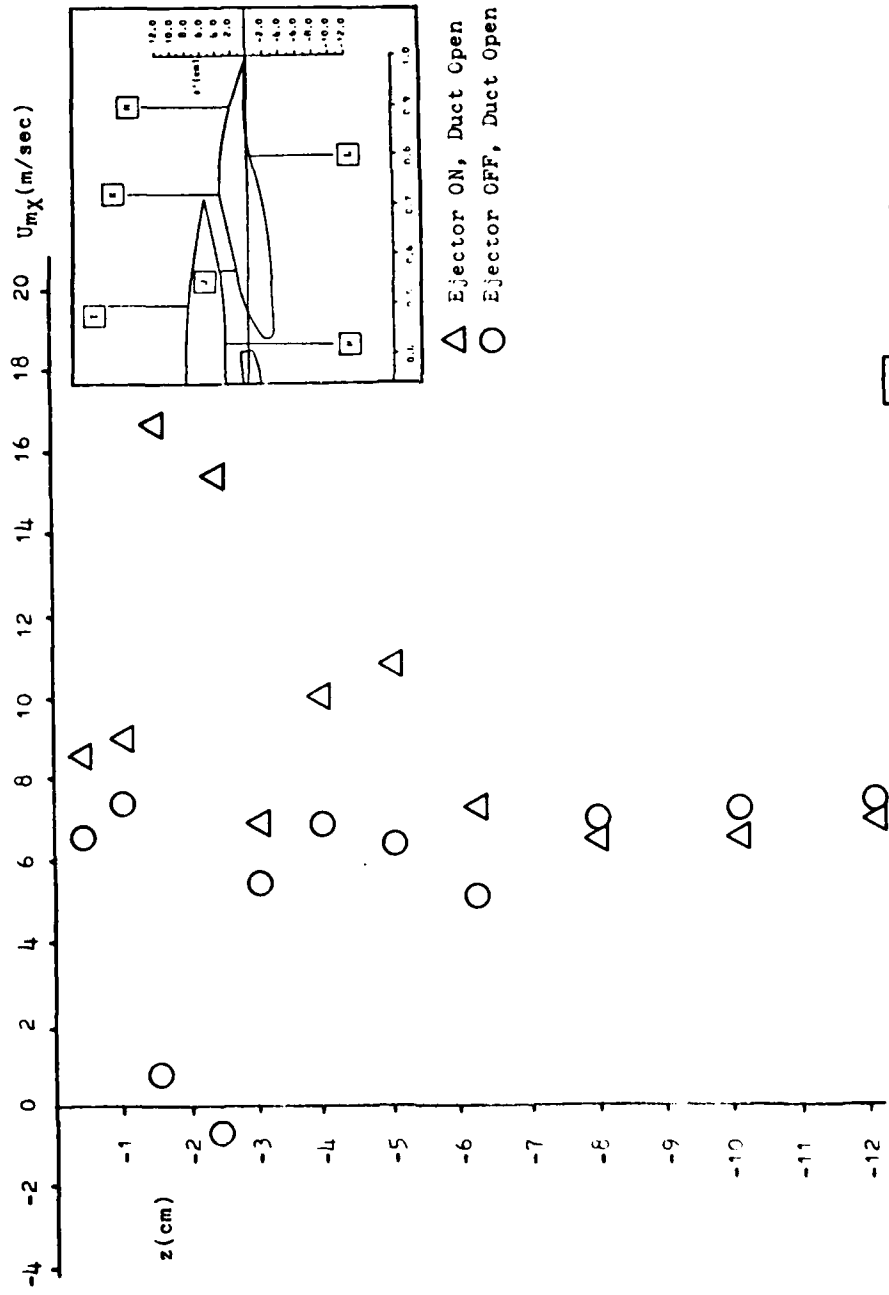


Figure 36 Mean Velocity Profile, Survey Location H, AOA = 15°

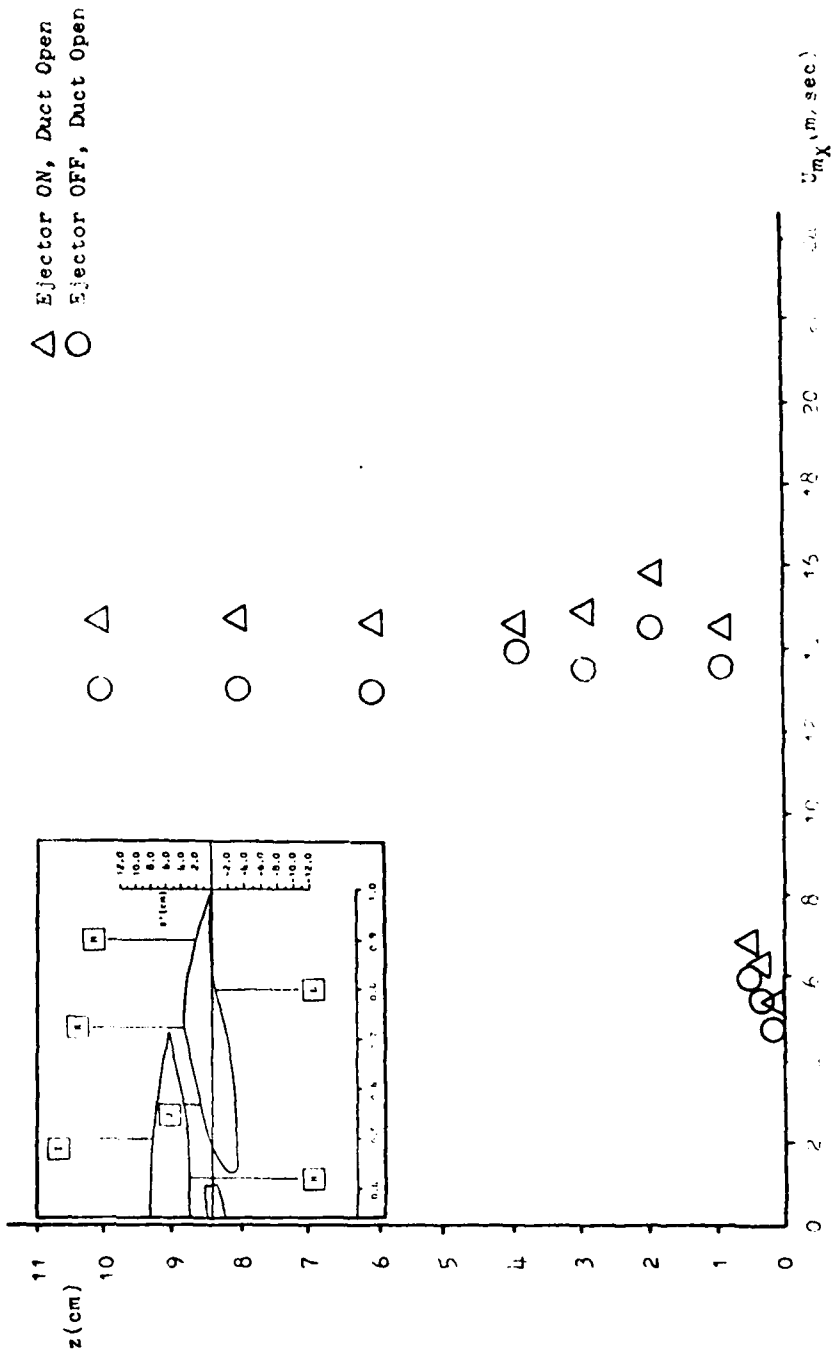


Figure 37 Mean Velocity profile. Survey Location I, $\alpha_{GA} = 15^\circ$

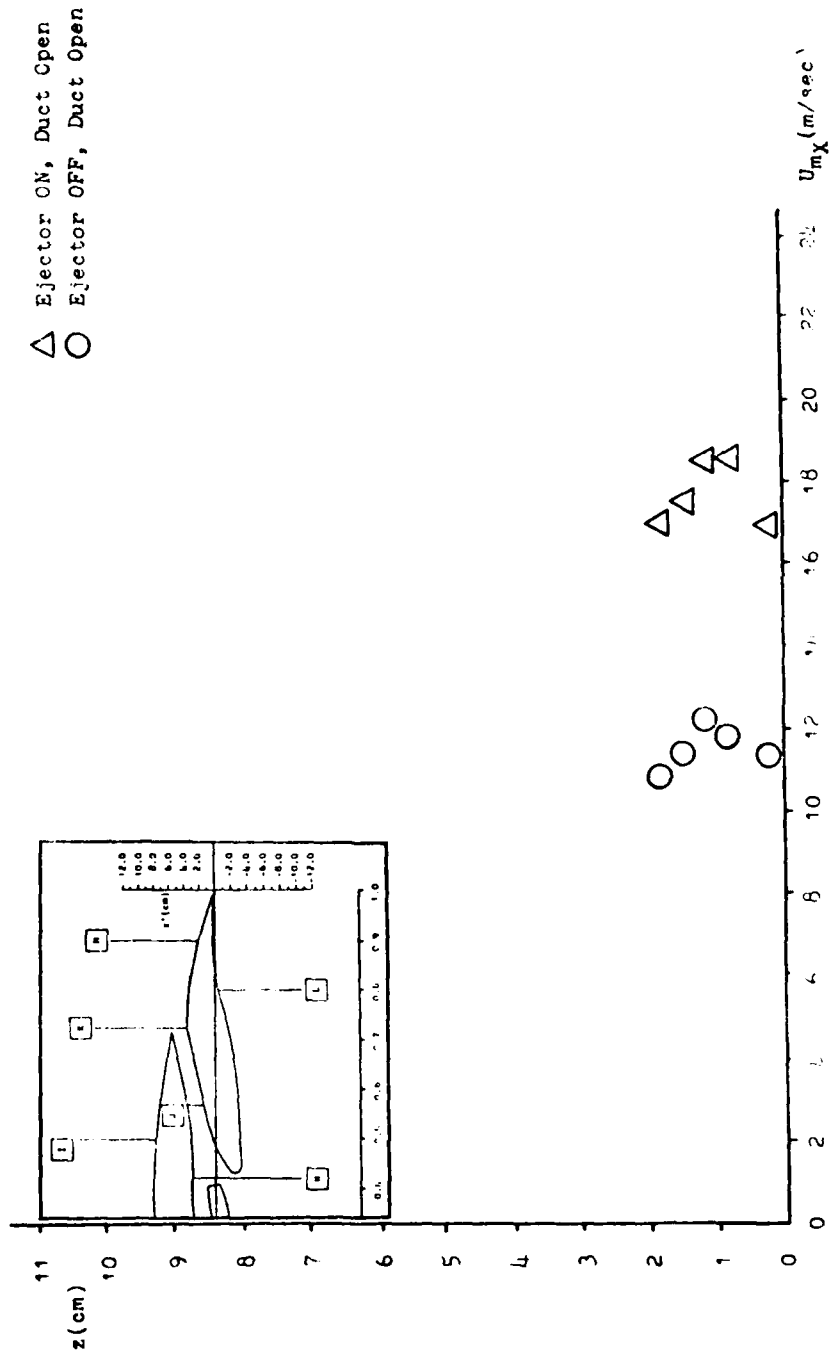


Figure 10 Mean velocity profile at burner location \square , ACP

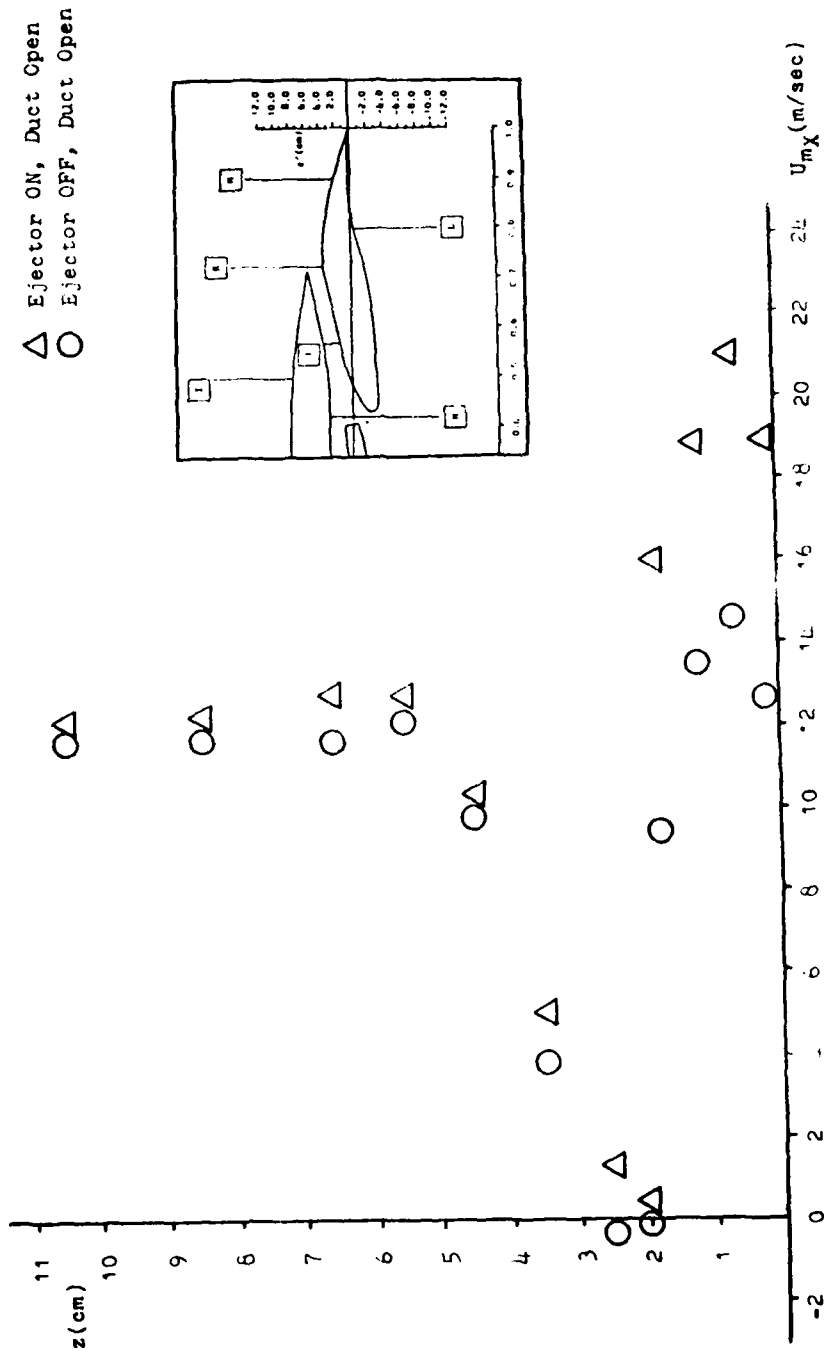


Figure 39 Mean Velocity Profile. Survey Location K , $AOA = 15^\circ$

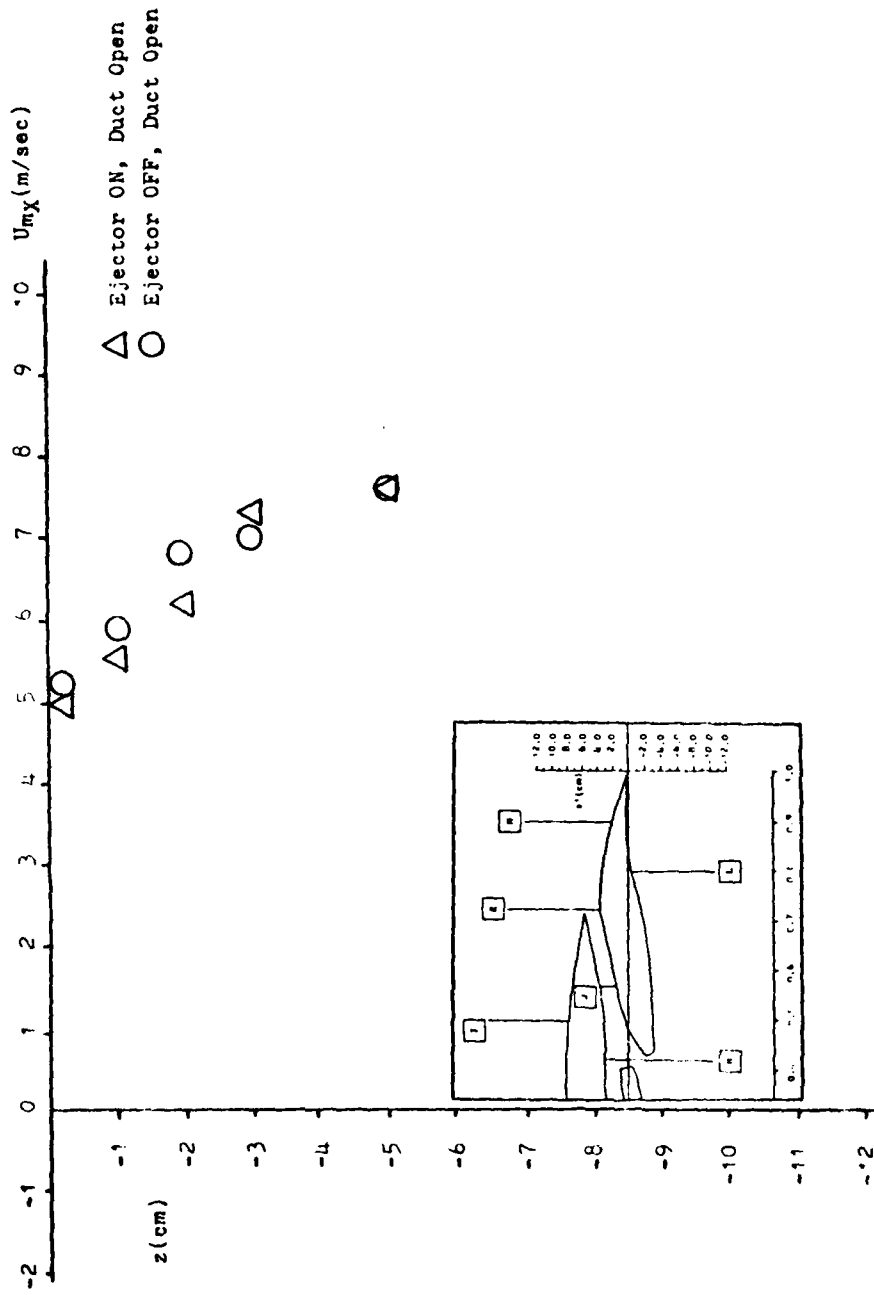
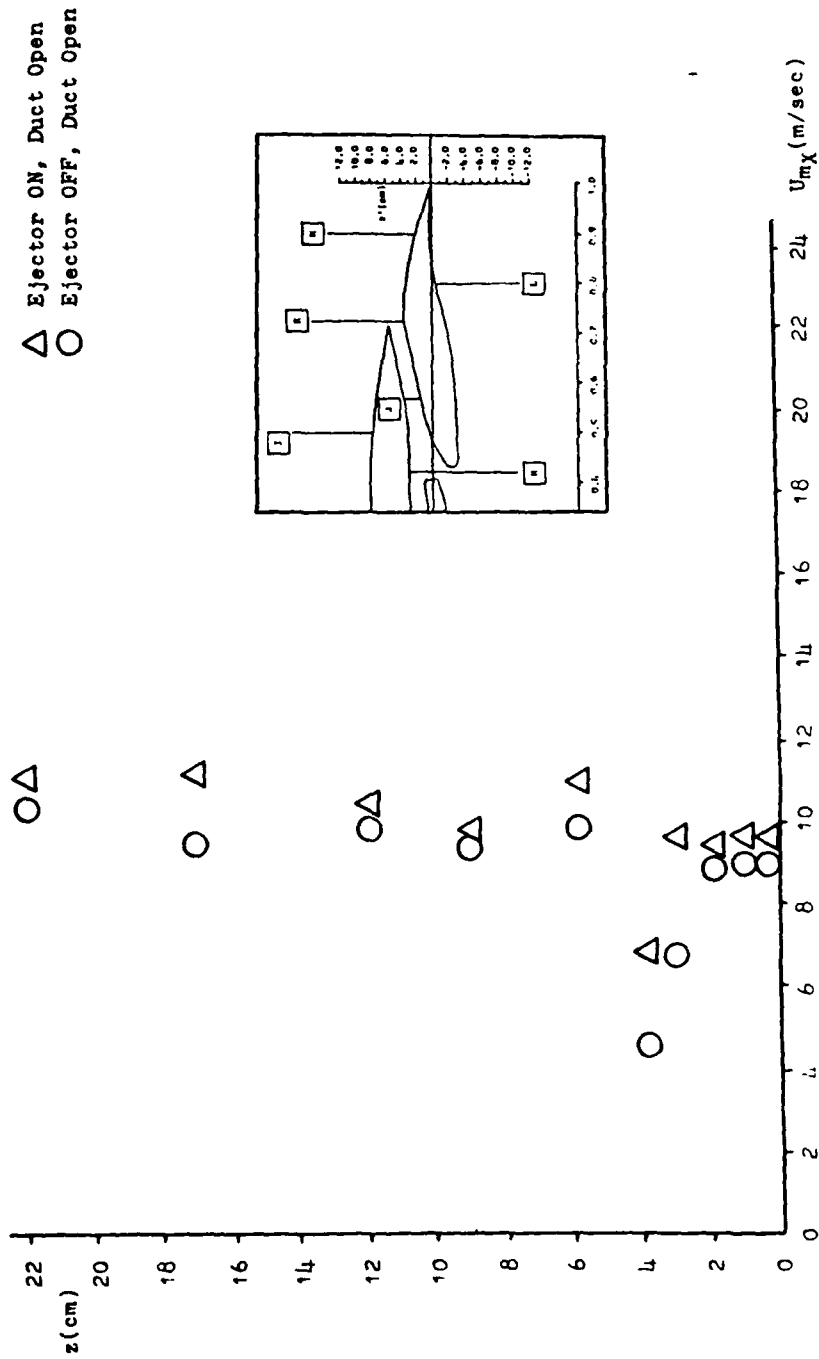


Figure 40 Mean Velocity Profile. Survey Location \square , AOA = 15°



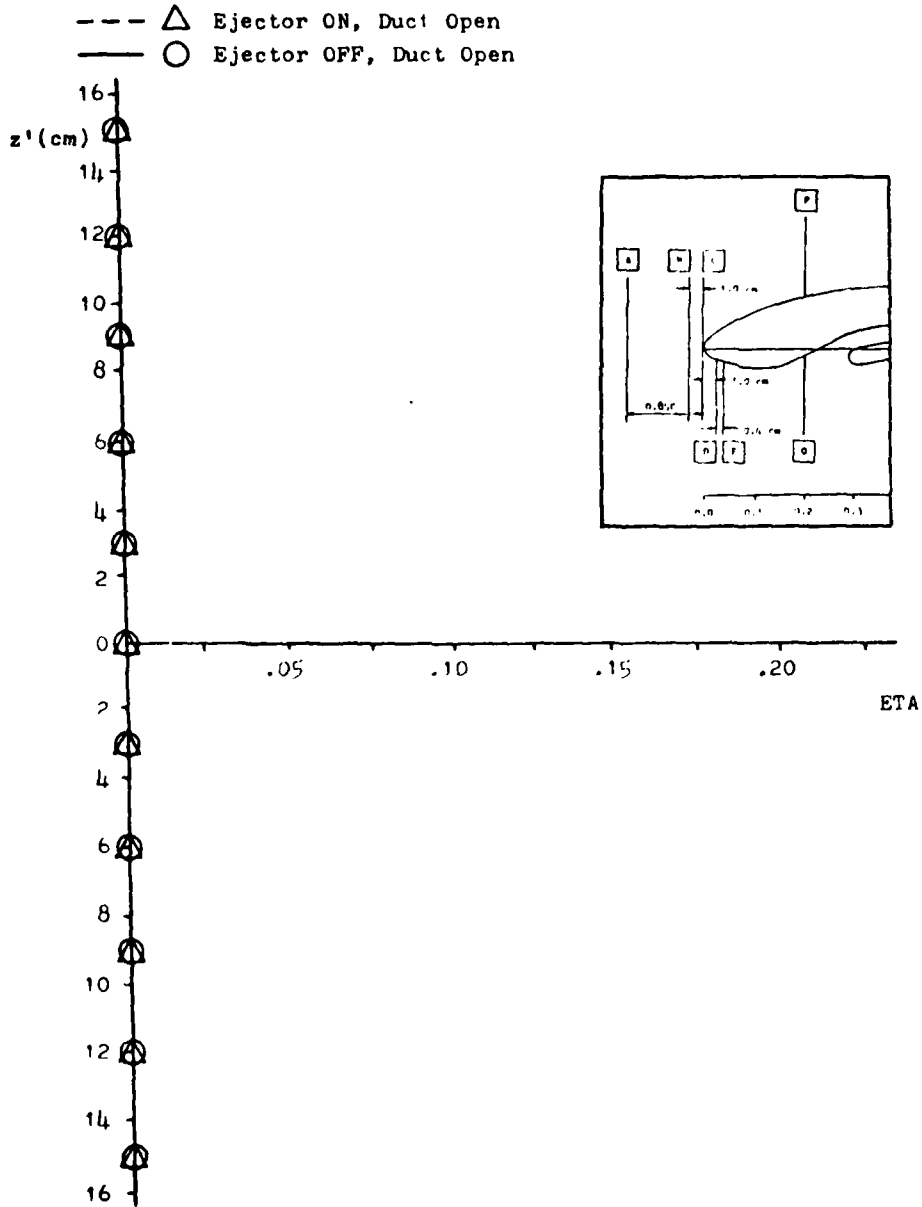


Figure 42 Turbulence Intensity Profile, Survey Location \square A , $AOA = 15^\circ$

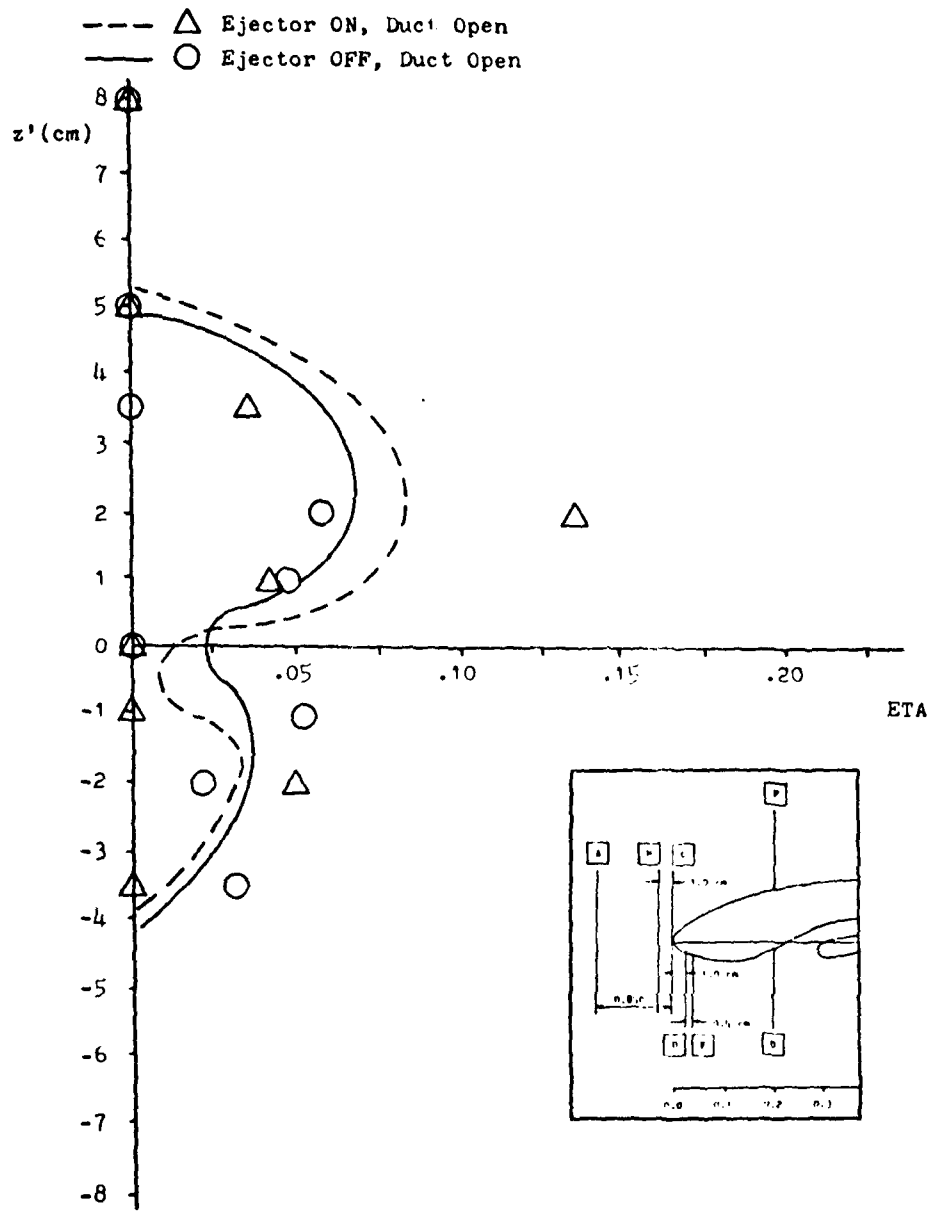


Figure 43 Turbulence Intensity Profile, Survey Location **B**, AOA = 15°

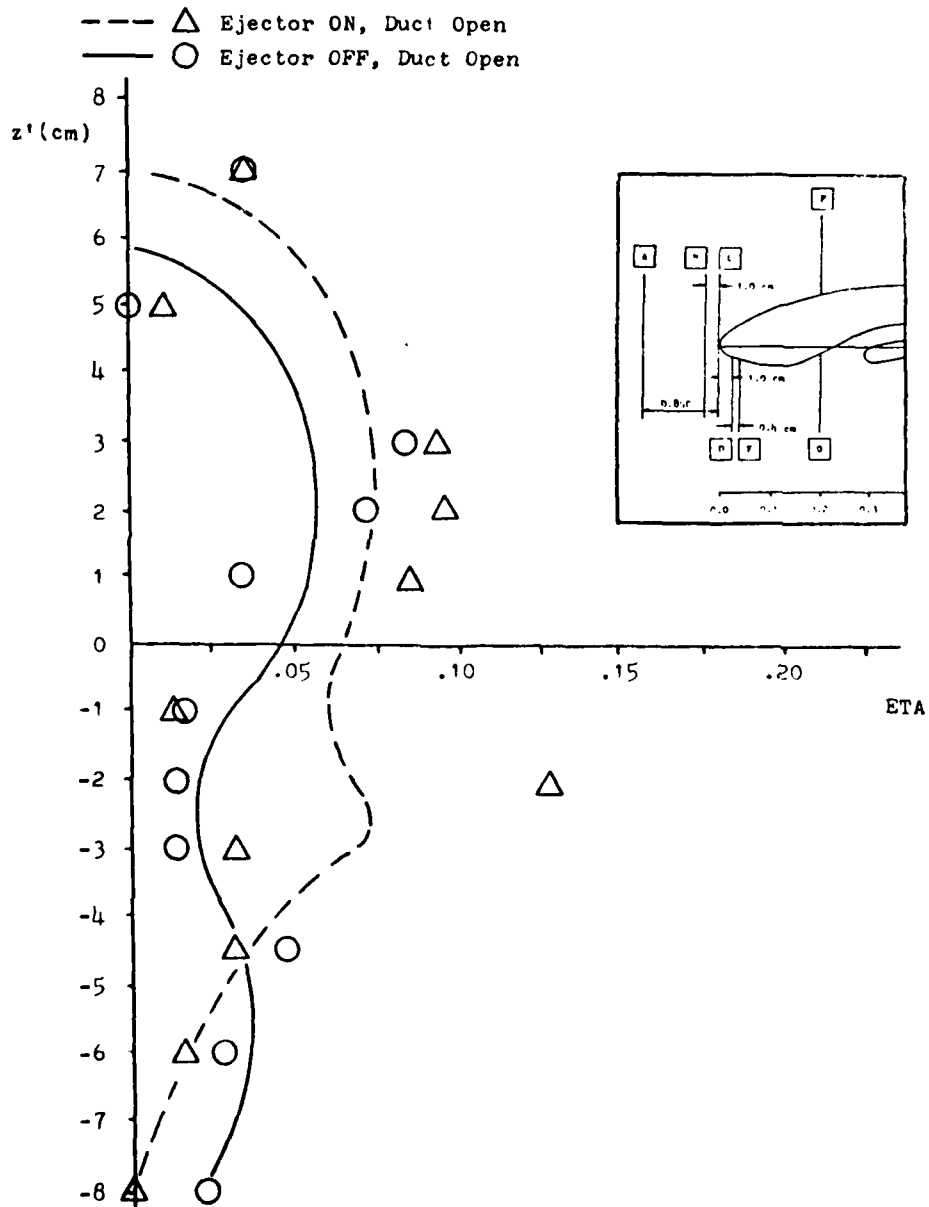


Figure 44 Turbulence Intensity Profile, Survey Location $\square C$, AOA = 15°

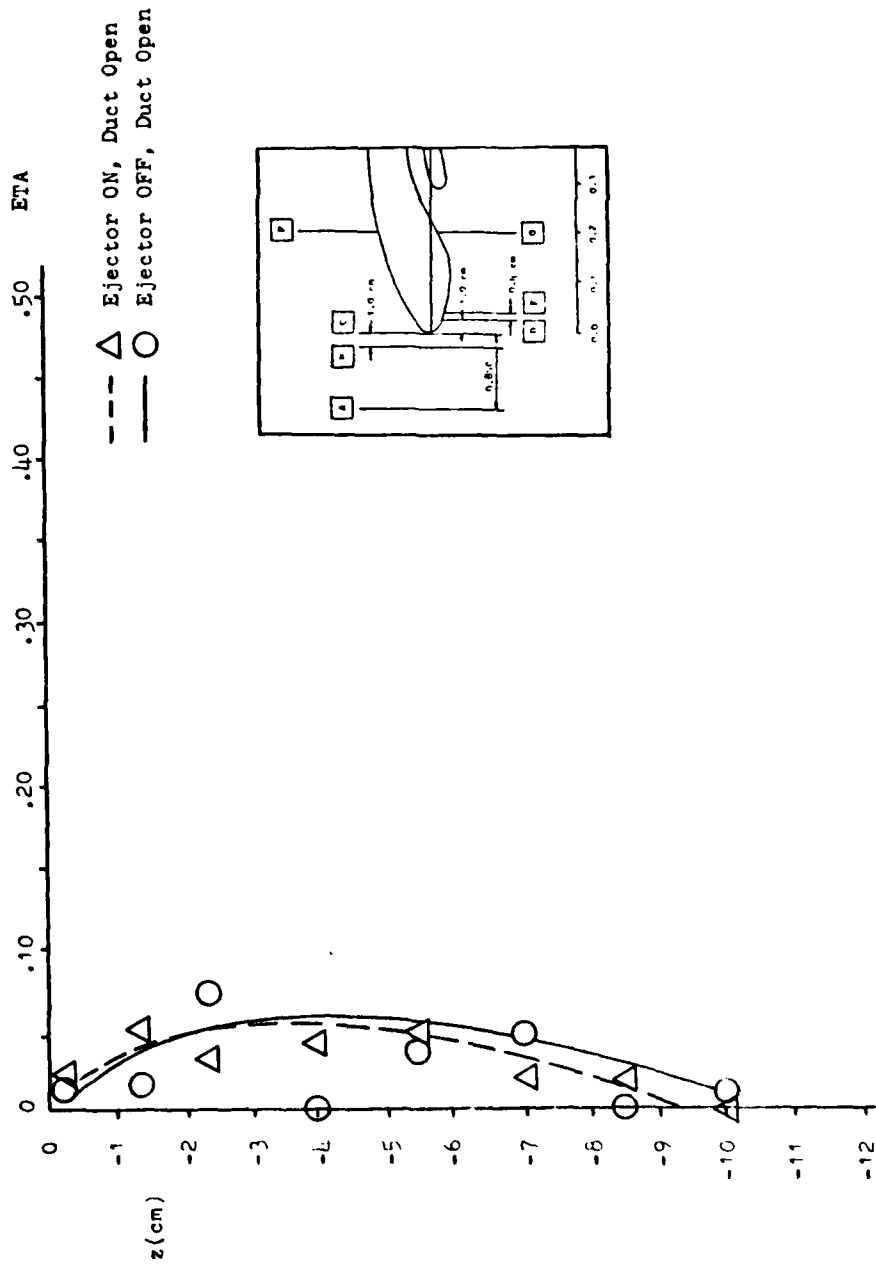


Figure 45 Turbulence Intensity Profile, Survey Location D , $AOA = 15^\circ$

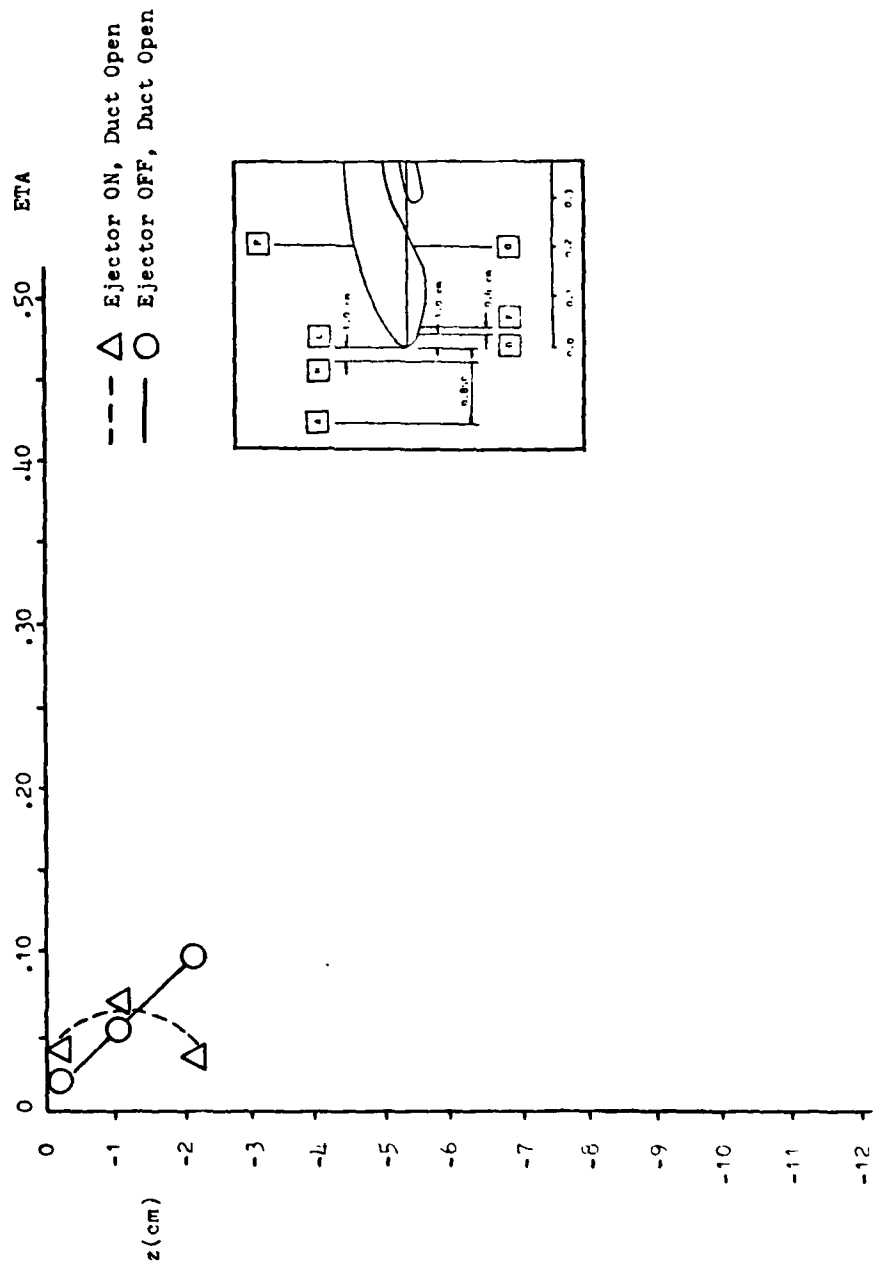


Figure 46 Turbulence Intensity Profile, Survey Location **E**, $\text{AOA} = 15^\circ$

--- Δ Ejector ON, Duct Open
 --- \circ Ejector OFF, Duct Open

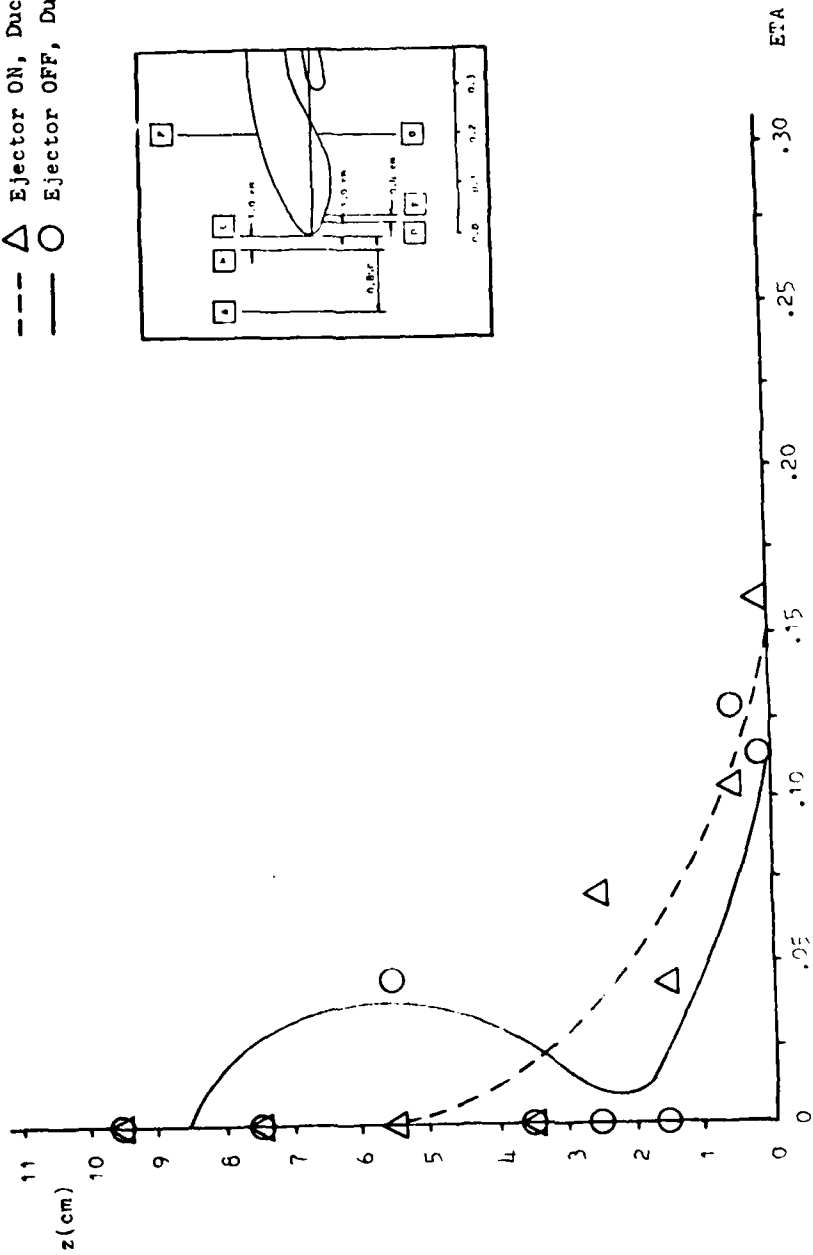


Figure 47 Turbulence Intensity Profile, Survey Location F , $AOA = 15^\circ$

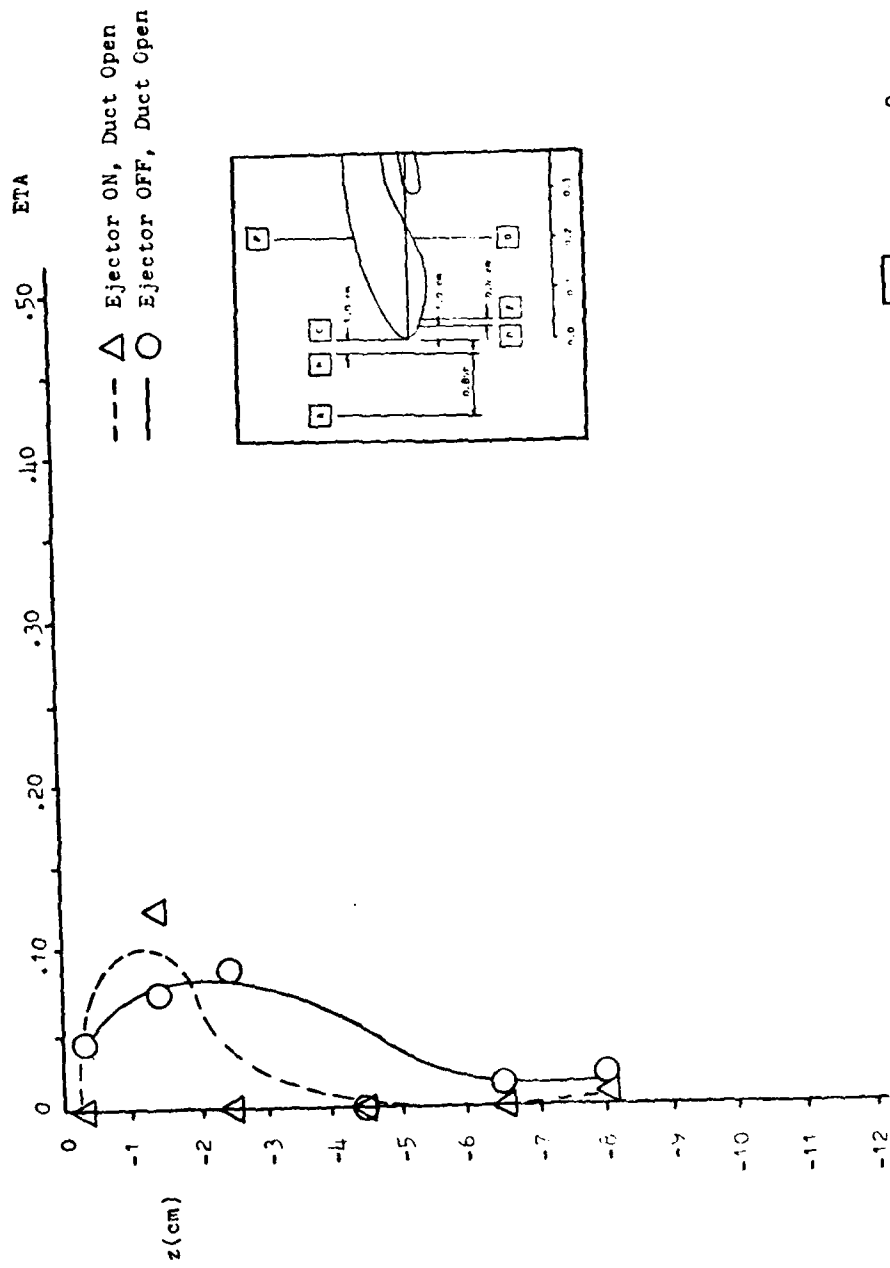


Figure 46 Turbulence Intensity Profile, Survey Location **G**, AOA = 15°

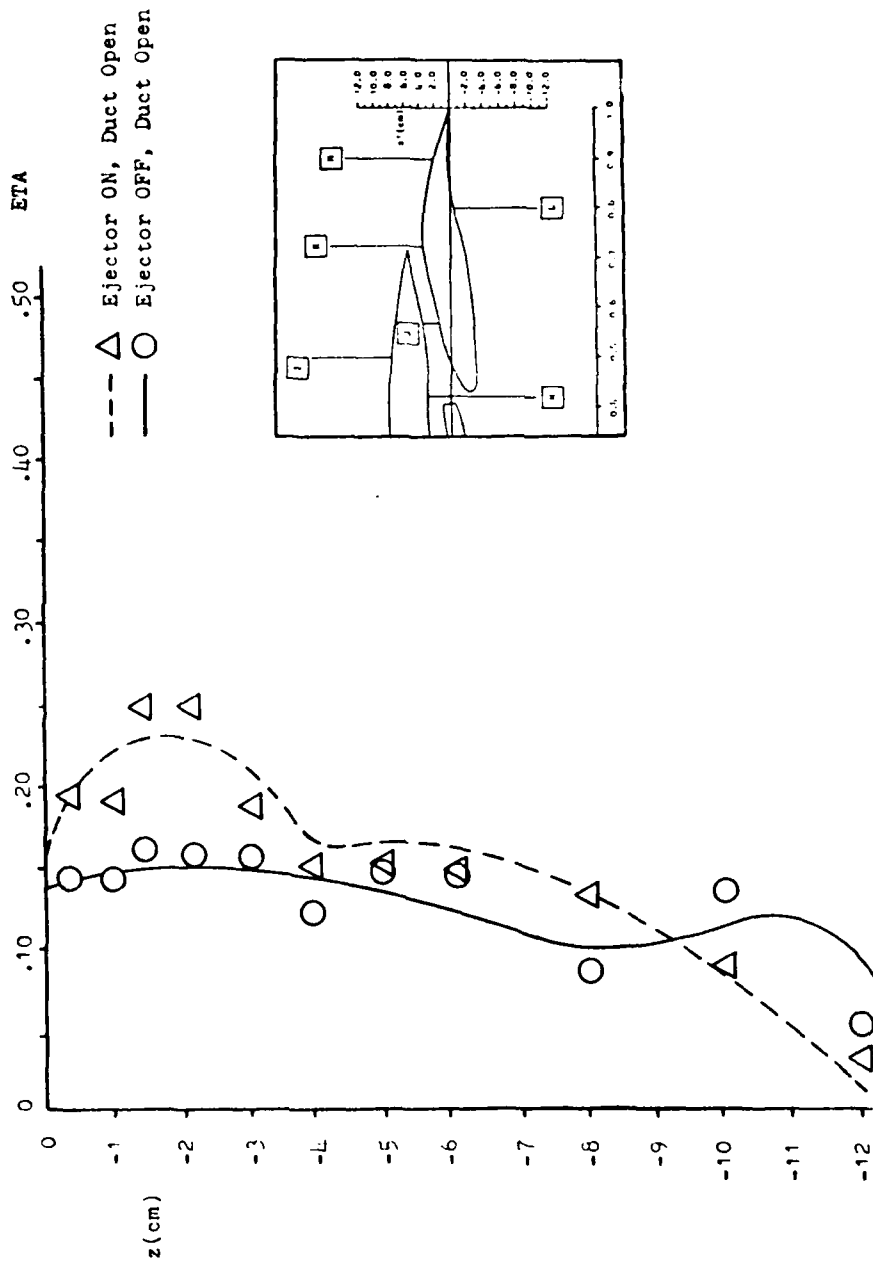


Figure 49 Turbulence Intensity Profile, Survey Location \square H, AOA = 15°

--- Δ Ejector ON, Duct Open
 --- \circ Ejector OFF, Duct Open

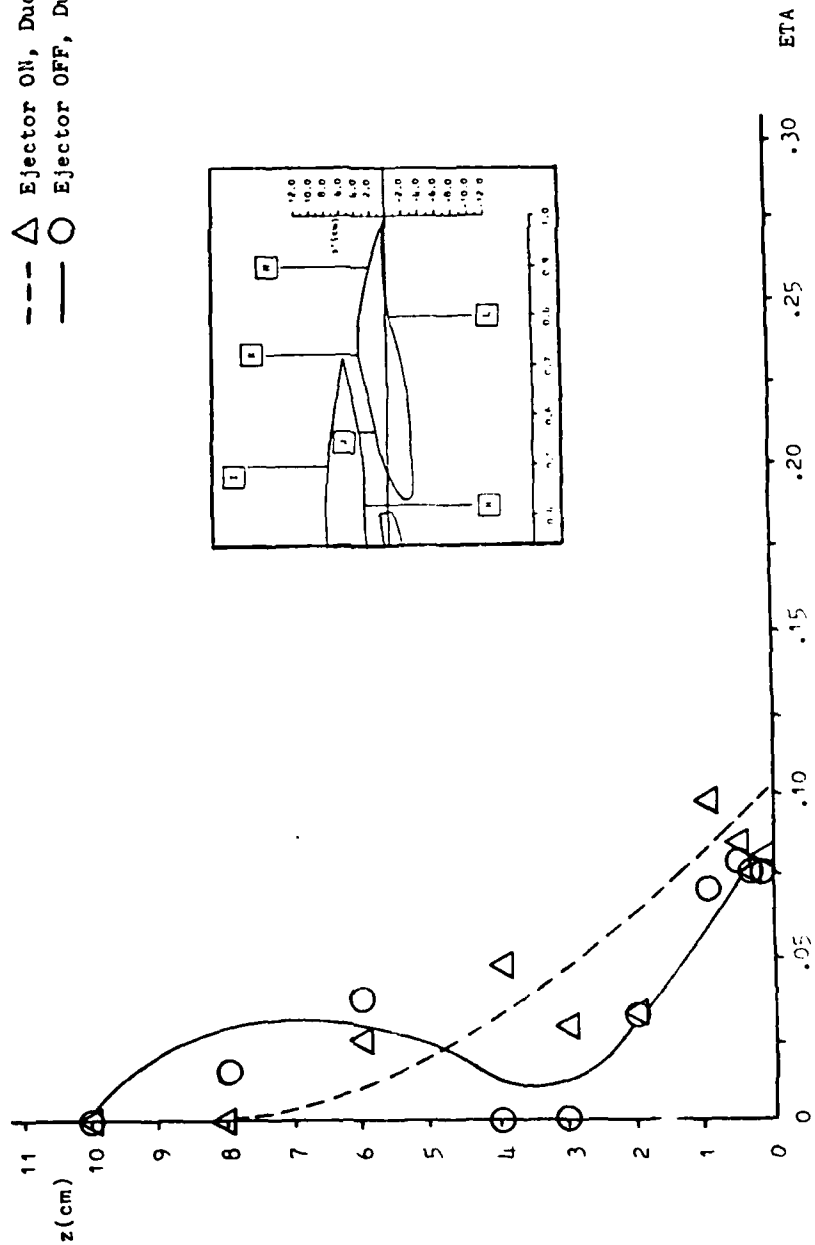


Figure 50 Turbulence Intensity Profile, Survey Location I, $\text{AOA} = 15^\circ$

--- Δ Ejector ON, Duct Open
 --- \circ Ejector OFF, Duct Open

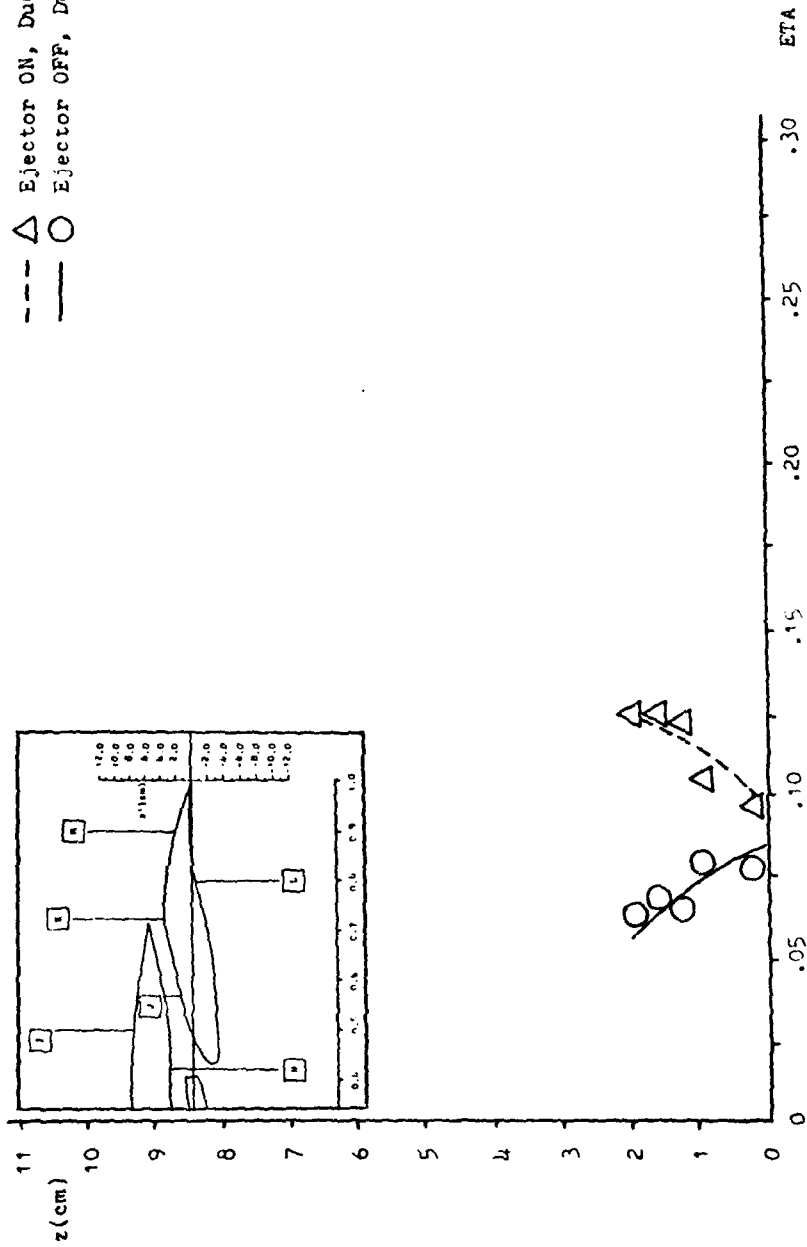


Figure 51 Turbulence Intensity Profile, Survey Location J_j , AOA = 15°

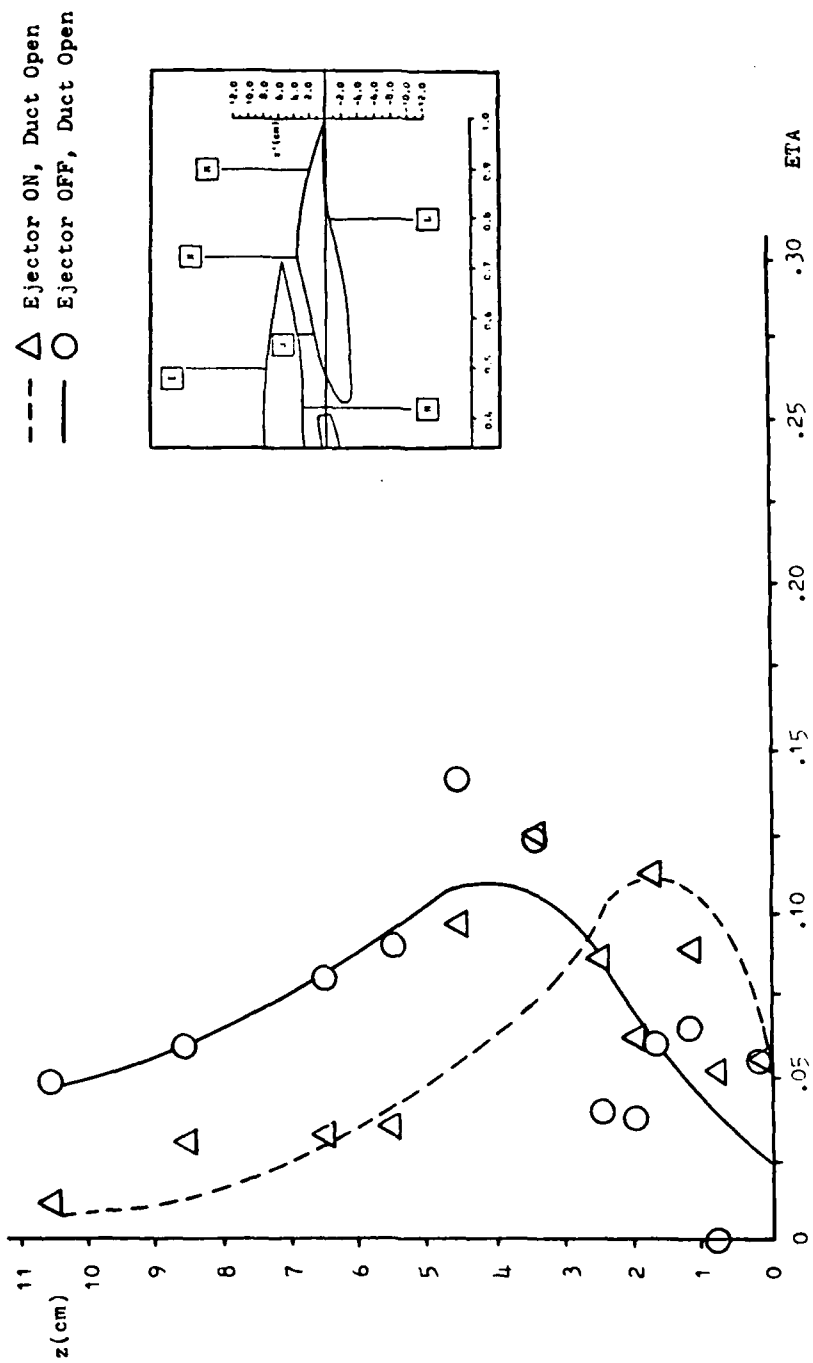


Figure 52 Turbulence Intensity Profile, Survey Location \square , AOA = 15°

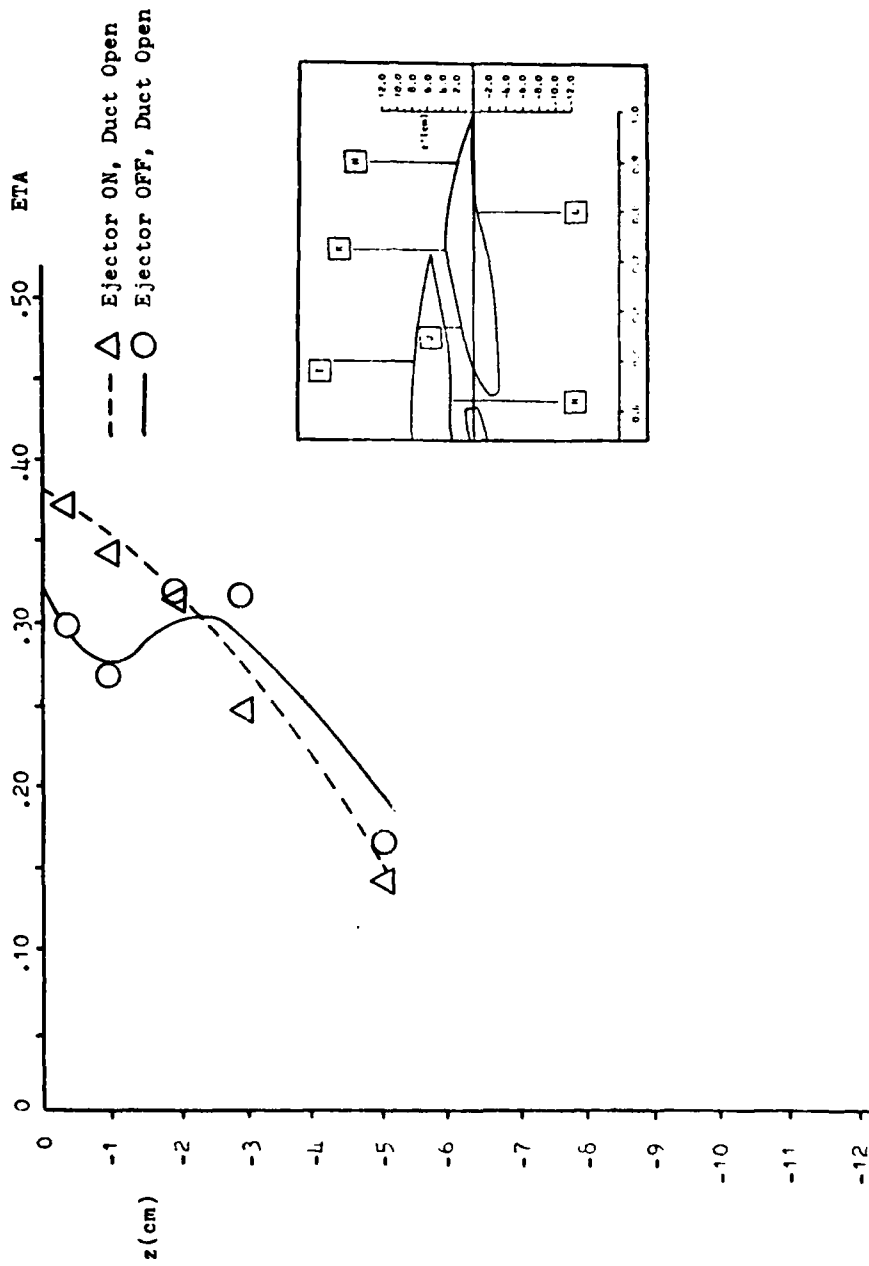


Figure 53 Turbulence Intensity Profile, Survey Location L , AOA = 15°

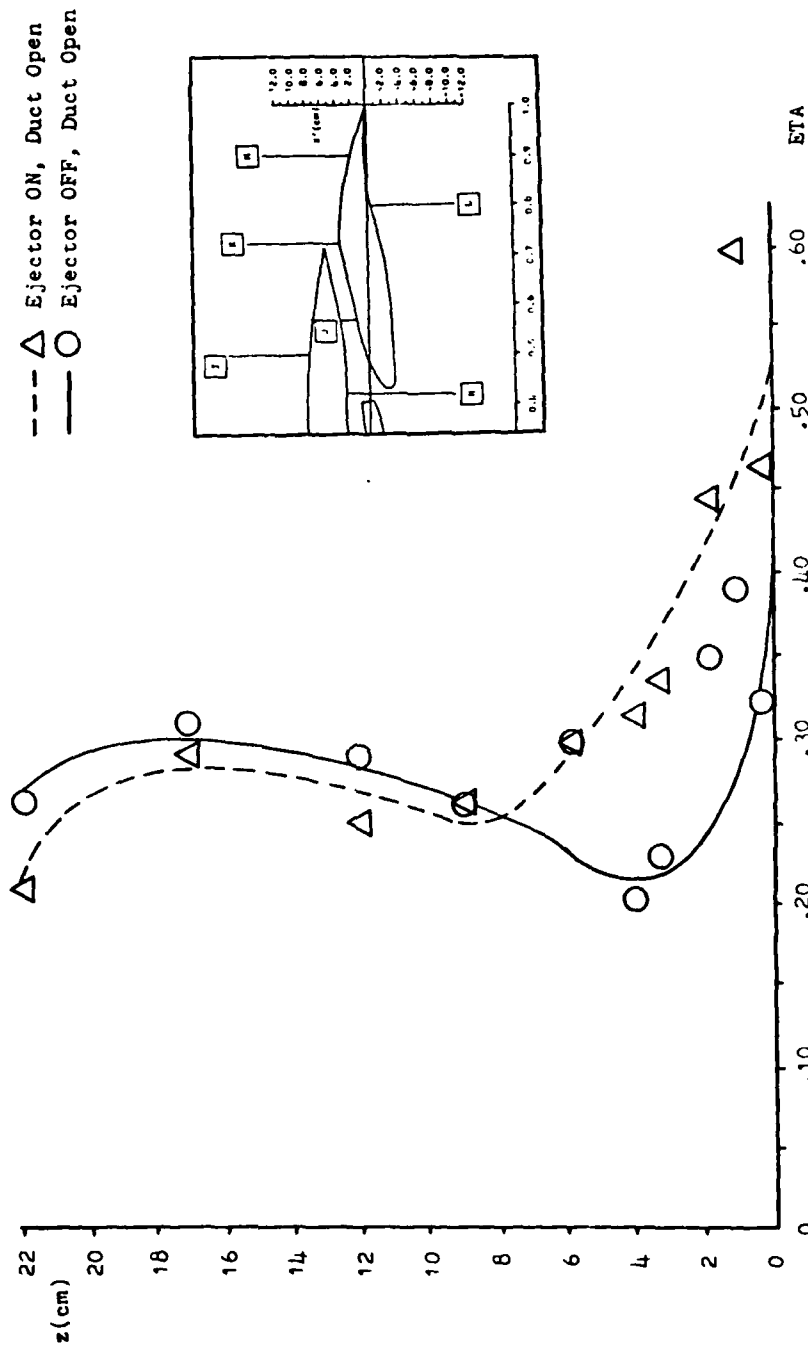


Figure 54 Turbulence Intensity Profile, Survey Location **M**, AOA = 15°

AOA = 0°:

The next angle of attack to be investigated with the LDV was 0°. Figure 56 shows the survey locations, lettered A through F which comprised approximately 100 data points. Since the relative benefit of ejector operation with the ejector duct open was documented at AOA = 15°, the investigation at AOA = 0° centered on comparing the relative performance of the model during ejector operation (ejector duct open) with an equivalent solid airfoil. Therefore, a plexiglass duct blockage element was designed and fabricated. With this blockage element and black tape the model could be temporarily converted to a solid airfoil.

In an attempt to determine relative drag, wake surveys (Survey Location F, Figure 62) were conducted as follows:

1. Ejector Duct Open (with and without blowing):

In this way the relative drag between the ejector on and ejector off operational modes with the ejector duct open can be compared.

2. Ejector Duct Blocked (solid airfoil, no blowing):

With this survey a drag comparison can be made between the ejector on mode with the ejector duct open and an equivalent solid airfoil.

In reviewing the data presented in Survey Locations A through E (Figures 57 through 67), which compares the model with ejector duct open and the ejector on to an equivalent solid airfoil, the same performance improvements doc-

umented at AOA = 15° can be observed:

1. Increased pressure differential with ejector operation due to faster mean velocities on the upper surface and slower mean velocities on the lower surface.
2. An apparently smaller, more well defined wake region above the aft airfoil with ejector operation.

From these results it appears that the ejector wing design is superior in performance to an equivalent solid airfoil.

As a measure of the relative drag/thrust augmentation of the ejector wing, wake surveys were conducted at a location 0.50C downstream of the trailing edge with the model at 0° AOA. The surveys are presented in Figure 62.

Wake survey data can be used to find the drag on any body through a control volume analysis involving the equation of motion (Reference 15). An equation for the drag can be written as:

$$D' = \int_w \rho V_{mX} (U_{fs} - V_{mX}) dz_w + (\dot{m}U)_e \cos(\theta_e)$$

- where D' = Drag per unit span (or thrust per unit span if negative)
 ρ = Air density = 0.0766 lb_m/ft³
 V_{mX} = Wake survey mean velocity component
 z_w = Coordinate measured normal to the mean velocity at the wake survey location
 dz_w = Differential area: $dz_w \times (1)$, i.e., unit span
 $(\dot{m}U)_e$ = Momentum flux of ejector

θ_e = Angle between ejector flux and the free stream with the model at 0° AOA, $\theta_e = 17^\circ$

Figure 55 illustrates the drag equation.

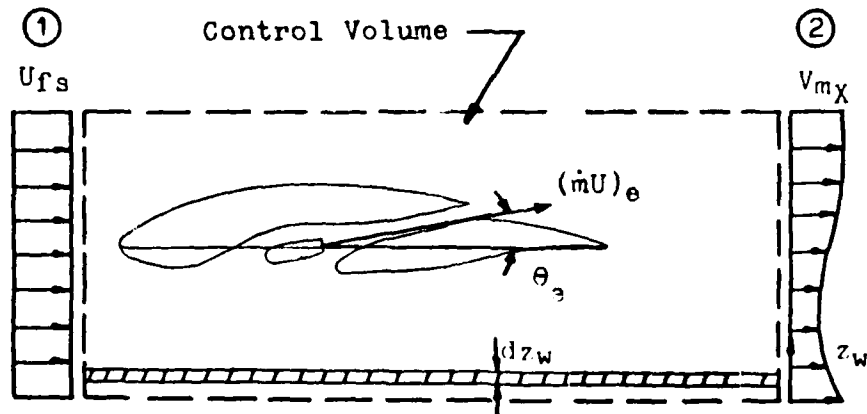


Figure 55 Wake Survey

The first term in the drag equation represents the momentum deficit per unit span between station 1 and station 2. The second term represents the additional momentum flux per unit span of the ejector. Since $\dot{m}_e = 0.046 \text{ lb}_m/\text{sec}$, $(\dot{m}U)_e = 0.315 \text{ lb}_f/\text{ft}$. Therefore, with the ejector off, only the first term is used to calculate the drag. But, with the ejector on, both terms are employed. In this way, the additional ejector momentum is accounted for in the control volume momentum balance. A drag reduction benefit due to ejector employment would thus be evident if:

$$D'_{\text{ejector ON}} < D'_{\text{ejector OFF}}$$

Other terms, such as, pressure differences between station 1 and station 2 due to the tunnel wall friction are

not considered significant and are equally present in both the on and off ejector modes.

Using this equation and graphical integration the drag per unit span of the model can be calculated. These values, however, are relative in nature and are used here only for comparative purposes to show the effect of ejector operation. Survey Location F (Figure 62) shows the effect of ejector operation with the ejector duct open (ejector ON and ejector OFF) and the ejector duct blocked (ejector OFF). Note that the velocity deficit is decreased with ejector employment.

The computed relative drag values are:

$$D' = 0.125 \text{ lb}_f/\text{ft} \quad (\text{Ejector OFF, Duct Blocked})$$

$$D' = 0.130 \text{ lb}_f/\text{ft} \quad (\text{Ejector OFF, Duct OPEN})$$

$$D' = 0.114 \text{ lb}_f/\text{ft} \quad (\text{Ejector ON, Duct OPEN})$$

Thus an apparent drag reduction for ejector employment as compared to the solid airfoil and the ejector off, duct open operational mode is evident.

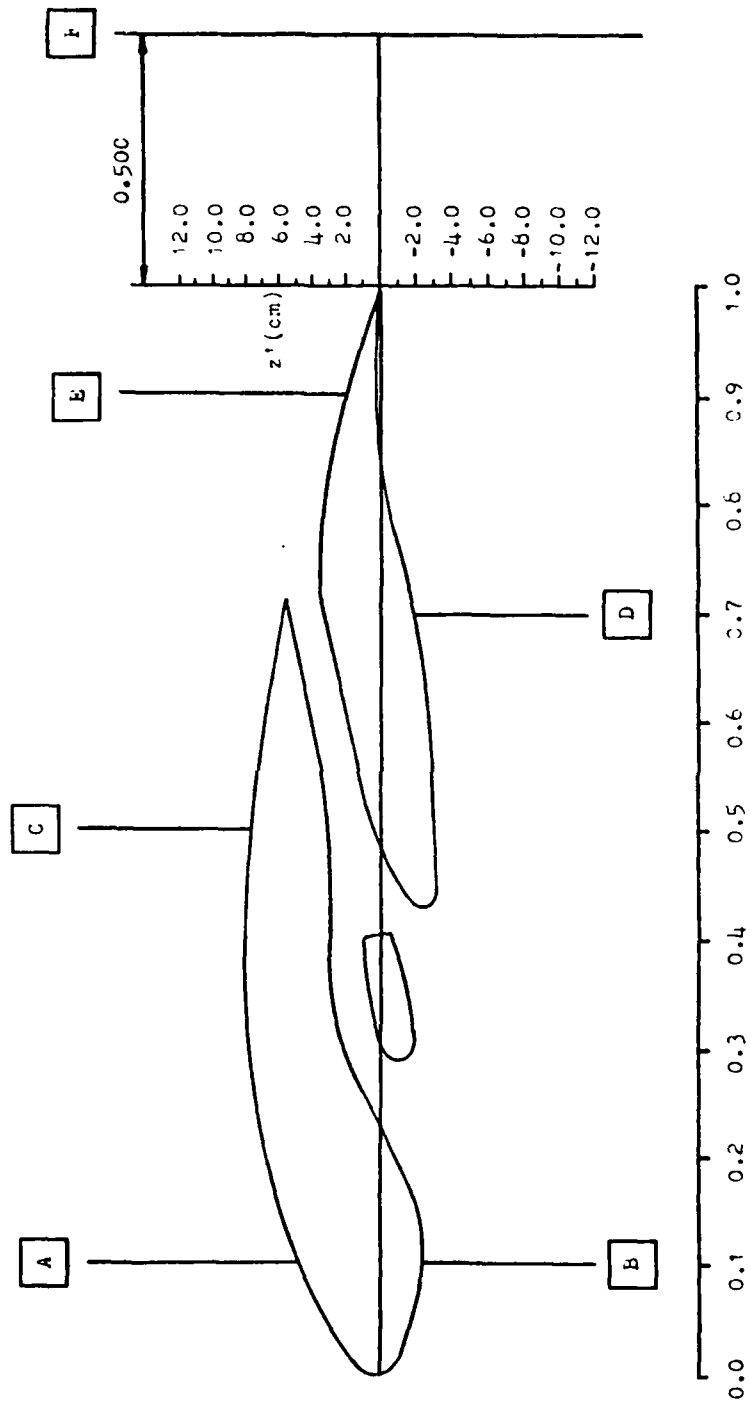


Figure 56 Survey Locations, $AOA = 0^\circ$

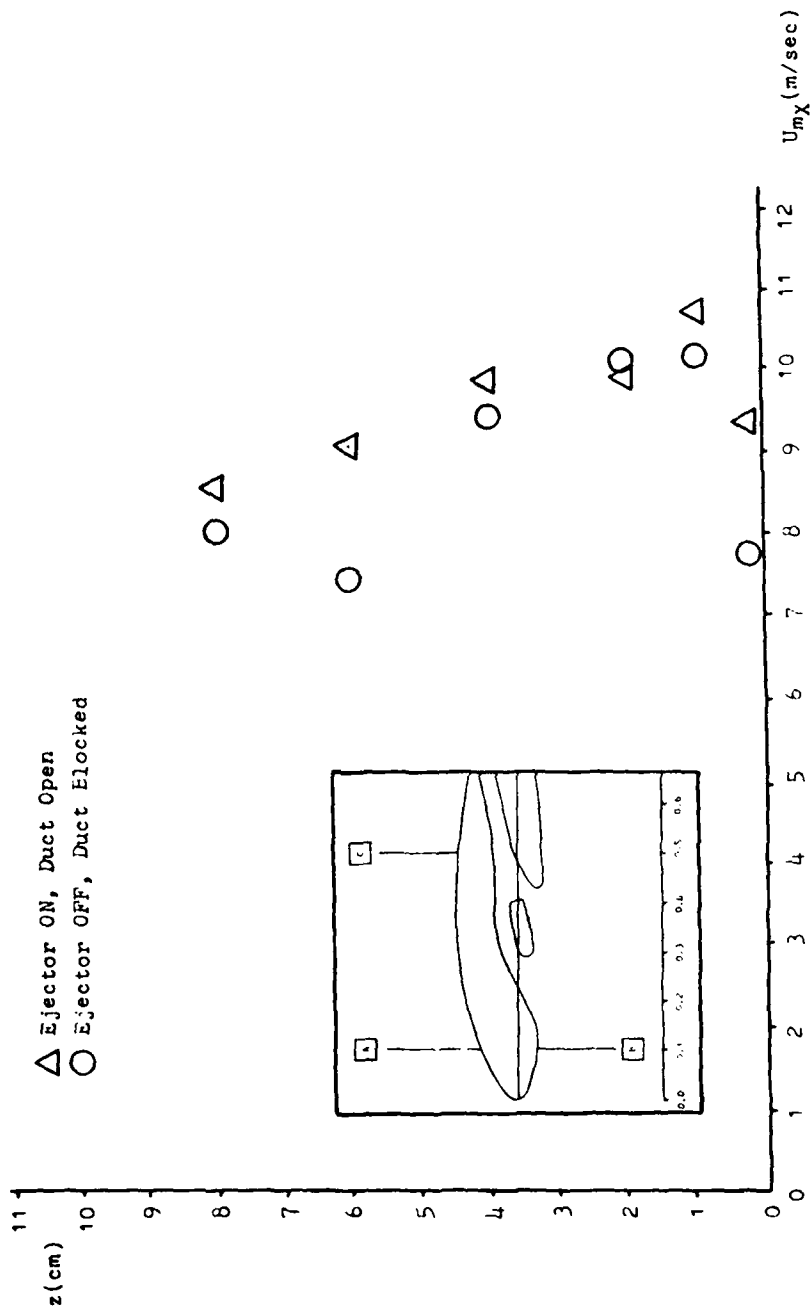


Figure 57 Mean Velocity Profile, Survey Location A, AOA = 0°

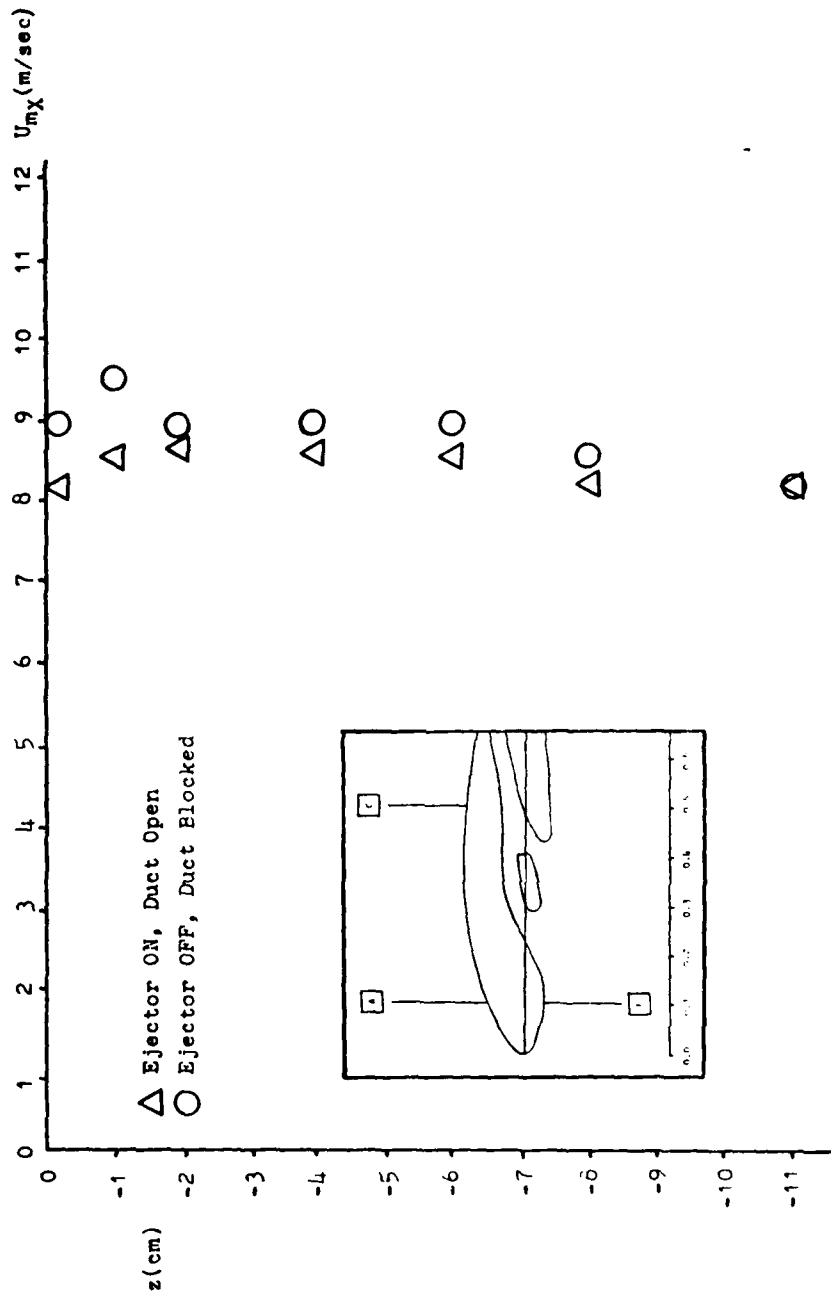
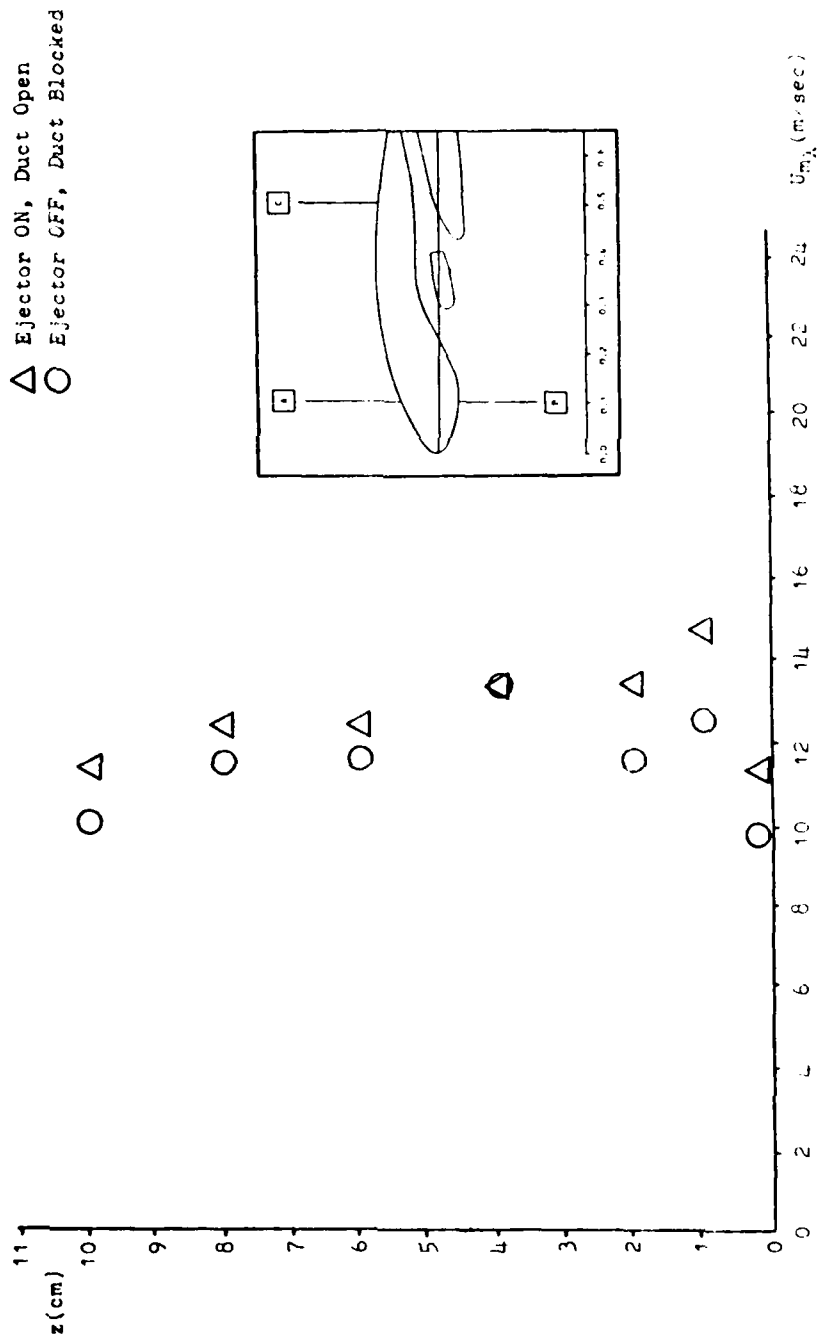


Figure 58 Mean Velocity Profile, Survey Location B, $\alpha_{OA} = 0^\circ$



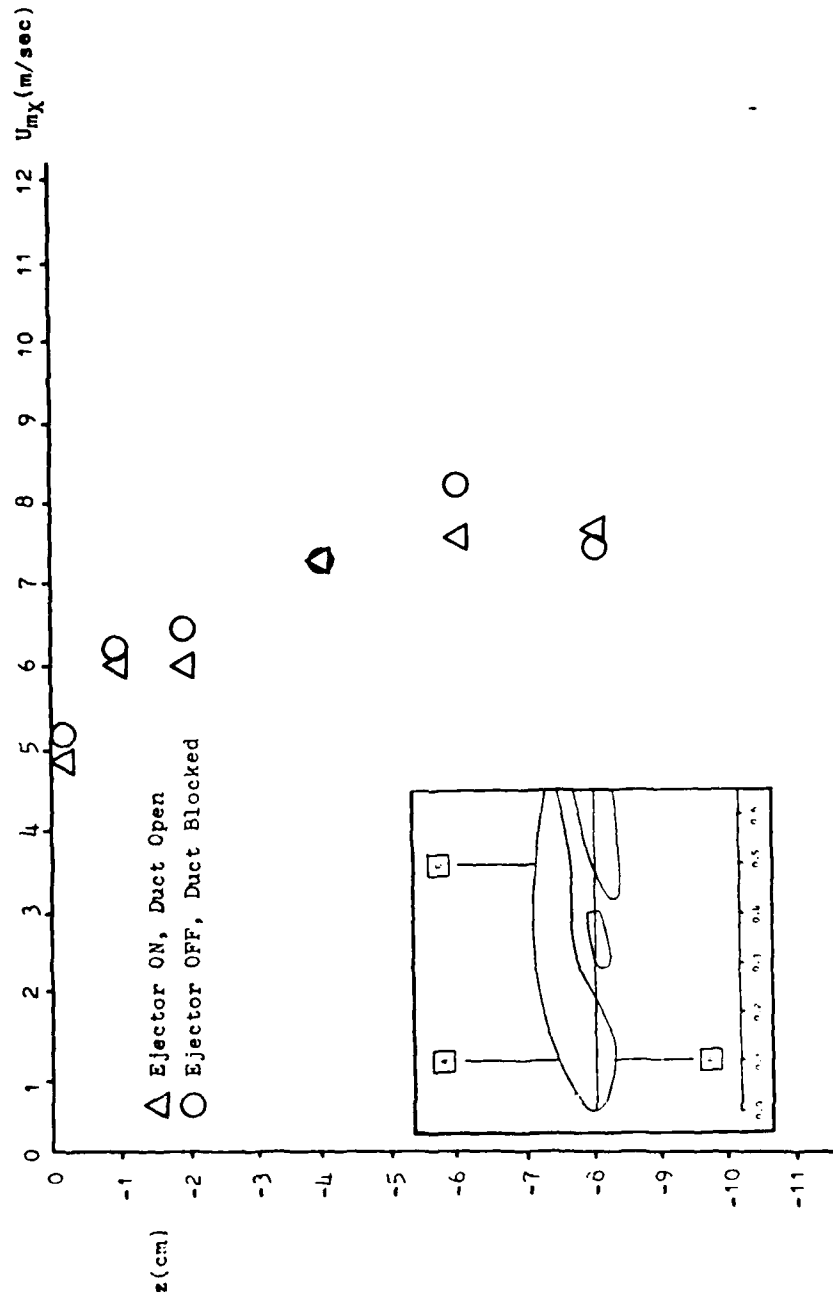


Figure 60 Mean Velocity Profile, Survey Location D, AOA = 0°

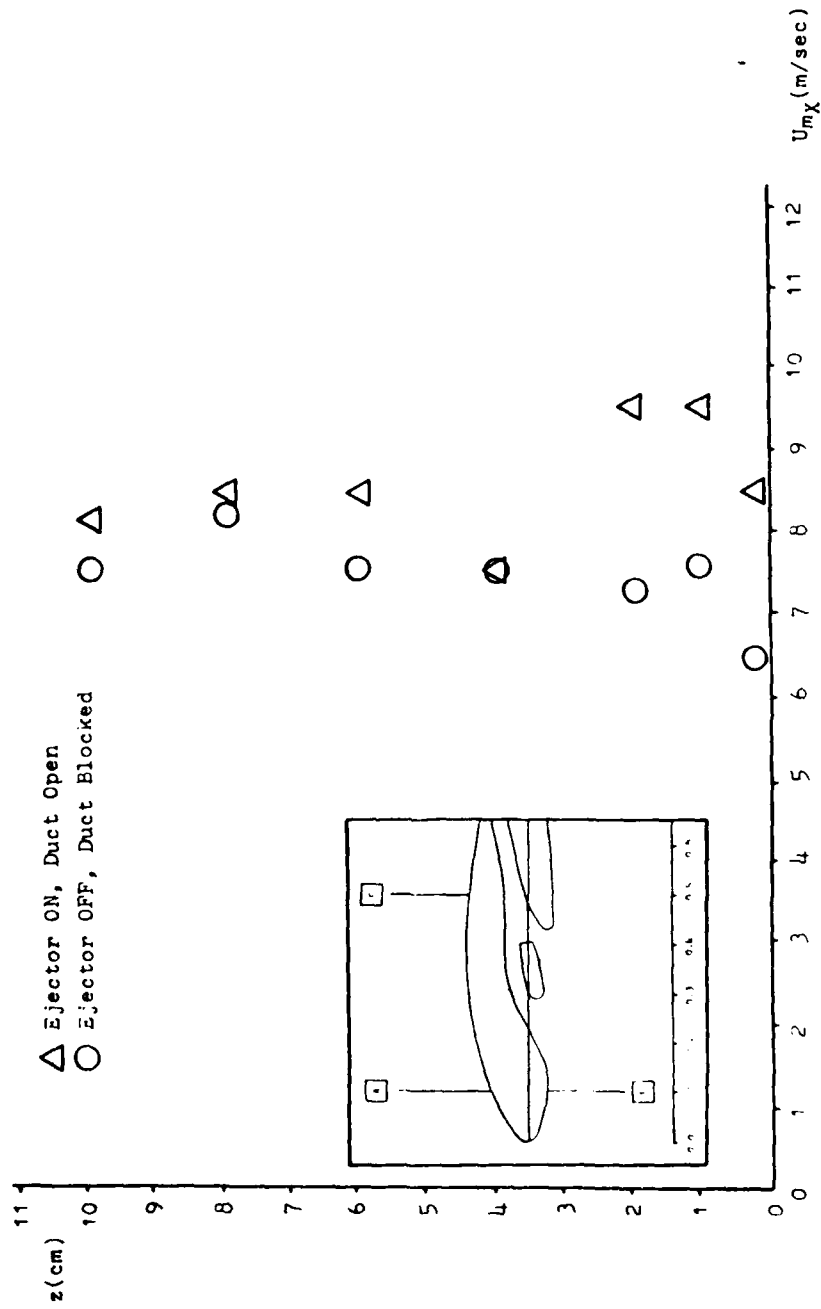


Figure 61 Mean Velocity Profile, Survey Location **E**, $AOA = 0^\circ$

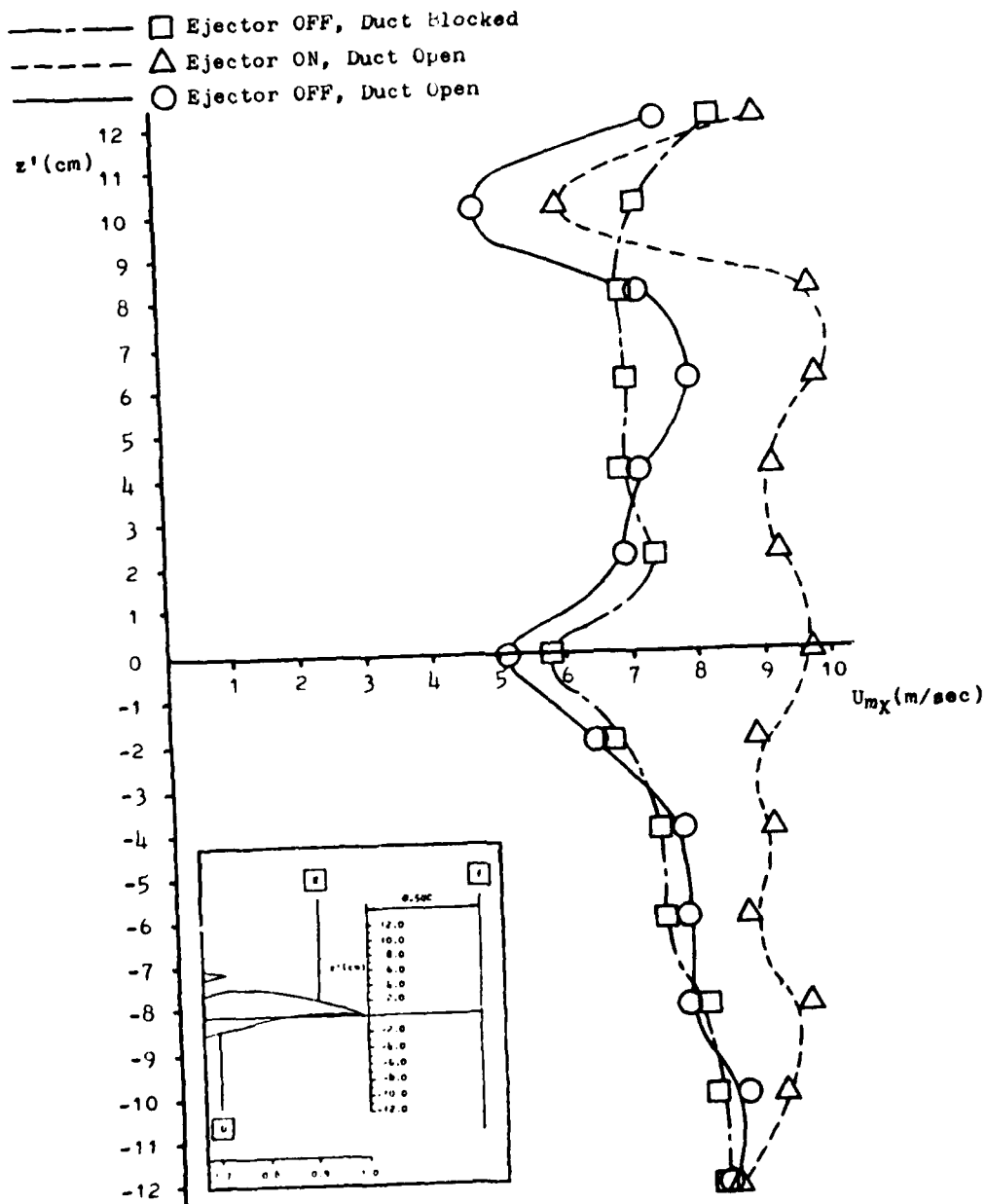


Figure 62 Mean Velocity Profile, Survey Location **F**, AOA = 0°

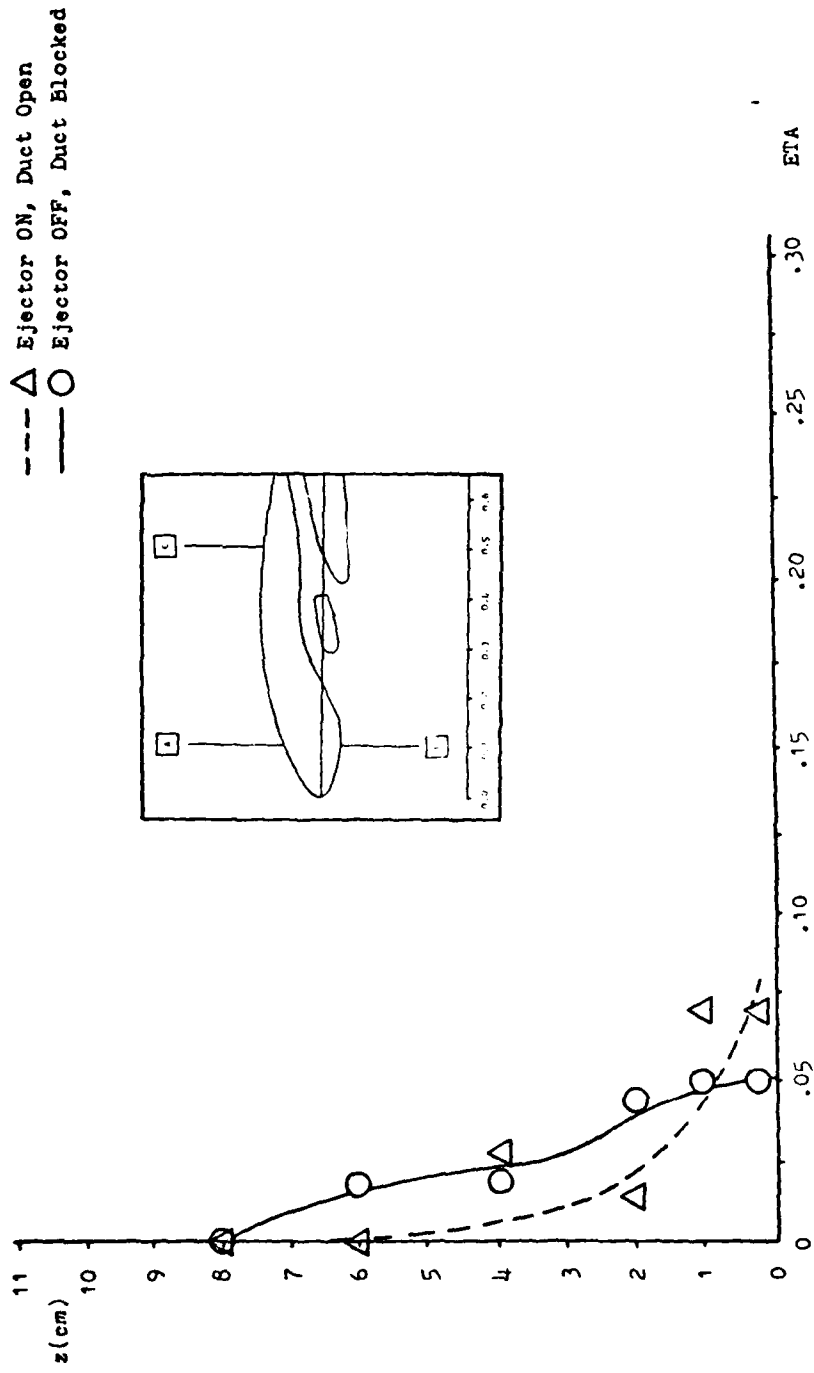


Figure 63 Turbulence Intensity Profile, Survey Location **A**, AOA = 0°

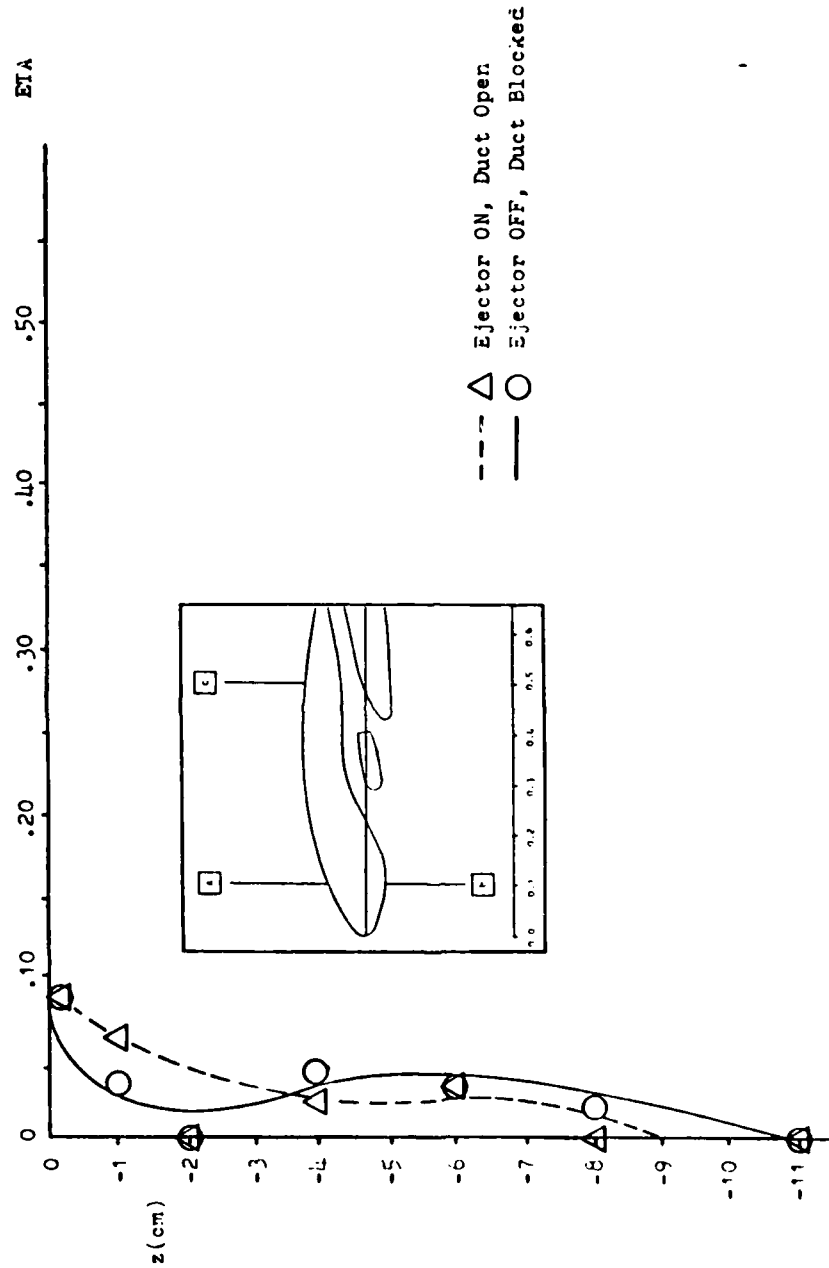


Figure 64 Turbulence Intensity Profile, Survey Location B, AOA = 0°

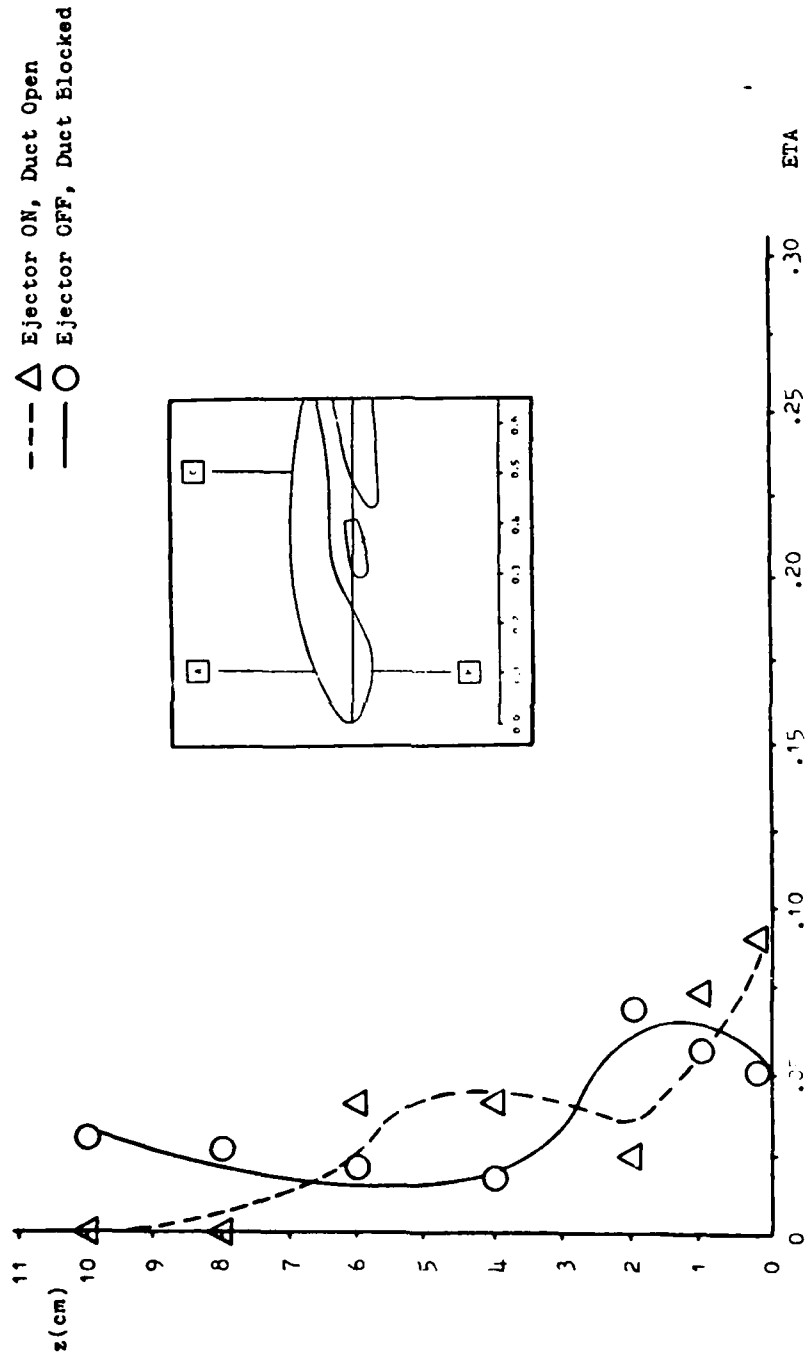


Figure 65 Turbulence Intensity Profile, Survey Location \square C, $AOA = 0^\circ$

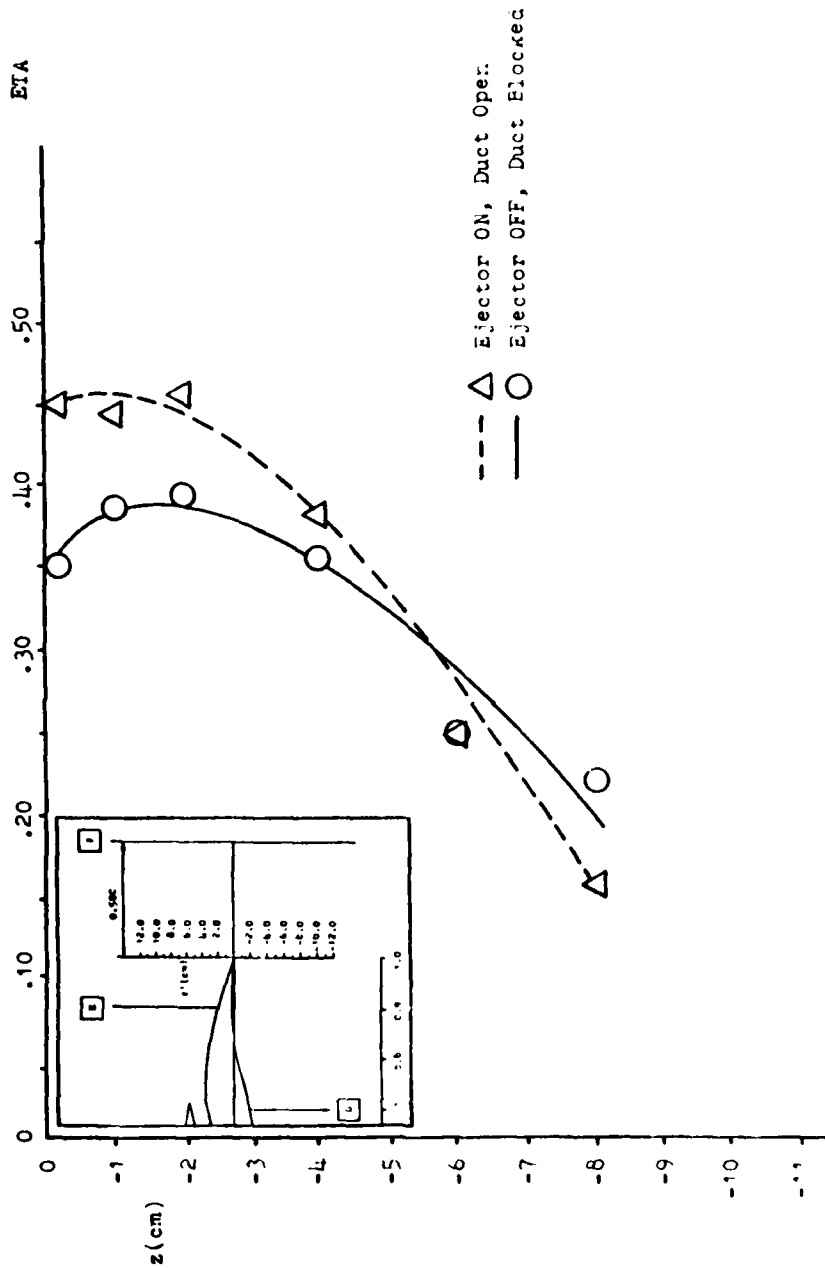


Figure 66 Turbulence Intensity Profile, Survey Location D, ACA = 0°

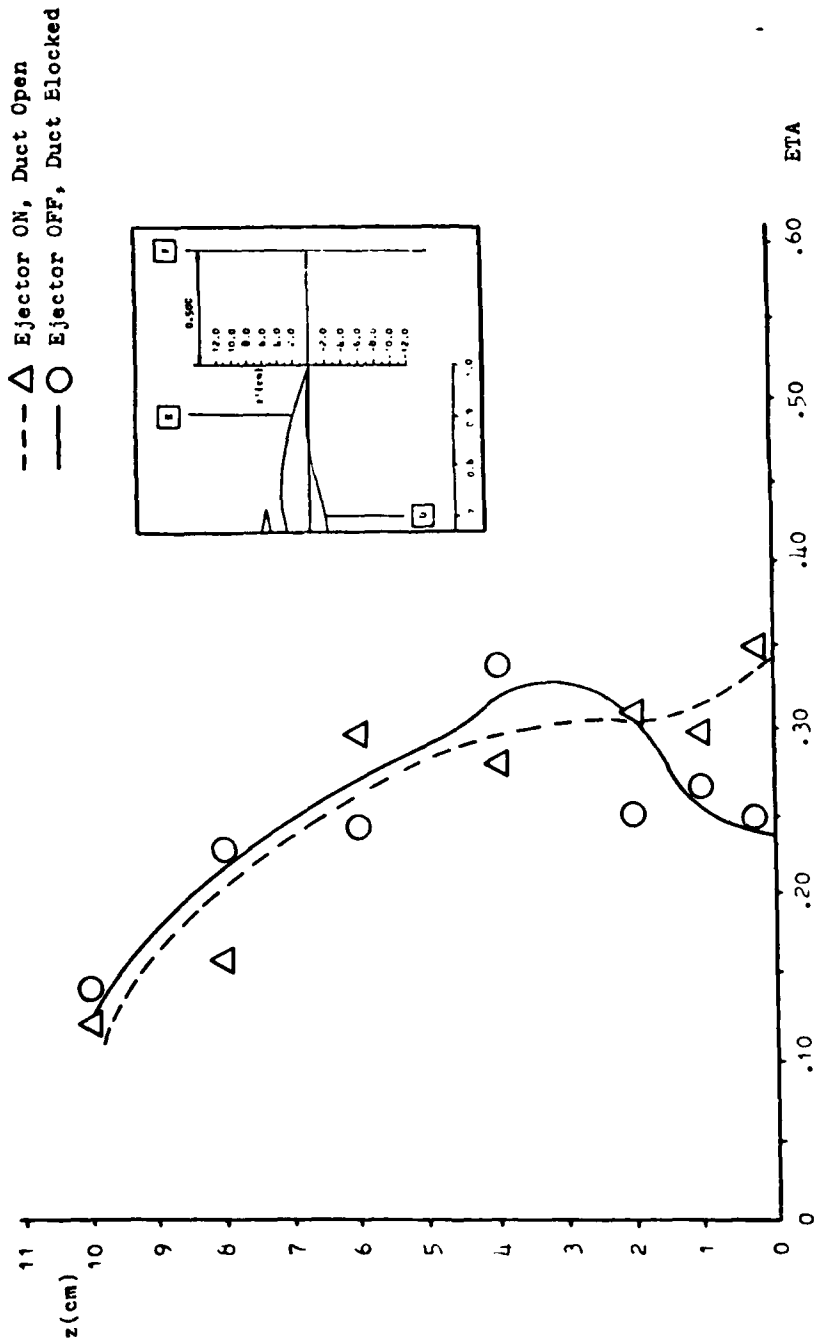


Figure 67 Turbulence Intensity Profile, Survey Location **E**, AOA = 0°

V. CONCLUSIONS

As a result of this research, conclusions can be drawn as to the aerodynamic benefit of this design. The conclusions that relate to enhanced lift are listed first followed by the conclusions that relate to reduced drag. Following these conclusions are three additional conclusions that are related to both increased lift and reduced drag.

The conclusions that impact lift are:

1. Ejector employment causes an increased pressure differential between the upper and lower surfaces of the airfoil.
2. The effective angle of attack of the model is increased with ejector employment.
3. The leading edge stagnation point appears to move down the forward airfoil's lower surface with ejector operation. This indicates an increase in circulation and thus an increase in lift.

The conclusions that impact drag are:

1. The flow on the upper surface of both the forward and aft airfoils is increased with the ejector on. This is an indication that the ejector energizes the upper surface flows and thus aids in fighting adverse pressure gradients. This may delay separation.
2. A less diffused, more well defined, and smaller wake region appears to exist above the aft airfoil

as a result of ejector employment.

3. With ejector operation turbulence levels near the surface of the airfoil are, in general, increased. This increase in turbulence level indicates a more energetic boundary layer which should be better able to overcome adverse pressure gradients.

4. The ejector's momentum flux contributes to a smaller velocity deficit in the wake region (wake survey location) as compared to an equivalent solid airfoil. A comparison of relative drag leads to the conclusion that the ejector provides a drag reduction.

The conclusions that impact lift and drag are:

1. The ejector entrains secondary fluid flow into the ejector duct thus increasing the momentum flux through the duct. This should further enhance the airfoil's lift increasing and drag reducing performance.

2. Flow in the ejector duct, both near the surface and about halfway down the duct is more turbulent with ejector operation. This increase in turbulence should aid mixing of secondary and primary flows and produce a more energetic flow exiting the duct and flowing over the aft airfoil.

3. The ejector wing design with the ejector duct open and the ejector operating appears superior in performance

(increased lift and decreased drag) to an equivalent solid airfoil.

On the basis of the presented results, analysis, and conclusions it appears that this unique ejector wing configuration is applicable to V/STOL aircraft.

Additional conclusions concerning equipment and procedures are as follows:

1. Extreme care must be taken when aligning and focusing the LDV optics. The sensitivity of the optics cannot be overemphasized.
2. Background scattered light must be reduced to the maximum extent possible. Steps toward this goal include:
 - a. Insure all optical surfaces and tunnel walls are clean and totally grease free.
 - b. Make maximum use of black paper and cloth materials to reduce reflections.
 - c. Insure that all background lights are extinguished prior to data acquisition.
 - d. For best results in avoiding scattered laser light, use plate glass rather than plexiglass.
3. Due to the limitation of 1 MHz maximum phase modulation, data near the airfoil's surface (less than 3 mm) and in other regions of high turbulence ($\text{ETA} > 60\%$) was unobtainable.

VI. RECOMMENDATIONS

Based on this study which utilized a LDV and the AFIT smoke tunnel to conduct an experimental investigation of an ejector wing design, recommendations for improvements and further projects are presented.

The recommendations are divided into two categories: those relating to the LDV and those pertaining to the ejector wing design model.

LDV

1. For ease of control volume translation a more sophisticated setup should be devised. A more stable, larger, and most importantly, stationary primary optical bench should be fabricated. Upon this stationary bench two secondary optical benches could be used to achieve translation in all three dimensions. The incorporation of remotely controlled traversing motors would greatly aid in control volume movement and should help alleviate alignment and maintenance nightmares. By constructing a more stable and more easily aligned optical setup the problem of floor/optical bench irregularities which prevented data acquisition very near the airfoil's surface may be avoided.
2. Incorporate an additional laser and beamsplitter whose control volume fringes are aligned perpendicular to the original fringes. In this manner two components

of velocity can be determined resulting in knowledge of the total velocity vector.

3. Increase the range of maximum phase modulation beyond the 1 MHz level. In this way data in areas of high turbulence ($ETA > 60\%$) could be obtained.

4. To reduce the arduous task of unskewing the displayed autocorrelation function and subsequent data reduction process, integration of the LDV system with a small desk top computer should be accomplished. This project is being conducted in parallel with this investigation using a Hewlett-Packard (HP) 3052A Automatic Data Acquisition System. This project should be completed as soon as possible. Once the entire LDV system is automated with traversing motors controlled by the HP for control volume placement and data reduction an excellent, real time, diagnostic tool will be available for future researchers.

Ejector Wing Model

1. Incorporate pressure transducers and/or pressure taps into the model. In this way pressure distribution can be plotted.

2. The model is equipped with trailing edge flaps on each airfoil. The forward airfoil has a 12% chord flap and the aft airfoil has a 19% chord flap. The flaps are capable of $\pm 4^\circ$ deflection. Flow field variations caused by the deflection of these flaps could

be the basis for a further study of this configuration.

3. An analytical analysis (finite element, paneling or other computational technique) should be conducted on this configuration. This experimental study could be used as a guide in modeling the analytical analysis. In this way the experimental findings and the analytical results could be compared resulting in a better understanding of the ejector wing concept.

REFERENCES

1. Abiss, J.E., Chubb, T.W., and Pike, E.R., "Laser Doppler Anemometry", Optics and Laser Technology, Vol. 6, pgs 249-261, Dec 1974
2. Baldner, J.L., Completion of the Development of the AFIT Smoke Tunnel, M.S. Thesis, Wright-Patterson AFB, Ohio: Air Force Institute of Technology, Aug 1959.
3. Bauer, J.S., "A New Family of Airfoils Based on the Jet Flap Principle", Douglas Aircraft Company Report No. MDCJ5713, Long Beach, California, Sep 1972.
4. Bendat, J.S. and Piersol, A.G., Measurement and Analysis of Random Data, New York: John Wiley & Sons, Inc., 1966.
5. Birch, A.D., Brown, D.R., and Thomas, J.R., "Photon Correlation Spectroscopy and its Application to the Measurement of Turbulence Parameters in Fluid Flows", Journal of Physics D: Applied Physics, Vol. 8, pgs 438-447, 1975.
6. Bradshaw, P., An Introduction to Turbulence and its Measurement, Oxford, England: Pergamon Press, Ltd., 1971.
7. Bradshaw, P., Experimental Fluid Mechanics, New York: The MacMillian Company, 1964.
8. Cebeci, T. and Smith, A.M.O., Analysis of Turbulent Boundary Layers, New York: Academic Press, 1974.
9. Durrani, T.S. and Greatel, C.A., Laser Systems in Flow Measurement, New York: Plenum Press, 1977.
10. Durst, F. and Mellin, A., Principles and Practice of Laser-Doppler Anemometry, London: Academic Press, 1976.
11. "Ejector Wing Design", Vought Corporation Advanced Technology Center, ATC Report No. R-91100/9CR-44, Sep 1979.
12. Fancher, R.B., "Why Ejectors for Aircraft Propulsion-Lift Systems and Where We Stand", Aerospace Research Laboratories (AFSC) Report No. 71-0140, Wright-Patterson AFB, Ohio, Aug 1971.
13. Hinze, J.O., Turbulence, New York: McGraw-Hill Book Company, 1959.

14. Johnston, J.P., "Internal Flows", Turbulence, ed. P. Bradshaw, Topics In Applied Physics, Vol. 12, New York: Springer-Verlag, 1978.
15. Kuethe, A.M., Chow, C.Y., Foundations of Aerodynamic Design, New York: John Wiley & Sons, 1976.
16. Malvern Instruments, Ltd., Operating and Installation Manual, Spring Lane Trading Estate, Malvern Link, Worcestershire WR14 1AL, England.
17. Rogers, H.J.V., Velocity Profiles in a Long Inlet Duct Employing a Photon Correlation Laser Velocimeter Without Seeding, M.S. Thesis, Wright-Patterson AFB, Ohio: Air Force Institute of Technology, Dec 1979.
18. Shepard, W.K., Turbulence Measurements in a Free Jet at High Subsonic Velocities, M.S. Thesis, Wright-Patterson AFB, Ohio: Air Force Institute of Technology, Dec 1974.
19. Smith, A.M.O., "High-Lift Aerodynamics", Journal of Aircraft, Vol. 12, pgs 501-530, Jun 1975.
20. Strand, T., "The Jet Flap- Review and Extension", General Dynamics/Convair Report No. ZA-255, San Diego, California, Nov 1956.
21. Tennekes, H. and Lumley, J.L., A First Course in Turbulence, Cambridge, Massachusetts: The MIT Press, 1972.
22. Thompson, H., Doyle, H., and Stevenson, W., eds. Laser Velocimetry and Particle Sizing. Washington: Hemisphere Publishing Corporation, 1978.
23. Walterick, R.E., An Experimental Investigation of the Near Wake of a Circular Cylinder, M.S. Thesis, Wright-Patterson AFB, Ohio: Air Force Institute of Technology, Sep 1980.
24. White, F.M., Viscous Fluid Flow, New York: McGraw-Hill, Inc., 1974.
25. Wagnanski, I., "The Effect of Jet Entrainment on Loss of Thrust for a Two-Dimensional Symmetrical Jet-Flap Aerofoil", The Aeronautical Quarterly, Vol. XVII, Feb 1966.

APPENDIX A

AUTOCORRELATION FUNCTION (Reference 4)

An autocorrelation function is a correlation between the same fluctuating random data measured at two different times at the same point in the flow. Thus, it is a time correlation rather than a spacial correlation. As an example, the velocity at a point in the flow field of the ejector wing may vary due to turbulent eddies in the following manner:

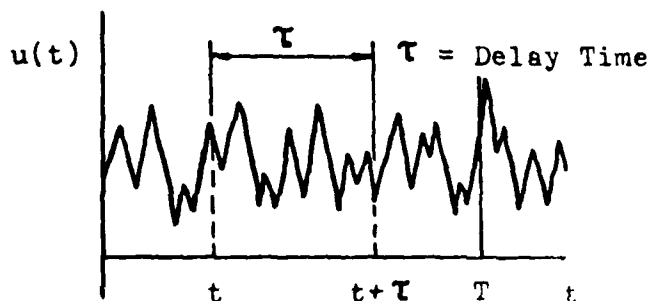


Figure 66 Autocorrelation of $u(t)$ and $u(t+\tau)$

Each value of the velocity, $u(t)$, at any instant in time is the instantaneous velocity. An estimate of the autocorrelation between values of $u(t)$ at time t and $t + \tau$ is obtained by taking the product of $u(t)$ and $u(t + \tau)$ and averaging over an observation time, T . Then as T approaches infinity the resulting average product will approach an exact autocorrelation function, defined mathematically as,

$$R_u(\tau) = \lim_{T \rightarrow \infty} \frac{1}{T} \int_0^T u(t)u(t+\tau)dt = \overline{u(t)u(t+\tau)}$$

In order to nondimensionalize the autocorrelation function, $G_u(\tau)$ is divided by:

$$\left[\overline{u^2(t)} \right]^{1/2} \left[\overline{u^2(t+\tau)} \right]^{1/2}$$

which is the product of the square roots of the time averaged instantaneous velocities at t and $t + \tau$.

This division yields:

$$G(\tau) = \frac{\overline{u(t)u(t+\tau)}}{\left[\overline{u^2(t)} \right]^{1/2} \left[\overline{u^2(t+\tau)} \right]^{1/2}}$$

Since $\overline{u(t)u(t+\tau)} \leq \left[\overline{u^2(t)} \right]^{1/2} \left[\overline{u^2(t+\tau)} \right]^{1/2}$ Schwartz's Inequality
(Reference 21)

then, $-1 \leq G_u(\tau) \leq 1$

A typical plot of the autocorrelation function versus delay time ($G_u(\tau)$ vs τ) is shown in Figure 69. Note that $G_u(0)$ has been normalized.

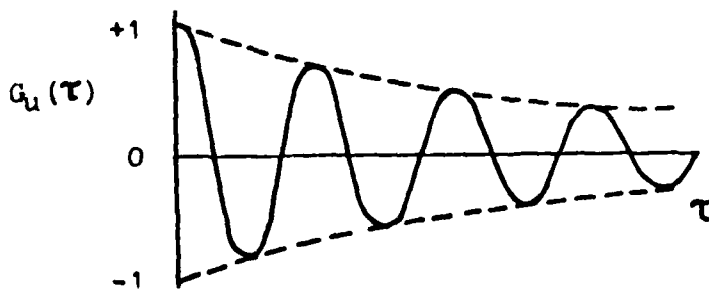


Figure 69 Autocorrelation Function

From this autocorrelation function mean velocity and turbulence intensity values can be obtained. However, before proceeding with a data reduction discussion an explanation of how the autocorrelation function displayed on the oscilloscope is transformed into a useful autocorrelation function of the form in Figure 69 will be given.

Since the oscilloscope cannot display the entire autocorrelation function, ie, $\tau \rightarrow \infty$, a sample of the function is generated by operator selection of an appropriate sample time. In general, a sample time is selected which yields the best presentation for data acquisition. Sample times ranging from 0 to 9.99 seconds in .05 μ sec increments are possible. Selected sample times are composed of 94 equal time steps numbered 5 to 99. Thus, the abscissa of the oscilloscope presentation represents the selected sample time. This sample time abscissa is "free floating" on the display requiring the operator to determine its location and orientation. Location and orientation of the abscissa will be discussed in detail shortly. The ordinate is the number of photon counts detected by the photomultiplier tube and processed by the digital photon correlator. These number of counts (count values) on the ordinate are totally arbitrary and will vary with sample time and oscilloscope/correlator settings. The arbitrary nature of the ordinate is of little concern since the function will be eventually nondimensionalized. Also, as previously stated, the sample time line (or zero ordinate line) is not displayed on the scope and; therefore, must be determined. This determination is made by fitting

one least squares second degree polynomial curve to the first three maximum count values and a second least squares second degree polynomial curve to the first three minimum count values as shown in Figure 70 .

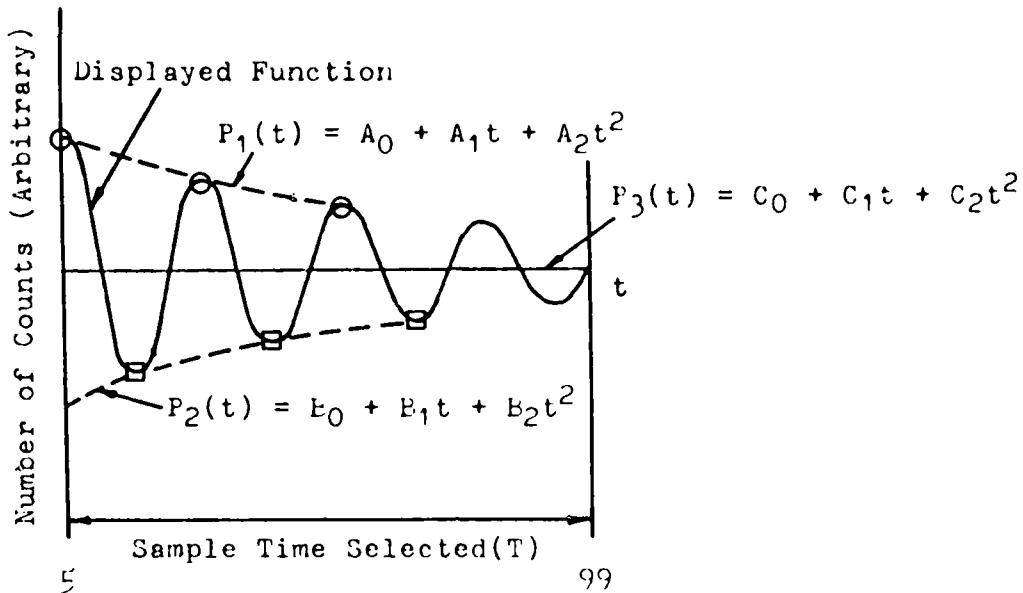


Figure 70 Oscilloscope Displayed Autocorrelation Function

The arithmetic mean of the coefficients is then calculated:

$$C_0 = \frac{A_0 + E_0}{2} \quad ; \quad C_1 = \frac{A_1 + E_1}{2} \quad ; \quad C_2 = \frac{A_2 + E_2}{2}$$

A new mean second degree polynomial curve is then drawn as shown and this represents the time abscissa (zero ordinate) line. That is, the number of counts corresponding to this line is considered the zero count line and all other count values are adjusted accordingly. This time abscissa line determination method is also very useful for correcting a skewed oscilloscope display. Skewedness is a frequent occurrence and is due to either an insufficient number of control volume fringes

or detection of background scattered light. Figure 71 shows a skewed oscilloscope display.

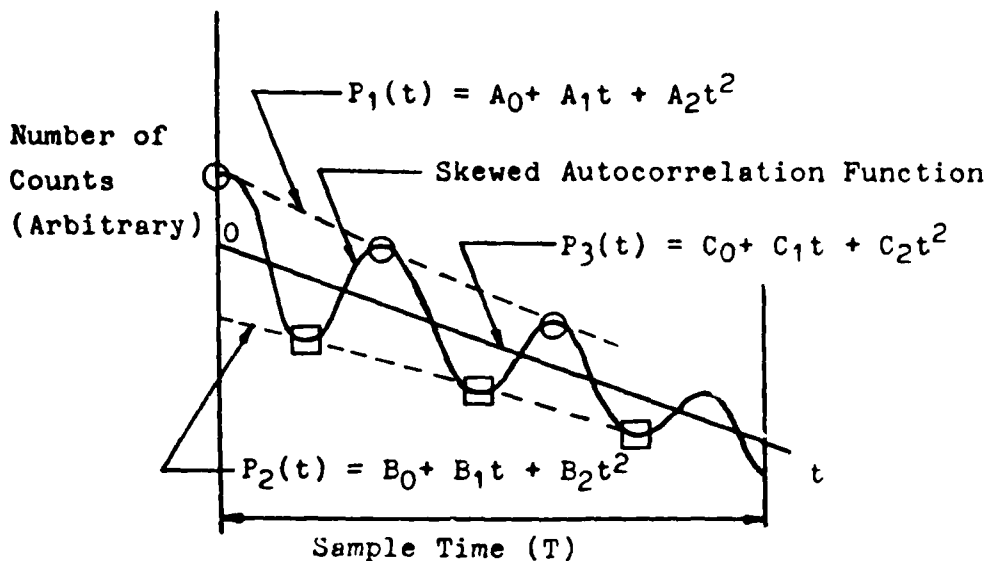


Figure 71 Displayed Skewed Autocorrelation Function

By subtracting the mean curve (P_3) from the minimum (P_2) and maximum (P_1) curve fits, the function can be replotted as shown in Figure 72 .

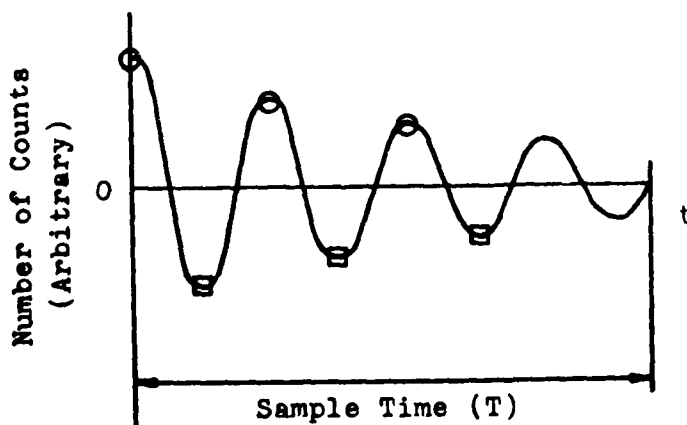


Figure 72 Replotted Unskewed Autocorrelation Function

Once an unskewed function with a zero ordinate line is obtained as in Figure 72 it is nondimensionalized. This is done by determining the difference between the number of counts at the zero ordinate line and the number of counts at the point where the function crosses the $t=0$ line (time step 5). This count difference is then divided into the count values at all points, thus nondimensionalizing the entire function. The resulting function is the desired autocorrelation function, $G_u(t)$ (Figure 73). Note that $G_u(0)$ has been normalized.

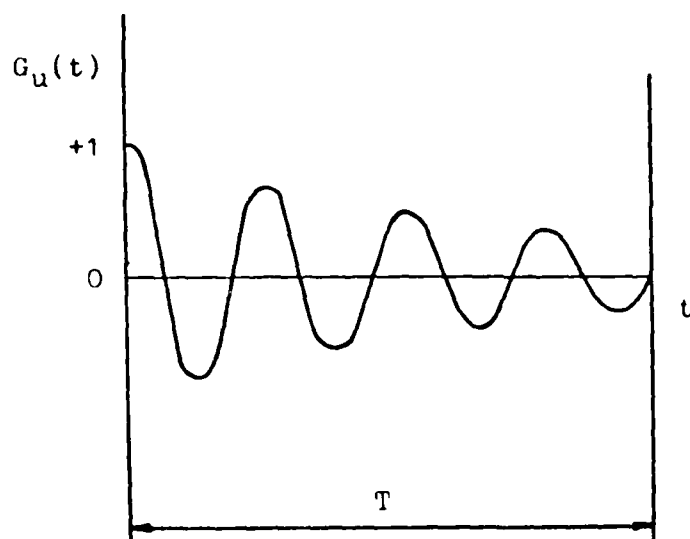


Figure 73 Autocorrelation Function

A computer program using the CDC 6600 computer was developed to determine the $G_u(t) = 0$ line, correct a skewed display and assist in plotting the autocorrelation function. Once the oscilloscope displayed autocorrelation function has been transformed into a usable function data reduction is the next step (Appendix B through D).

APPENDIX B

MEAN VELOCITY (Reference 8)

By definition mean velocity is the average velocity at a point, with respect to time.

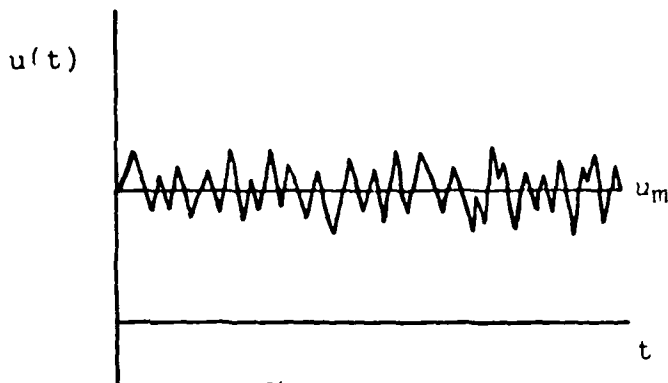


Figure 74 Mean Velocity

Mathematically, the mean velocity is expressed as:

$$u_m = \bar{u} = \lim_{n \rightarrow \infty} \frac{1}{n} \sum_{i=1}^n u_i$$

where n is the number of time samples taken.

In order to determine mean velocity from the autocorrelation function some preliminary calculations must be made. First, the fringe spacing, S , must be determined.

$$S = \frac{L\lambda}{D\mu}$$

where L = the distance from the laser beam intersection point (control volume) to a perpendicular reference surface

D = the distance the two beams are apart at the reference surface

λ = wavelength of helium-neon laser light = $.6328 \times 10^{-6}$ m

μ = refractive index of air = 1.0

Figure 75 illustrates L, D, and θ .

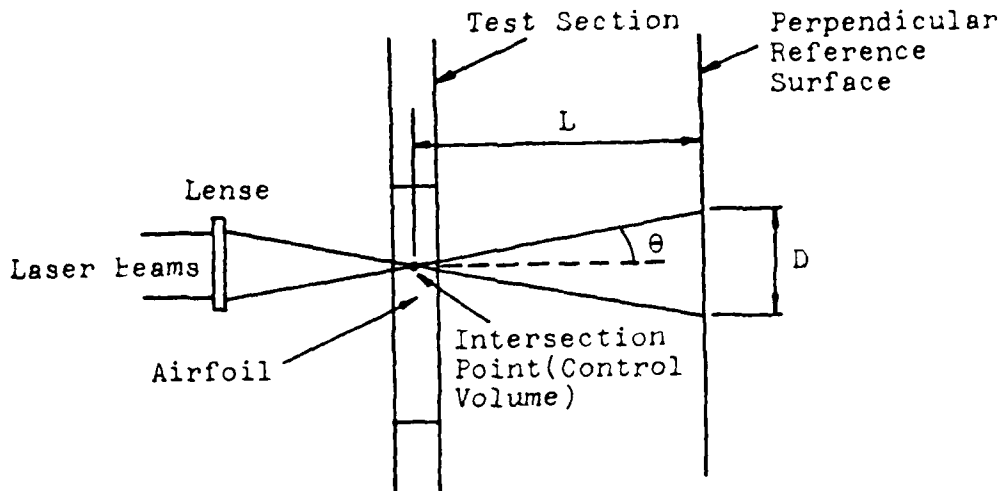


Figure 75 Illustration of L, D, θ

Then the formula for computing the mean velocity is:

$$U_{mX} = \frac{S}{(\text{Peak}-3)(T)}$$

where U_{mX} = the mean velocity component parallel to the free stream, X

Peak = the time step for the first peak after the first valley in the autocorrelation function (Figure 76)

T = sample time selected

Figure 76 identifies the important peaks and valleys of the autocorrelation function where:

G1 = the first valley

G2 = the first peak after G1

G3 = the second valley

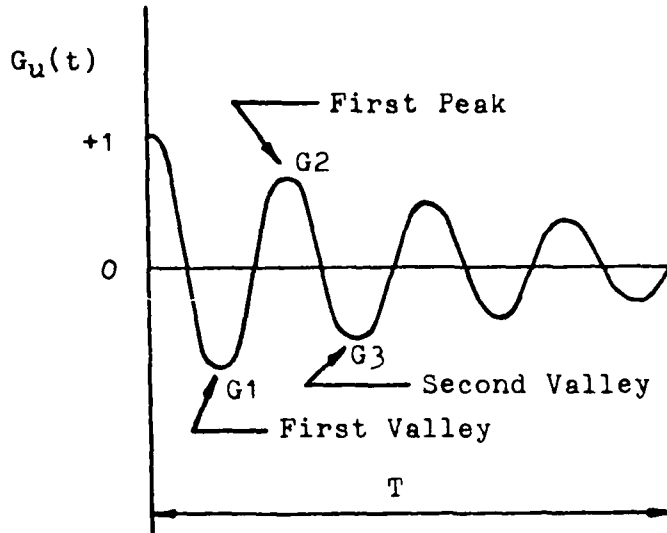


Figure 76 Autocorrelation Peaks and Valleys

In the event the phase modulator had to be employed during data acquisition a slightly different method is used for mean velocity determination. First, the included half angle, θ , is calculated:

$$\tan \theta = \frac{\frac{1}{2}D}{L}$$

$$\theta = \tan^{-1} \frac{\frac{1}{2}D}{L}$$

Next, the mean velocity is calculated as before:

$$U_{m\chi}^* = \frac{S}{(\text{Peak}-3)(T)}$$

where $U_{m\chi}^*$ = mean velocity with phase modulator employment

Then calculate the doppler shift frequency with phase modulator,

F_d^* :

$$F_d^* = \frac{2U_{m\chi}^*(\sin\theta)}{\lambda}$$

Next, calculate the doppler shift frequency without the phase modulator:

$$F_d = F_d^{\circ} \pm \Delta F$$

where F_d = doppler shift frequency without phase modulator employment

ΔF = the frequency shift imposed on the laser beams by the phase modulator

The sign of ΔF depends on the direction the fringes are made to move relative to the flow. If they move with the flow, ΔF is positive; against the flow ΔF is negative.

Then the actual mean velocity is:

$$U_{mX} = \frac{F_d \lambda}{2 \sin \theta}$$

It should be noted at this point for completeness that the function displayed on the oscilloscope can be used to determine mean velocities directly without correcting for skewedness or determining a zero ordinate line. By merely determining the time step at which the first peak occurs the formula for U_{mX} can be used to calculate the mean velocity. However, correcting for skewedness and determining a zero ordinate line is necessary for the calculation of turbulence intensity (Appendix C).

APPENDIX C

TURBULENCE INTENSITY (Reference 8)

The turbulence intensity parameter is a means of measuring the velocity fluctuations from the mean velocity in a turbulent flow (Figure 77).

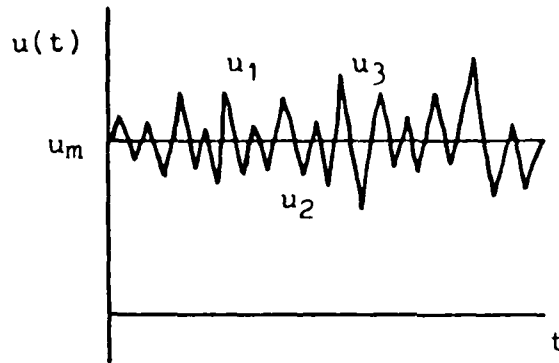


Figure 77 Velocity Fluctuations

Let the individual fluctuations about u_m be represented by:

$$\begin{aligned}u_1' &= u_1 - u_m \\u_2' &= u_2 - u_m \\u_3' &= u_3 - u_m, \text{ etc.}\end{aligned}$$

Then, the mean square of u' , U_{ms} , is:

$$\overline{(u')^2} = \lim_{n \rightarrow \infty} \frac{1}{n} \sum_{i=1}^n (u_i')^2 = U_{ms}$$

The root-mean-square (RMS) of this quantity is defined as the

turbulence intensity, U_{RMS} :

$$\left[\overline{(u')^2} \right]^{1/2} = U_{RMS} = \text{Turbulence Intensity}$$

To nondimensionalize the turbulence intensity, it is divided by the mean velocity, U_{mX} and given the symbol, ETA.

$$\text{ETA} = \frac{U_{RMS}}{U_{mX}}$$

The turbulence intensity is obtained from the autocorrelation function by the following method.

First, calculate R:

$$R = \frac{G2-G1}{G2-G3} \quad (\text{Figure 76})$$

where $G1$ = the first valley
 $G2$ = the first peak after $G1$
 $G3$ = the second valley

then,

$$\text{ETA} = \frac{1}{\pi} \left[\frac{1}{2}(R-1) + \frac{1}{2N^2} \right]^{1/2}$$

where $N = \frac{r_0}{S}$ = number of fringes in one half of the control volume

r_0 = laser beam radius = 0.55 mm

If the phase modulator is employed a slight variation in the above equation is used:

$$\text{ETA} = \frac{1}{\pi} \left[\frac{1}{2}(R-1) \frac{U_{mX}}{U_{mX}} + \frac{1}{2N^2} \right]^{\frac{1}{2}}$$

If during the calculation of the turbulence intensity an undefined or negative value is obtained, ETA is arbitrarily set to zero.

APPENDIX D

SAMPLE CALCULATIONS

In order to illustrate the data reduction process a sample calculation for a typical survey point is presented below.

The point is located 3.5 cm above the airfoil surface at Survey Location K with the model at 15° AOA. Phase modulation is employed and a skewed oscilloscope presentation was obtained. The necessary data for the reduction procedure is:

$$\text{AOA} = 15^\circ$$

$$U_e/U_{fs} = 2.0$$

$$\text{Sample Time}(T) = 0.10 \times 10^{-6} \text{ sec}$$

$$\text{Phase Modulation} = 201.9 \text{ KHz (against the flow)}$$

Time Step Number	Digital Count Number	Peak(P)/Valley(V)
5	32024548	P
17	30973870	V
31	31502864	P
47	30982591	V
58	31065118	P
75	30885595	V

Only enough data to allow the plotting of the first three autocorrelation maxima and minima are needed from the digital photon correlator. Therefore, although the data is correlated and stored out to 94 time steps (which when summed together equal the sample time selected, e.g., $T = .10 \times 10^{-6}$ sec) only data out to time step 75 is needed in this case. Also, under

certain turbulent conditions, more than 3 maxima and 3 minima are impossible to obtain. Figure 78 is presented as an illustration of this point.

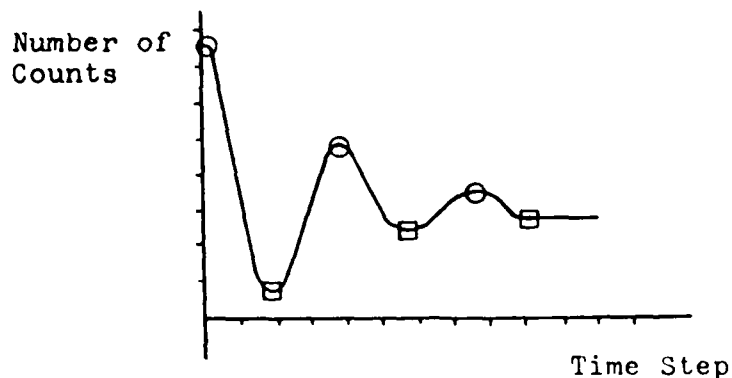


Figure 78 High Turbulence Displayed Autocorrelation Function

The first step in the data reduction process is to unskew the displayed autocorrelation function. The plot of the function at this sample point is shown in Figure 79. Next a least squares second degree polynomial curve is fit through the first 3 maximum points and a second least squares second degree polynomial curve is fit through the first 3 minimum points as illustrated in Figure 80.

Then the arithmetic mean of the coefficients is calculated:

$$C_0 = \frac{A_0 + B_0}{2} = 31526669.45$$

$$C_1 = \frac{A_1 + B_1}{2} = -9123.61$$

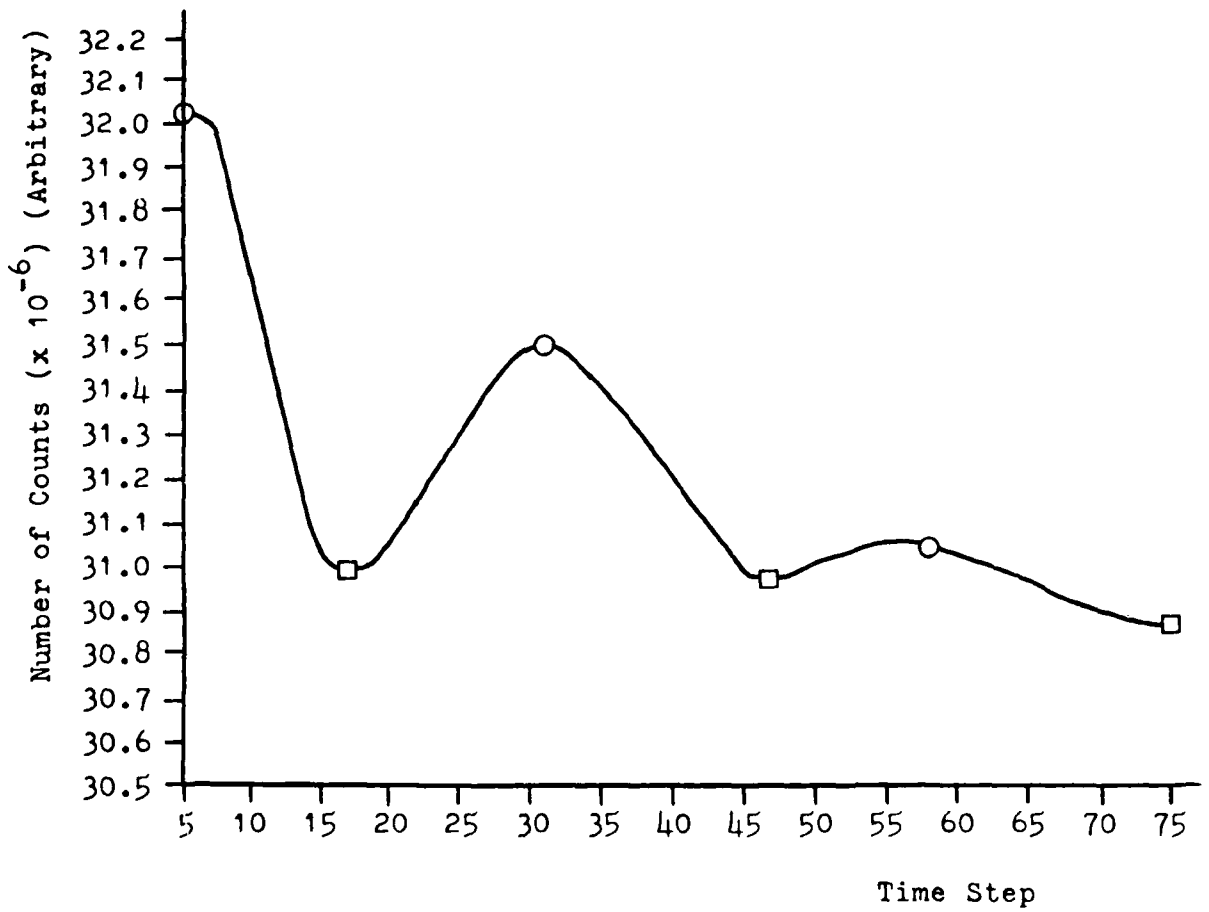


Figure 79 Plot of Displayed Skewed Autocorrelation Function (Sample Calculation)

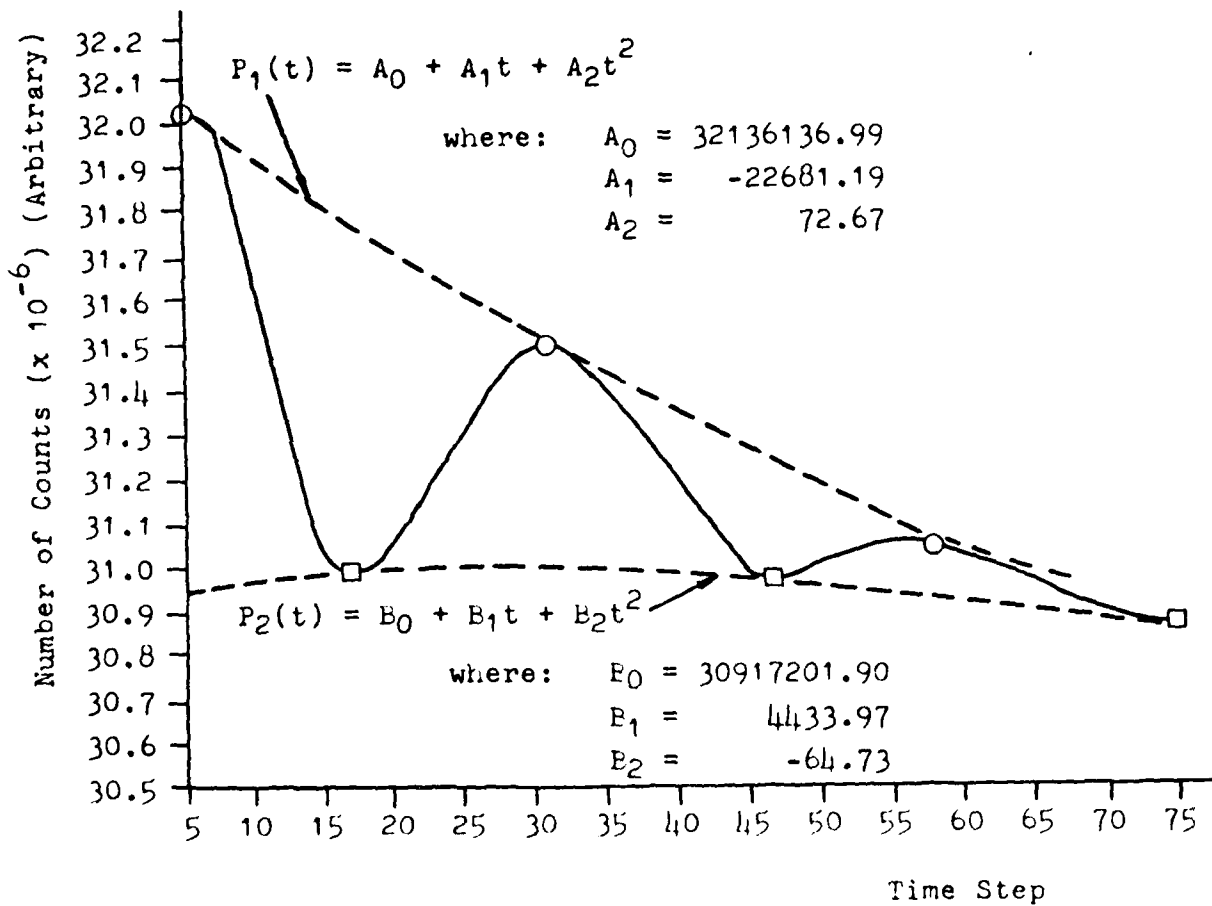


Figure 80 Least Squares Fit(Sample Calculation)

$$C_2 = \frac{A_2+B_2}{2} = 3.97$$

Next a new second degree polynomial curve is then drawn as shown in Figure 81 and this represents the zero ordinate line. The skewed displayed function can now be unskewed by subtracting the mean curve (P_3) from the minima (P_2) and maxima (P_1) curve fits, and replotting as illustrated in Figure 82 .

Finally, to complete the transformation to a nondimensionalized autocorrelation function the entire function is divided by the count difference at Time Step 5. This value is 543397.34 (Figure 83).

With the displayed function unskewed, mean velocity and turbulence intensity can be calculated as demonstrated below (See Appendices A,B, and C for equation details).

Mean Velocity

$$S = \frac{L\lambda}{D\mu} , \quad \sin \theta \cong \tan \theta = \frac{\frac{1}{2}D}{L}$$

$$L = 56.250 \text{ in}$$

$$D = 1.125 \text{ in}$$

$$\lambda = 0.6328 \times 10^{-6} \text{ m}$$

$$\mu = 1.0$$

$$S = \frac{(56.25 \text{ in})(.6328 \times 10^{-6} \text{ m})}{(1.125 \text{ in})(1.0)} = 31.64 \times 10^{-6} \text{ m}$$

$$\sin \theta = \frac{(.5)(1.125 \text{ in})}{(56.25 \text{ in})} = 0.010$$

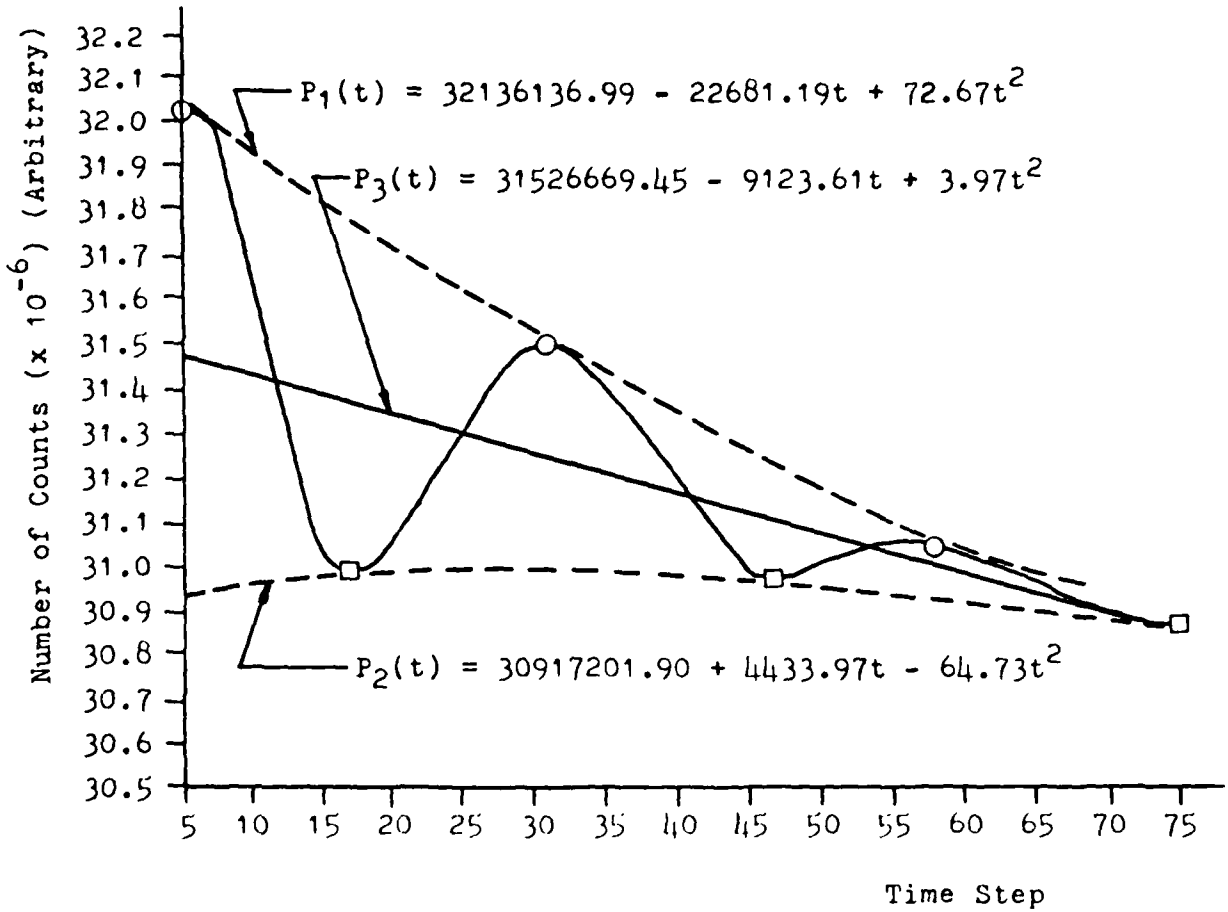


Figure 81 Least Squares Fit (Sample Calculation)

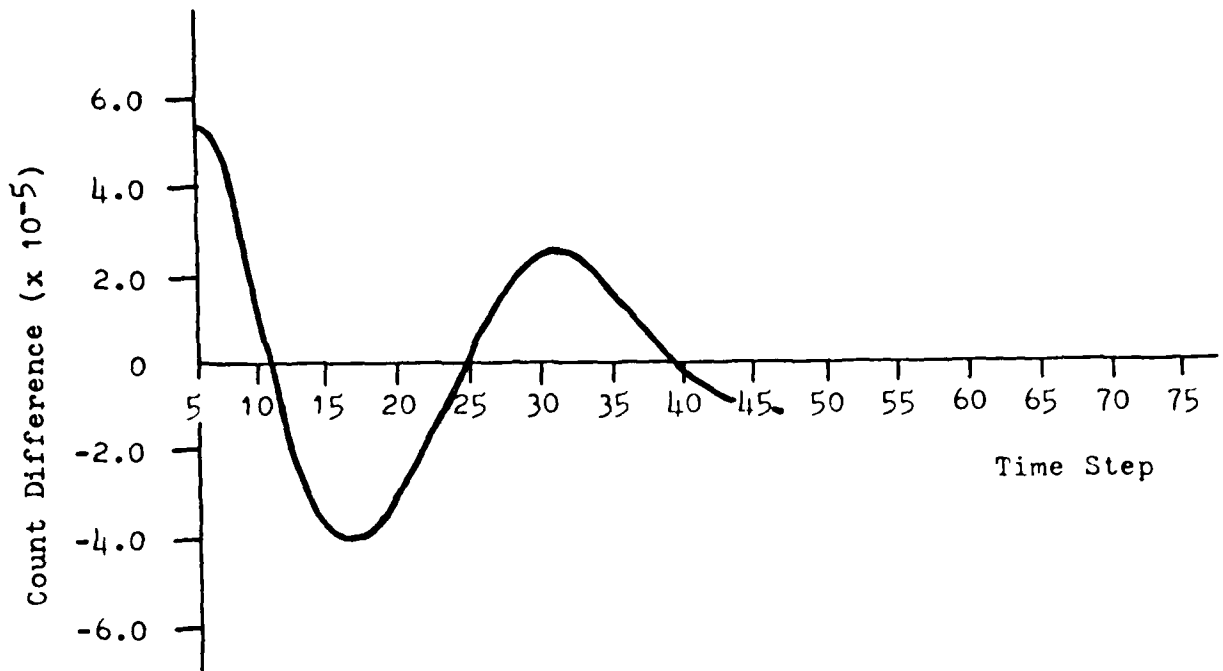


Figure 82 Unskewed Autocorrelation Function
(Sample Calculation)

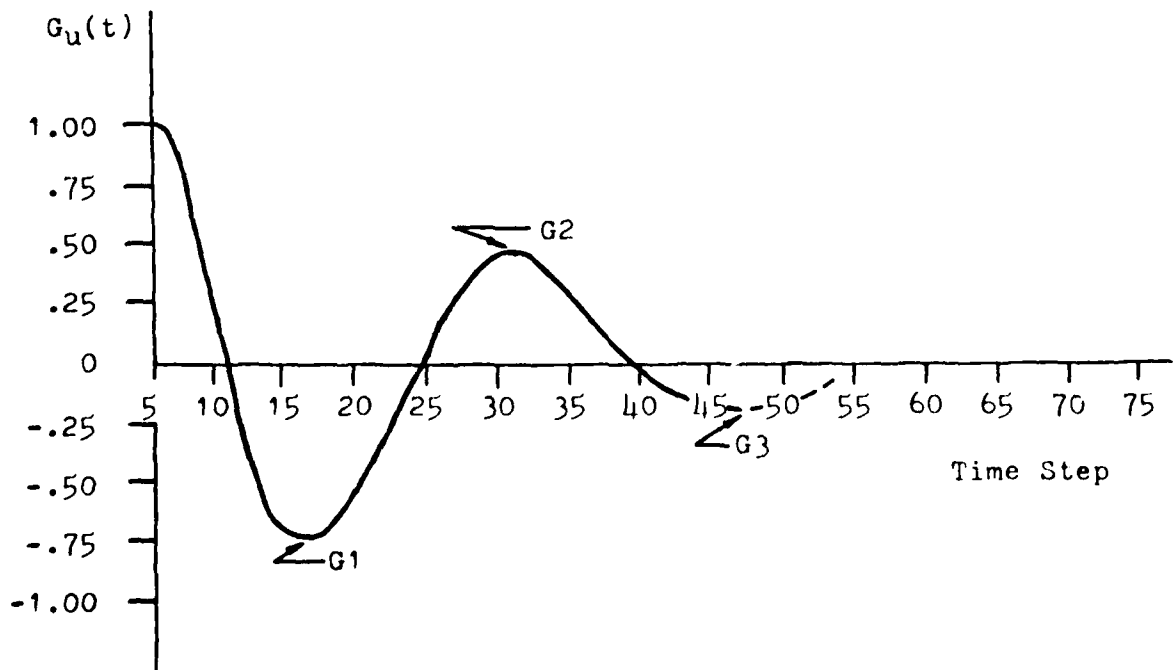


Figure 83 Nondimensional Autocorrelation Function
(Sample Calculation)

$$U_{mX}^* = \frac{S}{(\text{Peak}-3)(T)} = \frac{31.64 \times 10^{-6} \text{ m}}{(17-3)(0.10 \times 10^{-6} \text{ sec})} = 11.3 \text{ m/sec}$$

$$F_d^* = \frac{2U_{mX}^*(\sin \theta)}{\lambda} = \frac{2(11.3 \text{ m/sec})(.01)}{.6328 \times 10^{-6} \text{ m}} = 357.1 \text{ KHz}$$

$$F_d = F_d^* - \Delta F$$

$$F = 357.1 \text{ KHz} - 201.9 \text{ KHz} = 155.2 \text{ KHz}$$

$$U_{mX} = \frac{F_d \lambda}{2 \sin \theta} = \frac{(155.2/\text{sec})(.6328 \times 10^{-6} \text{ m})}{2(.01)} = 4.9 \text{ m/sec}$$

Turbulence Intensity

$$R = \frac{G_2 - G_1}{G_2 - G_3} = \frac{0.4696 - (-0.7339)}{0.4696 - (-0.2283)} = 1.724$$

$$N = \frac{r_0}{S} = \frac{.55 \times 10^{-3} \text{ m}}{31.64 \times 10^{-6} \text{ m}} = 17.383$$

$$\frac{1}{2N^2} = 0.00165$$

$$\text{ETA} = \frac{1}{\pi} \left[\frac{1}{2}(R-1) \frac{U_{mX}}{U_{mX}^*} + \frac{1}{2N^2} \right]^{\frac{1}{2}} = 0.127$$

VITA

PII Redacted

Captain Damon G. Stephens was born [REDACTED]. His family later moved to St Louis, Missouri, where he graduated from Ritenour Senior High School in 1969. Captain Stephens earned a Bachelor of Science Degree in Aerospace Engineering, Summa Cum Laude, from Parks College of St Louis University in 1972. He then entered the United States Air Force and upon completion of pilot training in 1974 spent six years flying B-52's at Castle AFB, California, and Minot AFB, North Dakota. In June 1980, Captain Stephens entered the Air Force Institute of Technology as a graduate student in Aeronautical Engineering.

Permanent Address: [REDACTED]
[REDACTED] [REDACTED]

UNCLASSIFIED

SECURITY CLASSIFICATION OF THIS PAGE (When Data Entered)

REPORT DOCUMENTATION PAGE		READ INSTRUCTIONS BEFORE COMPLETING FORM
1. REPORT NUMBER AFIT/GAE/AA/81D-30	2. GOVT ACCESSION NO. DDA 111 134	3. RECIPIENT'S CATALOG NUMBER
4. TITLE (and Subtitle) AN EXPERIMENTAL INVESTIGATION OF THE FLOW FIELD OF AN EJECTOR WING DESIGN EMPLOYING A PHOTON CORRELATION LASER VELOCIMETER		5. TYPE OF REPORT & PERIOD COVERED M.S. Thesis
		6. PERFORMING ORG. REPORT NUMBER
7. AUTHOR(s) Damon G. Stephens Capt USAF		8. CONTRACT OR GRANT NUMBER(s)
9. PERFORMING ORGANIZATION NAME AND ADDRESS Air Force Institute of Technology (AFIT/EN) Wright-Patterson AFB, OH 45433		10. PROGRAM ELEMENT PROJECT, TASK AREA & WORK UNIT NUMBERS
11. CONTROLLING OFFICE NAME AND ADDRESS		12. REPORT DATE December 1981
		13. NUMBER OF PAGES 121
14. MONITORING AGENCY NAME & ADDRESS (if different from Controlling Office)		15. SECURITY CLASS. (of this report) Unclassified
		15a. DECLASSIFICATION DOWNGRADING SCHEDULE
16. DISTRIBUTION STATEMENT (of this Report) Approved for public release; distribution unlimited		
17. DISTRIBUTION STATEMENT (of the abstract entered in Block 20, if different from Report) 28 JAN 1982 Air Force Institute of Technology Wright-Patterson AFB, OH 45433		
18. SUPPLEMENTARY NOTES Approved for public release; IAW AFR 190-17 <i>Fredric C. Lynch</i>		
19. KEY WORDS (Continue on reverse side if necessary and identify by block number) Laser Velocimeter Air Ejector Velocity Profiles Ejector Wing Mean Velocity Multi-Element Airfoil Turbulence Intensity Flow Visualization FREDRIC C. LYNCH, SC, PH.D., M.S. Instructor of Staff No. 254603		
20. ABSTRACT (Continue on reverse side if necessary and identify by block number) -The flow field about a dual element airfoil model employing an ejector for aerodynamic blowing is investigated. Flow visualization is obtained by smoke tunnel testing. Mean velocities and turbulence intensities are determined at various flow field locations. All data is obtained through the use of a Laser Doppler Velocimeter (LDV) using a photon correlation processing scheme.		

DD FORM 1 JAN 73 1473

EDITION OF 1 NOV 65 IS OBSOLETE

UNCLASSIFIED

SECURITY CLASSIFICATION OF THIS PAGE (When Data Entered)

UNCLASSIFIED

SECURITY CLASSIFICATION OF THIS PAGE (When Data Entered)

Flow field properties are computed from the LDV generated auto-correlation function.

The free stream velocity and Reynolds number based on model chord length are 8 m/sec and 325,000 respectively. Two ejector velocity ratios are investigated: $U_{\text{ejector}}/U_{\text{free stream}} = 0$ and 2. Flow visualization photography is conducted at seven angles of attack: -5° , 0° , 5° , 10° , 15° , 20° , 25° and LDV data is acquired at 0° and 15° angles of attack.

The results are presented in the form of flow visualization photographs and profiles of mean velocities and turbulence intensities. Conclusions are drawn concerning the aerodynamic benefit of the ejector wing design for possible V/STOL applications.

UNCLASSIFIED

SECURITY CLASSIFICATION OF THIS PAGE (When Data Entered)